ELECTROSPUN NANOFIBROUS METAL OXIDES AS REGENERABLE ADSORBENTS FOR DESULFURIZATION OF BIOMASS-DERIVED SYNGAS

BY

MAYANK BEHL

THESIS

Submitted in partial fulfillment of the requirements
for the degree of Master of Science in Chemical Engineering
in the Graduate College of the
University of Illinois at Urbana-Champaign, 2011

Urbana, Illinois

Adviser:

Professor Mark A. Shannon

Abstract

Gasification of biomass residue, a thermochemical conversion process, is fast becoming an attractive method of syngas production by extracting energy from the non-food based biomass feedstocks. Unlike the more popular biochemical processes, like fermentation of cellulosic biomass, it can operate with a wide range of biomass-feedstock in terms of feed's quality and consistency, thus expanding the available pool of feedstock and thereby reducing the overall costs. Moreover, by doing almost complete depolymerization of the source biomass to useful gaseous products like syngas, gasification currently is the only established technology that can theoretically make the most of the energy stored in the raw biomass.

However, on gasification, along with the syngas, gaseous impurities like sulfur containing species (H_2S, COS), ammonia, alkali oxides, halides etc are also generated due to the volatile contaminants present in the biomass residue. Many downstream processes, like Fischer Tropsch synthesis, Solid Oxide Fuel Cells and methanol production, use catalysts that have little tolerance with gaseous contaminants. Transition metal / metal oxide catalysts, typically employed for such value-addition processes, are especially vulnerable to sulfur containing gaseous species like hydrogen sulfide. Therefore, before this raw syngas can be used for different downstream applications, it needs to be cleaned. Among the different processes used for H_2S removal, wet amine scrubbing has been the most popular. However, such wet processes require comparatively low operating temperatures (35 - 55^oC). The cleaned syngas has to be subsequently reheated for the downstream processes (300 - 800^oC). Such consecutive cooling and heating can cause considerable thermal losses.

To avoid such energy losses, it is important to desulfurize the gas stream at suitably high temperatures. A solid-phase sulfur-sorbent material that has a high reactivity, good structural stability, and easy regenerability at such high temperatures can provide such an alternative. In past work, different bulk sorbents with different chemical and structural properties have been

tried for high temperature desulfurization. However, in spite of numerous efforts to modify chemical and compositional properties, only a limited success has been achieved. It is due to sorbent's failure in meeting one or more of the aforementioned criteria. For instance, in the past, it has been demonstrated that due to mass transfer limitations, if a bulk sorbent gets completely sulfided, it is almost impossible to achieve complete regeneration afterwards, regardless of process's favorable thermodynamics and chemical kinetics. This incomplete regeneration, partly due to mass transfer limitation and subsequent loss of sorbent's surface area, leads to underutilization of the sorbent material, which is typically a transition or rare earth metal oxide. To overcome these limitations, it seems necessary that one needs to go beyond doing modifications in sorbent chemical composition alone.

One option that has been little explored involves integration of tailored design and morphology of the sorbent with the process's favorable kinetics. The attempt in this work will be to describe how the structure-based modification of sorbents, specifically nanostructuring, can help in achieving improved sorbent performance for a process requiring reusable sorbents. Since the reaction time has been shown to be comparatively short, the approach here will be to come up with a sorbent design that facilitates short contact time so that deep sulfidation of sorbent can be avoided without affecting the sulfur removal capacity. As this would require high gas velocity along with sorbent's high specific surface area, the use of conventional bulk sorbent will lead to incomplete regeneration and significant pressure drop. Sorbents with tailored designs and sizes, however, can help in overcoming such limitations. The criteria for such designs should be to maximize available specific surface area along with short diffusion lengths. Nanosizing of sorbent seems as a good alternative. However, sorbent in the form of nanopowders tend to aggregate and cause mass transfer limitations similar to bulk sorbents. On the other hand, nanostructures having high aspect ratio, like nanofibers, can remain isolated; thus, potentially providing a more suitable framework for carrying out frequent cyclic sulfidation-regeneration operation. These high aspect ratio nanoscale structures can not only retain the properties from their bulk form such as favorable thermodynamics, chemical affinity etc., but they also tend to develop useful properties due to highly anisotropic geometry and

confined grain size. Because of the confinement of the grain size and short contacting time, nanofibers will tend to limit the large volume changes and accompanying grain boundary collisions which are typical during repeated sulfidation/regeneration. Thus, it is expected that the use of nanostructured sorbent will not only lead to high specific surface area and improved mass-transfer, it can also lead to an improved mechanical behavior during high temperature cyclic operation.

This work will present the results from the experimental investigation of such high-aspect ratio nanofibers for their potential to serve as a regenerable sorbents. Sol-gel based electrospinning was used to synthesize composite zinc and titanium oxide adsorbents in the form of non-woven fiber-mats. Two such samples, with different zinc-to-titanium atomic ratio were selected for further investigation. The Zn-to-Ti ratio for the first sample (Sample-1) was 3.69 and for the second sample (Sample-2a) it was 1.17. Salt solutions of the respective metals, with PVP (Mw ~ 1300000) as the binding polymer, were used to prepare the corresponding sol-gels, which were then used as the precursor solutions for electrospinning of the fibers. Calcination of the as-spun fibers at 600^{o}C for 4hrs resulted in zinc-titanate fiber-mats free from polymer. These fiber mats were characterized by substantially high specific surface areas: 151.7 and 90.1 m^2/g respectively. The average fiber diameter for Sample-1 (post-sintering) was found to be 435 nm and for the second sample it was 714 nm. Fibers were then characterized for their internal crystal structure and surface morphology using the techniques of XRD, SEM and TEM. XRD results and selected-electron-diffraction done using TEM revealed that the electrospun fibers, obtained after the heat-treatment, are multi-phase and polycrystalline in nature. The crystallites formed within a fiber are within the range of 10 – 15 nm in size. SEM allowed observation of surface morphology of the fiber mats. Fiber diameters, ranging from 165 nm to 830 nm, were obtained. It was found that the use of inorganic binders, like lithium polysilicate, can help in reducing the spread in the fiber diameters.

These specimens were subsequently tested for their high temperature reduction behavior. Testing of the reduction behavior is important as it determines the durability and resistance of the sorbent specimens in a cyclic sulfidation/regeneration operation. Temperature

controlled reduction was carried out using a Thermo-gravimetric Analyzer (TGA). Fiber-based sorbents with Zn-to-Ti ratio closer to one were found to be more resistant to deactivation caused by reduction. During the reduction reaction, different compositions of the mixed oxide sorbent exhibited different regimes with different rate-controlling steps. More zinc content in the sorbent implied that the overall reaction rate was controlled by the gas-film diffusion step. Product layer diffusion step becomes rate controlling if there is comparable zinc-to-titanium content (as in Sample -2a). In such sample, shrinking-core mechanism can be seen in operation in which inert product layer grows as the active core shrinks.

TGA was again used for the sulfidation experiments, carried out at isothermal conditions of 600°C with 1% H_2S (rest N_2) gas stream (with flow rate of 200 ml/min). It was found that the composite oxides (Zn-Ti ratio ≈ 1.1) based nanofibrous sorbent specimens (Sample-2a) were slightly more reactive than the specimens rich in free zinc oxide (e.g. Sample-1 with Zn-Ti ratio ≈ 3.7, both specimens being pre-reduced). This may be an indication of higher density of active sites and surface defects in polycrystalline complex oxides as compared to simple metal oxides. Equivalent grain model was used for identification of the rate-controlling step. For majority of the reaction duration, chemical reaction step was found to be the rate-controlling step rather than the product layer diffusion – an indication of minimal mass transfer resistance offered by the nanofibrous sorbent specimens.

During sulfidation, dendritic growth from the parent composite fibers was observed. This was attributed to specific local occurrences of the polar planes of ZnS/ZnO as fiber outer surface along with locally high gas (H_2S) / vapor (Zn) concentration. These structures may have contributed to increased specific surface area. Also, no sulfate formation was detected post-sulfidation, as confirmed by the results from the EDX and XPS analysis . Absence of formation of any sulfate compounds during the sulfidation of nanofibrous zinc titanate adsorbent is expected to improve the chances of achieving complete regeneration. In addition, formation of wurtzite phase during sulfidation, a distinct crystal form of zinc sulfide, was seen as another potential advantage of using nanostructured sorbent morphology. Although bulk wurtzite is only metastable at temperatures less than 1020°C, wurtzite, in its nanocrystalline form, was

apparently stable at lower temperatures (≈ 600°C). Wurtzite tend to oxidize directly to zinc oxide whereas oxidation of sphalerite (another ZnS crystal form) has been reportedly linked with the formation of $ZnSO_4$ and $Zn_3O(SO_4)_2$.

Regeneration experiments were carried out at the same temperature as the sulfidation (600^oC) with a gas stream containing 3% O_2 (rest nitrogen) flowing at 200 ml /min. Comparing the reaction data for the two different specimens (Sample-1 vs Sample-2a), sorbent specimens rich in zinc titanates (Sample-2a) showed faster kinetics than the zinc oxide sorbents (both pre-reduced). It was found that it is possible to achieve complete regeneration without raising the sulfidation temperature (600°C). Again, results from the XPS analysis confirmed no formation of sulfates on oxidation even when the regeneration temperature was kept same as the sulfidation temperature. Structural properties of the sorbent specimen like the fibrous morphology, grain size of the fresh sorbent mostly remained intact in the regenerated specimens. Multi-cycle sulfidation and regeneration tests found that the nanofibrous design of zinc titanate sorbents can successfully withstand repeated sulfidation-regeneration operations whithout suffering microstructure degradation while maintainng high sulfur capacities. Progressive improvement in the textural properties of the fiber was seen as the reason for better performance. Activation energy associated with the sulfidation reaction was also found to be atleast 3 times smaller than that needed for the other sorbent geometries.

All these observations promise an enhanced performance of composite oxides with nanofibrous morphology in a process requiring regenerable sorbents. These findings confirm the main propositions of this work that the sorbent morphology and overall structure influence the sorbent performance as much as the compositional modifications. The above-discussed modifications in the sorbent morphology helped in overcoming some problem areas generally associated with the compositionally-enhanced metal oxides; for instance their lower reactivity, the requirement of high regeneration temperatures, mass transfer controlled overall rate and the consequent incomplete regeneration, all were found to be absent in the above nanostructured sorbent specimens. Future studies will explore the extent to which these improvements can be sustained in a many-cycle operation.

ACKNOWLEDGMENTS

I would like to express my sincere appreciation to Professor Mark A. Shannon for his guidance during the course of this study. In particular, his willingness to support me in pursuing a thesis project that did not have any external funding was very generous of him. His deep insight of the various aspects of experimentation helped me in overcoming different challenges linked with this project.

In addition, I would also like to thank Dr. Junghoon Yeom and Dr. Glennys Mensing for showing interest in the project and providing useful consultation whenever the need arose.

I also wish to thank Dr. Mauro Sardela, Dr. Rick Haasch and Dr. Jim Mabon for familiarizing me with the various sample characterization instruments located at the Frederick Seitz Materials Research Laboratory's Central Facilities. These facilities are partially supported by the U.S. Department of Energy.

TABLE OF CONTENTS

List of symbols

N_{ZnO}	Number of moles of zinc oxide (moles)
A_{ex}	External surface area of the fiber-mat sample (m^2)
C_{H_2g}	Concentration of H_2 in the bulk gas phase (mol/m^3)
k_g	Mass transfer coefficient of the gas film ($m^3/m^2.s$)
b	Stoichiometric coefficient in a gas-solid reaction
Ř	Gas constant (=8.314 J/mol/K)
R	Effective spherical radius (m)
d_p	Effective sample diameter=2.R (m)
μ	Gas phase dynamic viscosity (Pa.s)
ρ	Mass density of the gas phase (kg/l)
y	Mole fraction of H_2 in gas phase
ρ_s	Being the molar density of zinc oxide (mol / l)
t	Time (s)
T	Temperature (^oC)
V	Specimen volume (l)
u_g	gas velocity (m/s)
Sc	Schmidt number $\frac{\mu}{\rho D}$

Re	Reynolds number $\frac{d_p \rho u_g}{\mu}$
X	Conversion or extent of reaction
$(dW/dt)_0$	Initial rate of change in the sample weight (in g/min)
α_0	Specific surface area as measured by BET (m^2 / g)
W_0	Initial sample weight (g)
W (t)	Sample weight at a time t (g)
W_f	Sample weight after the reaction (g)
A_0	Total area of the sorbent (in m^2) at t = 0 ($A_0 = W_0 * \alpha_0$)
M_{ZnO}	Molecular weight of Zinc Oxide = 81.4 g/g-mol
M_{ZnS}	Molecular weight of Zinc Sulfide = 97.47g/g-mol
C_{A0}	Concentration of gaseous reactant H_2S in bulk phase (mol / l)
r_{go}	Initial average grain radius inside a sorbent specimen (m)
k_0	Pre-exponential factor associated with reaction rate constant
E_{ar}	Activation energy associated with the chemical reaction step
k_r	Chemical reaction rate constant (m/s) = $k_0.\exp(-E_{ar}/\check{R}T)$
D_0	Pre-exponential factor associated with diffusion
E_{ad}	Activation energy associated with diffusion through the product layer
$\mathscr{D}$, D	Molecular diffusion coefficient in the gas phase (m^2/s)

$F_r(X)$	Conversion function defined as following: $\left(1-(1-X)^{1/3}\right)$
$F_d(X)$	Another Conversion function: $\left(1-3.(1-X)^{2/3}+2.(1-X)\right)$
P	A constant in the Grain model (time units): $\frac{\rho_m.r_{g_o}}{k_r.C_{A_0}}$
Q	Another constant in the Grain model (time units): $\frac{\rho_m.R_i^2}{6.D.C_{A_0}}$

Chapter-1

Introduction

1.1. Overview of desulfurization of biomass derived syngas

Production of syngas via gasification of cellulosic biomass has been gaining considerable attention primarily for its potential to contribute to the energy and environmental sustainability. There are several benefits that come with this technology especially when the syngas produced during gasification is used in an energy-related application. Using biomass residue as an energy source ensures that only non-food sources like crop residue, saw and paper mills discards and forest wood residue are used as a feedstock. Energy-crops like miscanthus and switchgrass that grow on marginal lands also contribute to biomass feedstock. Fig-1.1 gives the relative proportion of each of these feedstocks in constituting biomass resources of the United States.

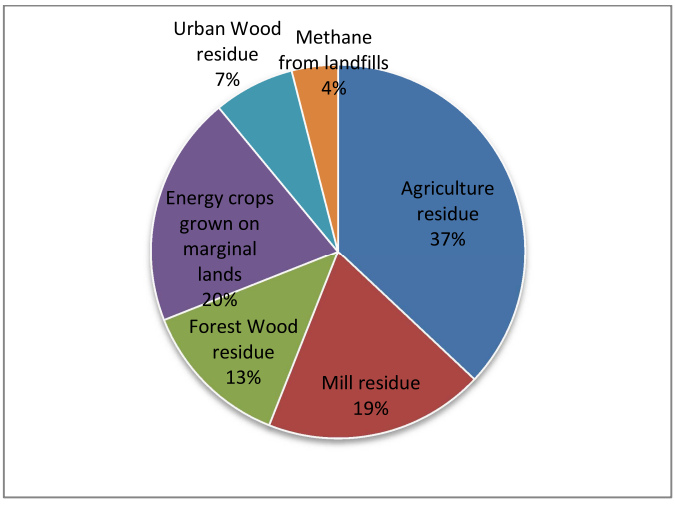

Figure-1.1: Contribution of different feedstocks to the cellulosic biomass resources of the United States (NREL, 2005)

Thus, unlike crop-based fuels (e.g. grain-ethanol), energy derived from cellulosic biomass feedstock does not interfere with food supply or the cost of the food products. In addition, such biomass is found abundantly with broad geographic distribution: the United States generates 423 million tons of dry biomass annually (Milbrandt, 2005), which has an energy content equivalent to 1.3 billion barrels of oil (boe). Moreover, its use as a energy source does not lead to any excess carbon dioxide emissions since any CO_2 released during its end-use (or during the conversion process) gets recycled during the growth of biomass by the process of photosynthesis. Biomass residue has high energy density, which is pertinent for energy and power applications. For instance, each ton of corn stover (with approximate energy density of 18MJ/kg) has an energy equivalent to 3 barrels of oil. The state of Illinois alone produces 28.3 million tons of biomass residue, which is equivalent to 9-15 billion gallons of gasoline (Milbrandt, 2005).

Currently, the most common ways of utilizing biomass for energy applications include processes like incineration and combined-cycle-power-generation. These processes come under the category of combustion-based methods, which are known to suffer from energy inefficiencies as these processes involve combustion (complete oxidation) of the biomass feedstock resulting mainly in gases like CO_2, water vapor (and tar as a solid by-product) which are less useful commercially and, while the remaining energy is released in the form of heat (byproduct of combustion) a portion of which is then used for running heat engines. That heat constitutes less than 50% of the actual energy of the feedstock. Furthermore, the efficiency of this heat engine is limited by Carnot's cycle law. Net result is a low efficiency process. An alternate approach is to use a 'thermo-chemical' process instead of a pure thermal process. Thermo-chemical processes aim at converting the energy present in the raw biomass into useful chemicals which can themselves be used as fuels or can be converted to other types of fuels or useful products. Partial oxidation, as in autothermal gasification, or heating of feedstock in complete absence of oxygen (as in pyrolysis) are examples of a thermo-chemical process. Biomass gasification is being considered as a particularly attractive technology as it can operate with a wide range in the quality and consistency of the feedstock, thus increasing the available feedstock and reducing the overall cost. Depolymerizing the source biomass right

down to the useful gaseous products like syngas makes this process currently the only established technology that can claim to extract most of the energy stored in the raw biomass (Seitarides et al., 2008).

The process involves conversion of the given feedstock into raw syngas, a gas mixture consisting mainly of hydrogen and carbon monoxide, by reacting the raw material at high temperatures with a controlled amount of oxygen and/or steam. Table-1.1 gives the typical range of composition of the gas thus produced. (Compositions can vary depending upon the ways in which gasification is carried out).

Table-1.1: Typical exit gas composition from a gasifier (Nagel et al., 2008)

Major components of raw syngas (dry basis, mol%)			
Type of gasifier	*Fixed bed (Downdraft)*	*Circulating Bed*	*Entrained Flow*
Gasification agent	Air	H_2O	O_2
H_2	15-21	17-36	29-40
CO	10-22	36-51	39-45
CO_2	11-13	7-15	18-20
CH_4	1-5	0.1-0.6	0.05-0.1
C_2	0.5-2	1.4-7.5	-
N_2	37-63	0-3	0.1-9

This raw syngas gas needs to be first cleaned (See Section 1.1) so that the undesired components are removed. After performing a gas treatment step, syngas can then be used for several commercially valuable applications like production of synthetic liquid fuel (Fischer-Tropsch Process), bulk chemical synthesis (methanol, methane, polymers etc), and also as a hydrogen source for other technologies like Solid Oxide Fuel Cells (SOFCs). A simplified block diagram of the process is shown in Fig-1.2.

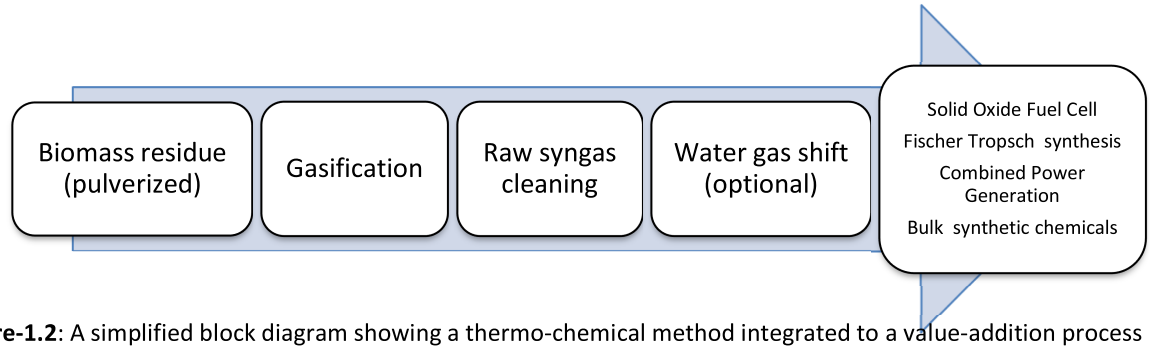

Figure-1.2: A simplified block diagram showing a thermo-chemical method integrated to a value-addition process

1.2. Challenges associated with the use of biomass-derived syngas

The foremost challenge in using gasification technology for energy-related application is the removal of the undesired gaseous components from the raw syngas. On gasification, along with the raw syngas (composition listed in Table-1.1), gaseous impurities like sulfur containing species (H_2S, COS), ammonia, alkali oxides, halides etc are also generated due to the volatile contaminants present in the biomass residue. The typical composition of some gaseous impurities is given in Table-1.2.

Table-1.2: Common gaseous impurities in Raw syngas (via gasification), Cheah et al. (2009)

H_2S (ppmv, dry)	**HCl (ppmv, dry)**	**NH_3 (ppmv, dry)**
50–230 (wood residue)	1–200 (wood, verge grass)	1,000–13,000 (wood, verge grass)

Many downstream value-addition processes, like Fischer Tropsch synthesis, power generation from Solid Oxide Fuel Cells and methanol production, use catalysts that have little tolerance with gaseous contaminants. Transition metals / metal oxide catalysts, typically employed for such value-addition processes, are especially vulnerable to sulfur containing gaseous species like hydrogen sulfide. Apart from being a well-known catalyst poison, presence of H2S in the gas stream is the leading cause of corrosion of the pipelines that are used for gas transport. Therefore, before raw syngas can be used as an input to a particular downstream application, the concentration of gases like H_2S need to be brought down to that process's acceptable limits (See Table-1.3). Beside gaseous impurities, tar (condensable heavier hydrocarbons) is also generated during gasification, although the amount produced is

significantly lesser than that produced during combustion (incineration), it needs to be converted into lighter gaseous components. Otherwise, tar will condense later and cause premature loss of catalyst activity or clogging of pipelines.

Table-1.3: Acceptable limits on impurities in inlet gas composition for different value addition processes (Torres et al., 2007. Cheah et al., 2009)

Process	Sum of all Sulfur containing species (Typically H_2S, COS)	Sum of all halide containing species (Typically HCl, HF)	Sum of all Nitrogen containing species (Typically NH_3, HCN)
Fischer Tropsch Synthesis	Less than 1 ppmv	Net less than 10 ppbv	Less than 1 ppmv
Methanol production	Less than 0.5 ppmv	Less than 1 ppbv	NA
Solid Oxide Fuel Cell	Less than 1 ppmv	Less than 10 ppbv	-
Water gas shift reaction	Less than 1 ppmv	Less than 10 ppbv	-

An analysis of thermochemical ethanol production conducted at NREL revealed that tar reforming, acid gas and sulfur removal processes together with the subsequent syngas compression, comprise 31% of the total fuel production cost (Phillips et al., 2007). Thus, a more efficient method of H_2S and tar removal can significantly reduce the overall operation cost.

Following is a list of the different categories of contaminants found in the biomass derived syngas and the commonly used cleaning methods associated with each of the categories:

- Removal of nitrogen containing species (NH_3, HCN)
  - Wet scrubbers using H_2SO_4, or Sulfinol-D®
  - Acidic adsorbents, acid coated molecular sieves
- Removal of sulfur containing components (H_2S, COS)
  - Wet amine scrubbing (operates between 35-50 C)
  - Metal or Mixed Metal oxide adsorbents (ZnO, ZnTiO3, MnO, FeO, ZnFe2O4), Operating temperature (350 – 900 C)
- Removal of chlorine containing species (HCl)

- Wet scrubbers using NaOH
- Sorbents like Na_2CO3, Trona ($NaHCO3.2H2O$)

- Removal of Ash / silica,
  - Particulate filters – Cyclone separators

- Removal of Tar (Condensable heavy hydrcarbons)
  - Thermal cracking, Catalytic process
  - Optimum operating temperature (350 – 600 C)

It can be seen that removing gaseous impurities can be categorized in to two different groups: wet gas cleaning techniques & hot gas cleaning techniques. Following sections describe the difference between the two with focus mainly on H_2S removal.

1.3. Different ways of removing H_2S

Wet gas cleaning

In general, wet gas cleaning technologies typically employs a series of low-temperature solvent absorption and gas scrubbing steps so as to reduce the concentration of the contaminants to an acceptable level. Among the many methods of H_2S removal, wet amine scrubbing has been the most popular one. It requires the raw syngas from the gasifier to be cooled down to 35 and 50°C and scrubbed with a liquid solvent (amine) which physically absorbs most of the hydrogen sulfide contained in the gas. Some absorbents may require hydrolysis conversion of COS to H2S to achieve high levels of sulfur removal. One of the most effective absorbents for removing sulfur is methanol but it needs temperatures as low as -75 degrees Celsius. Commercially, this process is known as Rectisol® desulfurization process (with methanol as solvent). It does not require hydrolysis of COS to H2S and can reduce sulfur concentrations to relatively low levels in syngas. However, the Rectisol process requires a substantial investment in equipment and incurs high power costs

The cleaned syngas has to be subsequently reheated for the higher temperature downstream processes (like Fischer Tropsch ~ 350 – 500°C, SOFCs ~ 800°C). Such consecutive

cooling and heating is not only expensive but also incurs significant thermal inefficiencies that can bring down the overall energy recovery of the process. Moreover, such sort of cooling causes immediate tar condensation. Tar condensation causes plugging and fouling of the condenser and downstream process piping. This presents significant operating challenge. Use of solvents to absorb H_2S causes an additional problem of wastewater generation, and subsequent water treatment will increase the operating cost. Thus to avoid such problems, it is important to desulfurize the gas stream at suitably high temperatures.

Hot dry gas cleaning

Hot dry gas cleaning technique, as the name suggests, operates at a temperature that is closer to overall process temperature (~600 – 900°C) and does not use any liquid solvent for gas treatment. Instead, it employs solid metal oxides as adsorbents for selectively adsorbing hydrogen sulfide. Most of the metal oxides are regenerable. Based on the study of equilibrium thermodynamics for H2S adsorption, Westmoreland and Harrison (1976) showed that oxides of barium, calcium, cobalt, copper, iron, manganese, molybdenum, strontium, tungsten, vanadium, and zinc are capable of being used as sulfur adsorbents. All these metal oxides are known to remove H_2S by the following general reaction (also known as sulfidation reaction):

$$M_xO_y + y.H_2S \Leftrightarrow M_xS_y + y.H_2O$$

This reaction denotes a non-catalytic gas-solid reaction where 'M' represents a viable metal. The above overall sulfidation reaction is typical of transition metal oxides. Rare-earth metal oxide-based sulfur adsorbents, like CeO_2 (reacts with H_2S as Ce_2O_3 in presence of reducing atmosphere, as is the case with syngas desulfurization) and La_2O_3, tend to undergo the following overall reaction with H_2S:

$$2CeO_2 + H_2 \Leftrightarrow Ce_2O_3 + H_2O$$
$$Ce_2O_3 + H_2S \Leftrightarrow Ce_2O_2S + H_2O$$

Sulfidation temperature typically reported in the literature lies in the range of 400 to 900°C. However, in an industrial plant, the upper temperature limit is determined by process

equipment restrictions, for instance, valve limitations. Operating temperature and pressure should be selected such that the valves are able to withstand alternating reducing and oxidizing conditions. This limits the upper temperature to somewhere around 600°C (Slimane et al., 2002). The lower limit, as discussed earlier, is limited by thermal efficiency

Regeneration, for a transition metal sulfide, is supposed to proceed by the following overall reaction:

$$M_x S_y + \frac{3}{2} y.O_2 \quad \Leftrightarrow \; M_x O_y + y.SO_2$$

For rare-earth metal sulfides, like Ce_2O_2S, regeneration leads to a direct recovery of sulfur:

$$2Ce_2O_2\,S(s) + 2O_2(g) \Leftrightarrow 4CeO_2(s) + S_2(g)$$

Regeneration is done with a stream of air passed through the oxide bed countercurrent to the direction of the process stream during sulfidation. Oxygen present in the air reacts with the metal sulfide and returns the original metal oxide form. It is generally carried out at temperatures couple of hundred degrees higher than the sulfidation reaction, typically between 600 -1000°C.

Besides thermodynamics, there are other factors, like kinetics, cost, side reactions, oxide's catalytic properties, which can play an important role in making sorbent choice. Based on these additional criteria, zinc, manganese, copper, iron, and calcium sorbents have shown to be more promising. Several studies indicated the intrinsic reaction kinetics of the sulfidation of ZnO, MnO, CaO, FeO, and Cu on ceria to have first-order dependence in H_2S (Flytzani-Stephanopoulos & Li, 1998). An Oxide's catalytic properties may prove to be an additional benefit, for instance, iron oxide acts as a water gas shift catalyst (downstream of cleaning unit) that promotes conversion of CO and H_2O to CO_2 and H_2.

Cheah et al. (2009) suggested certain selection criteria for choosing a sorbent:

- High adsorption capacity (favorable thermodynamics)

- Fast kinetics
- Mechanical Strength to withstand high temperatures
- Chemical properties to withstand highly reducing conditions
- Easy regeneration
- Multi-component adsorption capability

Thus, a metal oxide having high reactivity, good structural stability, and easy regenerability at high temperatures can provide such an alternative. In past work, different types of bulk sorbents with different chemical and structural properties have been tested for the applications involving high temperature desulfurization, pertaining mainly to the research in the field of treatment of syngas generated by **coal gasification** (Gibson & Harrison, 1980; Lew et al., 1992; Kobayashi et al., 1997; Harrison, 1998; Jothimurugesan et al., 1989). It should be noted that although literature available on sorbents developed for coal-derived syngas at high-temperatures is being used as the starting point here, desulfurization of syngas derived from biomass involves some aspects that are unique to it. For instance, coal gasification is usually a direct oxygen-blown process conducted at higher temperature than biomass gasification, which typically employss steam/air mixture. As a result, the syngas from biomass typically has a higher water (steam ~ 30 – 65%) and hydrocarbon content (Phillips et al., 2007). On the other hand biomass-derived syngas obtained from has comparatively less sulfur content as compared to coal-derived syngas. Sulfur content of biomass-derived syngas varies from 50-600 ppmv where as coal-derived syngas has sulfur content in the range of 1000 to 15000 ppmv (Cheah et al., 2009).

Among various metal oxides, zinc oxide is the one of the most extensively studied oxide for desulfurization applications. Zinc oxide is known for its high sulfidation capacity, favorable thermodynamics and high efficiency when it comes to sulfur removal. However, as shown by Harrison (1998), ZnO starts getting reduced to zinc metal at high operating temperatures (>550

C) due to the presence of gases like H_2 and CO in the exit gas stream of a gasifier. Thus, the use of ZnO is limited to only few-cycles at mid-high temperatures.

Most of the simple metal oxides, however, show limited performance when operating at high temperatures. In particular, for temperatures in excess of 550°C, oxide of highly volatile Zinc metal (ZnO) tends to get chemically reduced to zinc vapors due to the reducing gases present in raw syngas mixture (Jothimurugesan et al., 1998). Furthermore, many single oxide sorbents tend to suffer from loss in surface area and consequent decline in sulfur capacity due to sintering caused by high temperature. Carrying out desulfurization at lower temperatures may seem to be an option, but it not only leads to slower kinetics but also leads to formation of metal sulfates (Ryu et al., 2004; Siriwardane & Poston, 1990), which are thermodynamically stable and harder to regenerate. In addition, volumetric changes caused by oxide-sulfide-oxide conversion, may mean increased sorbent spalling and decreased mechanical strength during high temperature multi-cycle operation.

To overcome these limitations, use of mixed metal oxides became popular. When metal oxides are mixed together and calcined, it was found that new composite compounds are produced with considerably different thermodynamic, kinetic and physical properties. Mixed metal oxides have shown better mechanical strength and stability, less reduction tendency & improved regenerability (Harrison, 1998). For instance, with an aim of stabilizing zinc oxide against reduction, Titanium oxide (TiO_2) is typically added to ZnO to generate complex oxide phases like zinc titanate ($ZnTiO_3$). Addition of iron oxide has also been tried but Zinc ferrites have been found to suffer from similar problems as of their individual components: at high temperatures they tend to decompose to individual oxide components, which subsequently reduce towards their metal form. Zinc titanates, however, have been shown to be much more effective against reduction. Lew et al. (1989, 1992) studied the performance of zinc titanate as adsorbent for H_2S. Authors found that on comparing sorbents containing ZnO alone to sorbents containing mixed Zn-Ti-O, rate of zinc loss is five to ten times slower during sorbent-reduction reaction. In a later publication, Lew et al. (1992) conducted studies on the kinetics of Zn−Ti−O reduction and found that in H_2−N_2 gas mixtures, Zn−Ti−O solids have a lower reduction rate

than ZnO in the temperature range 550−1050°C and the associated activation energies for Zn−Ti−O and ZnO reduction were calculated to be 37 and 24 kcal mol^{-1} respectively. They also concluded that zinc titanate sorbents (with less than 50% TiO_2) had higher surface area and pore volume than ZnO sorbents. It was proposed that TiO_2 inhibited the sintering of ZnS by acting as a physical barrier to the growth of ZnS particles. All these properties make certain mixed metal oxides more suitable candidates for high temperature multi-cycle operation.

However, although the presence of Titania does decrease the reduction tendency of the Zn-Ti-O system, it has also been linked to sorbent's lower specific sulfur removal capacity and slower initial reaction rate during sulfidation (Lew et al., 1992; Ryu et al., 2004). This has been attributed to the fact that titania does not take part in the desulfurization reaction.

In short, despite of numerous efforts to modify chemical and compositional properties, only a limited success has been achieved. It is primarily due to sorbent's failure in meeting one or more of the above-mentioned criteria. In addition, it has been demonstrated that due to mass transfer limitations (Focht et al., 1989), it is highly unlikely to achieve complete regeneration if a bulk sorbent is allowed to get completely sulfided, regardless of process's favorable thermodynamics and chemical kinetics. Such incomplete regeneration, partly due to mass transfer limitation and subsequent loss of sorbent's surface area, leads to underutilization of the sorbent material, which is typically a transition or rare earth metal oxide. To overcome these limitations, it seems necessary that one needs to go beyond doing modifications in sorbent chemical composition.

1.4. Motivation

One option that has been little explored involves investigation of structured sorbent materials having microstructures and surface morphologies that can be tailored to suit the process. Integration of such capability with the material's inherent favorable thermodynamics and kinetics can lead to a better sorbent performance. However, conventional bulk scale sorbent designs will not be able to fully utilize the benefits that arise from the control of the

microstructure and associated sorbent morphology. The approach, therefore, should be to come up with a sorbent architecture that facilitates such control so that it is able to maximize the advantages associated with the nanostructuring. This aspect becomes particularly important for some adsorbent applications; for instance, mass-transfer controlled processes which involve relatively fast chemical reactions. High temperature desulfurization is one such case. Focht et al., (1989) and Harrison (1998) argued that the time for intrinsic chemical reaction between Zinc oxide and hydrogen sulfide is comparatively short and gas & product layer diffusion are the controlling steps. Wang & Flytzani-Stephanopoulos (2005) reached a similar conclusion with cerium oxide as the desulfurizing agent. Authors recommended short contact time so that deep sulfidation can be avoided and it becomes feasible to carry out complete sorbent regeneration in the subsequent step. As short contact time necessitates the use of high gas velocity, the use of conventional bulk sorbent will not only lead to significant pressure drop but will also lead to underutilization of the sorbent material because of the large diffusion lengths. Sorbents with tailored designs and sizes, however, can help in overcoming such limitations by providing considerably higher specific surface area and short diffusion lengths for minimizing the mass transfer resistances. Nanosizing of the sorbent seems to be a good alternative. However, nanosizing alone cannot solve the problem. Sorbent in the form of nano-particles will tend to aggregate and can lead to diffusion limitations similar to bulk sorbents. Dispersion of the particles on a support structure seems to be another option; however, being adsorbent (and not catalyst), they will be needed in comparatively larger quantities and catalyst-like dispersion on a support surface may limit the sulfur removal capacity. Therefore, what is needed is a synthesis technique that can produce nanoscale sorbent structures that do not tend to aggregate and are amenable to scale up so as to retain high sulfur removal capacity.

Ceramic nanofibers prepared using the process of electrospinning can demonstrate such potential (Li & Xia, 2004; Sigmund et al., 2006, Yuh et al., 2007, Dai et al., 2011). This process can be used to synthesize high surface area fiber mats made up of metal oxide fibers with diameter as small as 50 nm. Because of their high aspect ratio, these nanofibers tend to remain isolated; thus, potentially providing a more suitable framework for carrying out frequent cyclic

sulfidation-regeneration operation. Such high aspect ratio nanoscale structures not only retain the favorable thermodynamics and chemical affinity of their bulk equivalents but also develop useful properties due to anisotropic geometry and reduced grain sizes. Given that the reactions involved are inherently fast, abovementioned properties of the nanofibers, along with the operating conditions that facilitate short contacting time, can help in limiting the excessive volumetric changes that typically result in sorbent failure in cyclic sulfidation/regeneration operation. Thus, it is expected that the use of sorbents in the form of stacked fiber-mats made from such nanofibers can not only lead to considerably higher specific surface area and improved mass-transfer, but they may also contribute to an improved mechanical integrity during high temperature multi-cycle operation.

1.5. Process of electrospinning

The setup for electrospinning consists of three major components: a metallic needle, high voltage source and a metallic collector (See Fig-1.3). The metallic needle is called spinneret. It is attached to syringe that contains a polymeric solution homogenously mixed with a salt or a propoxide solution of the given metal. A syringe pump is used to feed this mixture through the spinneret at a controllable rate.

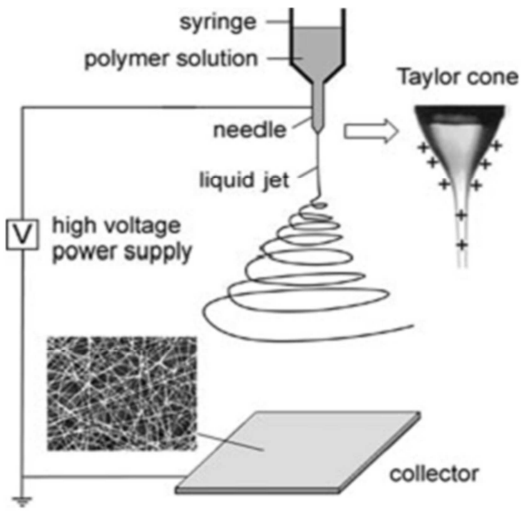

Figure-1.3: The basic setup for electrospinning process (Li & Xia, 2004)

When a high voltage is applied (typically via DC power), the pendant drop at the tip of the metallic needle becomes highly charged with charges induced all over the surface of the drop. In addition to the solution's own surface tension, the drop also experiences two other forces: electrostatic repulsion due to surface charges and Coulombic force exerted by the external electric field. Under the action of these forces, the shape of the drop will distort from spherical to conical, commonly known as Taylor cone. Once the strength of the electric field exceeds the surface tension of the solution, a liquid jet will be ejected from the nozzle (Li & Xia, 2004). This electrified jet then undergoes stretching and whipping process, leading to a long, thin thread. Solvent evaporates as the jet continuously elongates, and in the process, the thread's diameter starts reducing by several orders. This charged fiber is deposited on the grounded collector as a randomly oriented, non woven web or mat. This fiber-mat is first vacuum dried and then sintered at elevated temperatures, removing all the organic compounds present in the green fibers. Ramaseshan et al. (2007) recently used electrospinning to successfully produce ZnO/TiO2 fibers. They investigated these fibers for their reactivity against chemical warfare agents. They reported satisfactory performance in detoxifying CEES (2-chloroethyl ethyl sulfide) which was being used as a liquid phase simulant for mustard agents.

Process of electrospinning has been discussed in more detail in Chapter – 2.

1.6. Thesis objectives

The overall objective of this thesis is to investigate the nanostructured fiber-mats produced via electrospinning for their potential to provide a sorbent architecture that is amenable to a fast and a fully regenerable operation, specifically when being used as a multi-cycle, high temperature adsorbent during the removal of H_2S from the biomass-derived syngas. The sol-gel based electrospinning was used to synthesize composite nanofibers containing mixed metal oxides of zinc and titanium. Zinc oxide was chosen because of its high sulfur removal capacity due to its favorable thermodynamics and reasonably fast kinetics. However, as discussed in earlier sections, ZnO needs to be mixed with titanium dioxide to limit its tendency to get reduced to the highly volatile zinc metal when operating at high temperatures (> 550°C).

In order to achieve this objective, electrospun zinc titanate fiber-mats were subjected to reduction (with 4% H_2 gas), sulfidation (with 1% H_2S) and regeneration reactions (with 3% O2) and a detailed investigation of the overall reaction rates and the associated compositional and morphological changes was carried out. The technique of thermo-gravimetric analysis (TGA) was used to measure the chemical reaction rates for each of the operations mentioned above. Kinetic parameters, like the activation energy and the rate constant involved, will be estimated. Using the values of these kinetic parameters, the effect of unique microstructure (nanoscale grain sizes, higher density of grain boundaries etc.), generated as a result of employing nanostructuring technique of electrospinning, will then be studied. The reaction rate parameters obtained for these nanofibrous sorbent will be compared with the values reported for their bulk-counterparts as reported previously in the published literature. In particular, attention will be paid to the effect of nanostructuring on the mixed sorbent's ability to resist deactivation caused by reduction.

In addition to measurement of the regeneration kinetics, regeneration performance will be evaluated by investigating the compositional changes that occur during the process. This is important for monitoring the formation of compounds like zinc sulfate during regeneration, which, on successive regenerations, can quickly shorten the sorbent life. This will be carried out by making use of the analytical techniques like XPS, which can easily capture the difference

arising from the changes in the element's (here zinc) bonding by causing shift in the spectral peaks. Also, changes in specific surface area, surface morphology, composition, and crystalline phases will be studied by characterizing the specimen from techniques of BET, SEM, EDX and XRD.

In short, the main objectives of this thesis can be summarized as follows:

- To investigate if a fibrous sorbent architecture, as provided by the electrospun fiber mats, is more effective in extending the lifetime of a given sorbent during a multi-cycle operation.
- To investigate how surface reconstruction during gas adsorption affects the subsequent regeneration properties of the sorbent
- To study the effect of nanostructuring on the adsorption & structure-related properties of metal oxide sorbents. In particular, determining the extent to which nanocomposite Zn-Ti-O fibers impact sorbent's overall resistance to the deactivation, which occurs during the reduction reaction.
- To determine the extent to which the reaction is surface sensitive by relating the estimated the reaction data with the observed microstructure.
- To carry out mathematical modeling of the sulfidation reaction for determining the rate-controlling step in the overall non-catalytic gas-solid reaction between the H_2S and the nanofibrous zinc based sorbents.

1.7. Organization of the text

- Chapter-2 provides the details of the electrospinning process that was employed during the preparation of electrospun adsorbents preparation.
- Chapter-3 discusses the results obtained from the experimental investigation of the response of the sorbent when exposed to the reducing atmosphere of hydrogen gas.

- Chapter-4 begins by describing the setup used for carrying out the sulfidation and regeneration experiments with the electrospun adsorbents. An attempt is made to correlate the results obtained from the reaction experiments with the results from the characterization of microstructure of the sorbent specimens. The chapter also proposes a mathematical model for the sulfidation reaction based on the reaction rate data collected using the TGA setup.
- Chapter-5 summarizes the major findings of this work. Important conclusions drawn using these findings are then presented. Chapter-5 ends with couple of recommendations and some ideas for the direction of the future research work.

Chapter-2

Preparation of oxide fiber-mats using electrospinning

2.1. Need for nanostructured adsorbents

The unique properties of nanostructured adsorbents have the potential to solve many of the problems presently faced by the sorbents during high temperature adsorption and regeneration operations. The nanometer-sized grain size in a polycrystalline metal oxide means higher specific surface area with relatively high grain-boundary density. This results in improved gas sensitivity and adsorbent reactivity, implying that the adsorbent can be potentially be used at lower to mid-high temperatures (400-600^{o}C) instead of conventional 600 to 900^{o}C. Gas-cleaning in mid-high temperature is gaining significant interest in industry because of some practical reasons. Slimane (2002) argued that due to the various process equipment limitations and other process variables such as the alkali content of the raw syngas, the optimum desulfurization temperature is in the range of 316 to 540^{o}C instead of the commonly recommended 650 to 900^{o}C (based on thermal efficiency criteria alone). This relatively lower temperature operation offers solution to many problems associated with high temperature operation. For instance, sintering and subsequent loss of surface area, reduction to volatile metallic forms, and heat related volumetric changes can all be avoided or minimized which otherwise would have led to chemical deactivation and mechanical degradation of the adsorbent. However, at these lower temperatures the reactivity of the sorbent gets diminished. Therefore, a sorbent structure with high specific surface area and sensitivity, like that of

nanofibrous metal oxides, can prove to be a good alternative to the conventional bulk sorbents, especially at mid-high temperature operating conditions.

In addition to causing higher specific area to the nanostructured adsorbents, the smaller grain size, on the of the order of few nanometers, imply that their size (5 – 10 nm) is comparable to the Debye length (Huang & Wan, 2009), which is responsible for the higher sensitivity of nanostructured materials to the polar gases like H2S than their bulk counterparts. Moreover, the surfaces of such nanostructured polycrystalline metal oxides are known to carry high density of grain boundaries (Ra et al., 2010). The increased density of grain boundaries not only increase the number of active adsorption sites but it is being hypothesized here that they may also act as a nano-scale expansion joints which can compensate for any thermal or reaction induced volumetric changes. Molar volume of ZnS being 1.64 times larger than that of ZnO, volumetric changes have been identified by Harrison (1998) and Poston (1996) as one of the main causes of sorbent degradation.

Furthermore, nanostructuring leads to smaller diffusion lengths, thus minimizing the diffusion resistances involved. This improved mass transfer is especially desirable when reactions involved have reasonably fast inherent kinetics but are mainly limited by the poor mass transfer (the case of sulfidation reaction between H2S and ZnO, as shown by Focht et al., 1989). Fig 2.1 shows a micrograph of the cross-section of a 4 mm ZnO pellet after sulfidation (Engelhard® Zn-9201E). Clearly, sulfidation (ZnS formation) was limited only to a region that was close to the outermost surface and much of the remaining pellet remains un-utilized.

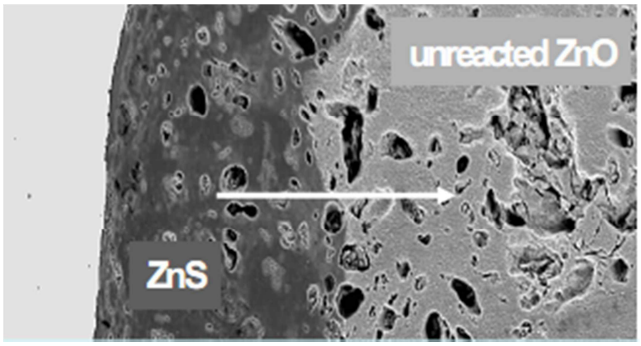

Figure-2.1: Adsorption of H2S on a commercial ZnO pellet (4mm diameter, Engelhard® Inc. Zn-9201E). Reaction limited to outermost region.

All the above-mentioned advantages of the nanostructured sorbent promises improved utilization of the sorbent material along with the prospects of longer adsorbent life even with operations involving repeated regeneration.

However, the above stated benefits can be practically realized only if a nano-fabrication technique can lead to quantities that are adequate for large-scale production. The common techniques currently popular for the nanostructuring or nanofabrication of a material like metal oxides include processes like hydrothermal growth (Du et al., 2006), electrochemical deposition (Li et al., 2007), vapor-phase transport (Huang et al., 2001), pulsed laser deposition (Sun et al., 2004), thermal oxidation (Guo et al., 2008) and microwave thermal evaporation (Cheng et al., 2007). Currently, none of these techniques can claim to have production rates compatible with a commercial-scale application. Recently, however, the process of electrospinning, a top-down nanofabrication process mainly known for polymeric nanofibers, has been successfully employed for the synthesis of ceramic fiber-mats with the size of the individual fibers reported to be in the range between 40 nm to 700 nm (Park et al., 2010; Sigmund et al., 2006, Ramaseshan et al., 2007). The process of preparing non-woven fiber mats by continuous fiber-spinning using electrospinning has been shown to be easily scalable to operations requiring large production (Ramakrishna, 2005).

The non-woven fiber-mat-based architecture of the electrospun sorbents has a potential to offer an alternative design to the conventionally used sorbent structure, which is typically in the form of pellets-base active oxides inside packed beds. In order to increase the available surface area of conventional pellet-based sorbents, each pellet has to be made porous. But increasing surface area means decreasing pore sizes. The size of the pores varies inversely with the specific surface area of the sorbent. Thus, it is possible to synthesize very high surface area pellets but the resultant sorbent may not be very effective due to the excessive mass transfer resistance generated by the extremely small pores, which limits gas penetration and as a result much of the surface area remains underutilized. This problem of poor gas penetration on increasing surface area gets decoupled when a fiber-mat based structure with porous fibers is used. The pores in such structures can be categorized as having

two types: the ones that are present within the fibers (1-5 nm), and the other types of pores (> 100nm) which are present as the voids between the fibers (Fig-2.2). Because of this bimodal (or multimodal) distribution of the pore sizes, large specific surface areas can be achieved without affecting the gas penetration. This feature makes electrospun fiber mats potentially a good alternative to the current sorbent designs.

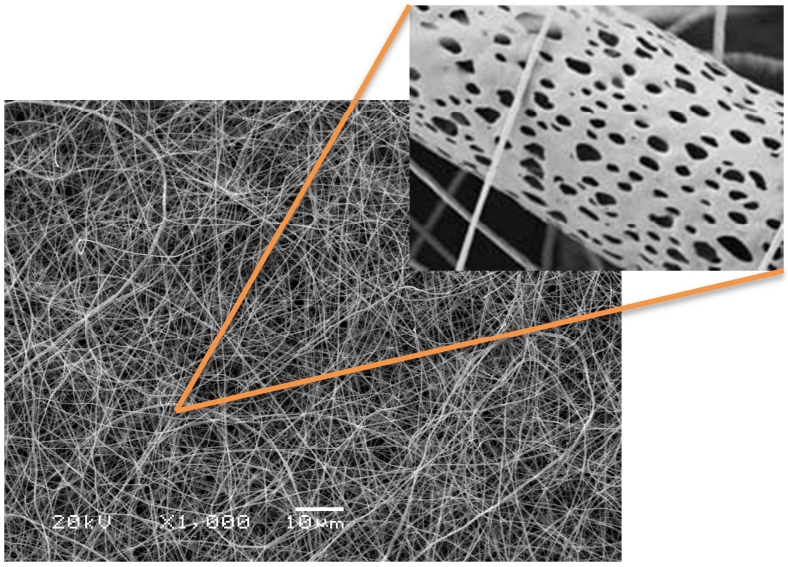

Figure-2.2: Illustration emphasizing the types of pores present in the electrospun fibers mats

2.2. Ceramic nanofibers via sol-gel based electrospinning

As discussed in the previous sections (Section 1.4, 2.1), the process of electrospinning is a straightforward technique used primarily for the fabrication of one-dimensional nanostructures such as nanofibers and if needed, can easily be scaled to on an industrial-level production (Dai et al. 2010). The process has shown good control over the fiber-diameters, compositions, and morphologies. It is versatile in terms of starting materials too. Polymeric fibers via electrospinning have been well-explored. Recently, the fabrication of ceramic nanofibers through a combination of electrospinning and sol–gel method, first described by Li & Xia (2003), is fast becoming a popular technique for synthesizing metal oxide nanostructures. Many important oxide materials (like ZnO, TiO_2, CeO_2, Mn_3O_4, Fe_2O_3 & SnO_2) have been

successfully spun into nanofibers via electrospinning. A number of morphologies and structures, other than conventional solid fibers, have also been reported, including core–shell (Wang et al., 2010), hollow (Zhang et al., 2009), hierarchically structured, and segmented.

Preparation of the precursor solution using sol–gel process

The sol–gel process can be described essentially as a network-forming process which broadly consists of two steps: solution preparation and subsequent gel formation on ageing. The starting materials for the process are typically metal salts or metal alkoxides, which are reacted in an organic / aqueous solvent whereupon water molecules perform hydrolysis of metal alkoxides/salts. Further condensation of the forming compounds leads to formation of a gel. The overall acidic hydrolysis and subsequent condensation can be represented by the following set of reactions:

$$M(OR)_4 + 4H_2O \rightarrow M(OH)_4 + 4ROH \quad (2.1)$$

$$mM(OH)_4 \rightarrow (MO_2)_m + 2mH_2O \quad (2.2)$$

So to obtain fibers of a desired metal oxide, one needs to start with a salt or alkoxide of the metal involved along with an appropriate solvent (to make a composite, salts of two or more metal will need to be used). Due to the small reactant diffusion lengths, much better homogeneity can be obtained using this method as compared to methods like oxide-slurry mixing or powder mixing.

In order to make this process compatible with the electrospinning technique, a polymer is typically added during the solution preparation step (before the gel-formation occurs). Although direct-spinning without a polymer has also been reported in literature, but it has been observed that adding a polymer significantly facilitates the spinning process due to polymer's favorable rheological properties which provide much better control over the process. Poly(vinyl pyrolidone) (PVP) is one of the most commonly used polymer due to its high solubility in ethanol or water and its good compatibility with many metal alkoxides and salts, including titanium isopropoxide and zinc acetate dihydrate. Other polymers, such as poly(vinyl alcohol)

(PVA), poly(vinyl acetate) (PVAc), polyacrylonitrile (PAN), poly(methyl methacrylate) (PMMA), have also been popular.

Inclusion of some additives, such as salts and catalysts, is sometimes carried out to stabilize the precursor and assist the jetting process. Although only a small amount is required, these additives play an important role in stabilizing the solution as well as the jet. Catalysts, such as acetic acid can be used to adjust both the hydrolysis and gelation rates (Ramaseshan et al., 2007), preventing the solution from blocking the spinneret, thus ensuring a continuous spinning. Addition of salt, such as sodium chloride, can increase the charge density on the liquid jet and thus reducing the tendency of bead formation during fiber-spinning (Ramakrishna, 2005).

Once a gel of desired viscosity is obtained by adjusting the polymer content, it is loaded in a syringe with a metal needle and the electrospinning is carried out (See section 1.4).

Heat treatment of the green-fibers

The as-spun fibers, or otherwise known as green fibers, are composite of inorganic material and a polymer template. After lifting the fiber-mat from the metal collector, it needs to be sintered at an elevated temperature to burn-off the polymer and obtain the desired crystalline phase of the oxide. Due to the polymer removal and sintering of the ceramic phase, the diameter of the nanofibers often decreases. The sintering temperature often depends on the nature of the oxidic phase that is to be generated. By controlling the sintering temperature, the ramp rate and the duration of heating, properties of the resultant oxide, like the composition, phase, and surface roughness, can be varied considerably. These parameters become even more important when composite metal oxides are being produced. For instance, in this study, in order to make the fibers more resistant to reduction than the fibers with ZnO alone, composite fibers of zinc and titanium oxides were prepared using sol-gel technique (Sec-2.3). Various crystalline phases of Zn-Ti-O system that can be obtained depend not only on the atomic ratio of Zn/Ti in the precursor solution but also on the temperature and the duration of sintering. It has been reported earlier (Dulin & Rase, 1960) that as the proportion of titanium in the precursor solution is increased, following phase transformations occur during sintering (at

temperatures below 1000C): ZnO $\rightarrow$ $ZnTi_2O_4$ $\rightarrow$ $ZnTiO_3$ $\rightarrow$ TiO_2. Few researchers have also reported formation of another Zinc titanate phase: $Zn_2Ti_3O_8$ alongside $ZnTiO_3$ (at titanium percentage > 50%). For instance, Yang & Swisher (1996) proposed a phase diagram for the ZnO-TiO2 system as shown in Fig-2.3. They prepared mixed oxides by solid-solid mixing of sub-micron sized powders of ZnO & TiO2, followed by heat-treatment of 3 – 48 hrs.

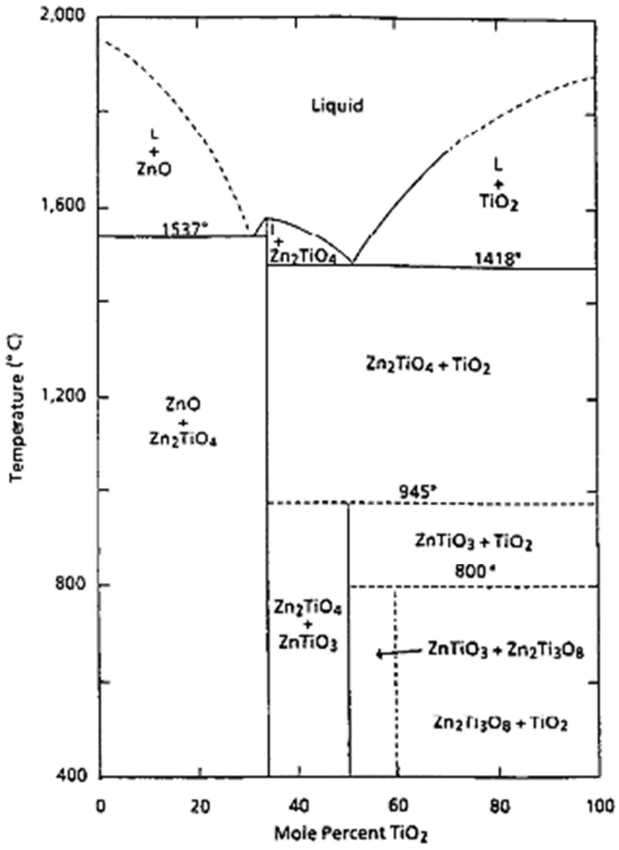

Figure-2.3: Phase equilibrium diagram for ZnO-TiO2 system as proposed by Yang & Swisher (1996).

Fig-2.3 also helps in understanding the effect of temperature on the stabilities of different phases. As can be seen, for titanium percentage greater than 60%, following transformations occur as the temperature is raised from 600°C to 800°C and then to 945 °C:

$$ZnTi_3O_8 \rightarrow ZnTiO_3 \rightarrow ZnTi_2O_4$$

In addition to the sintering temperature and the composition, duration of sintering can also impact the fiber morphology. Formo et al. (2009) reported that the surface roughness of electrospun nanofibers can be tailored by varying the duration of the sintering. Smooth surface was observed after calcination at 500°C for 3hr while a rough surface was obtained at 550°C for at least 6hr.

2.3. Experimental

2.3.1. Materials

Sol-gel based approach was used to prepare the precursor solution for electrospinning zinc titanate fibers. Zinc acetate dehydrate 97% $\{CH3COO\}_2Zn.2H_2O$ (Alfa Aesar, CAS #5970-45-6) and Titanium (IV) isopropoxide 97%, $C_{12}H_{28}O_4Ti$ (Sigma Aldrich, 97%, CAS#546-68-9) were used as the starting chemicals. Ethanol (ACS grade, 99%) was used as the solvent. Glacial acetic acid was also added to prevent titanium isopropoxide from precipitating. It also helps in catalyzing the hydrolysis step (Sec-2.2, Eq.-2.1) during the early stages of sol-gel process. To obtain specific Zinc-to-Titanium ratio in the final sorbent, the relative amounts of the zinc salt and the titanium isopropoxide need to be varied accordingly at this stage. A solution of titanium isopropoxide in acetic acid (1.0 : 2.25) was added to the solution of zinc acetate and ethanol. All the chemicals were mixed at 55 °C using a magnetic stirrer until a clear solution was obtained. This ceramic precursor solution was then mixed with a polymeric solution prepared using PVP (M_w ~ 1300000, Sigma-Aldrich, CAS#9003-39-8) dissolved in ethanol. As discussed in the previous section, PVP serves as a fiber-template and imparts the necessary rheological properties to the solution. Table – 2.1 gives the quantities of different chemicals used for preparing two such solutions.

Table-2.1: Chemicals used for the Sol-gel based Zinc Titanate fibers (for Sample-1)

Component	Amount in Sample-1	Amount in Sample-2a
$Zn(CH3COO)_2.2H_2O$	5.6 g	10.2g
$Ti(O\text{-}iPr)_4$	4.0 ml	10.0ml

Table-2.1 (cont.)

Acetic acid	9.0 ml	3.5 ml
PVP	2.4 g	4.6g
Ethanol (99%)	22.0 ml	40 ml

2.3.2. Electrospinning of zinc titanate fibers

Fig-2.4 shows pictures of the electrospinning setup. The ceramic precursor and polymer solution were mixed for 6hrs at 55^{o}C. The solution thus obtained was drawn into a 10 ml syringe. Syringe was equipped with a 20 gauge blunt metal needle. Two types of geometries of aluminum collector were used: mesh and plate type (Fig-2.5). It was found that mesh based geometry led to easier fiber lift-off from the collector's surface. A voltage of 19kV was applied to the needle while the collector was grounded. The distance between the needle tip and the collector was fixed at 17 cm. The feed rate was fixed at 1.2 ml/hr using a syringe pump.

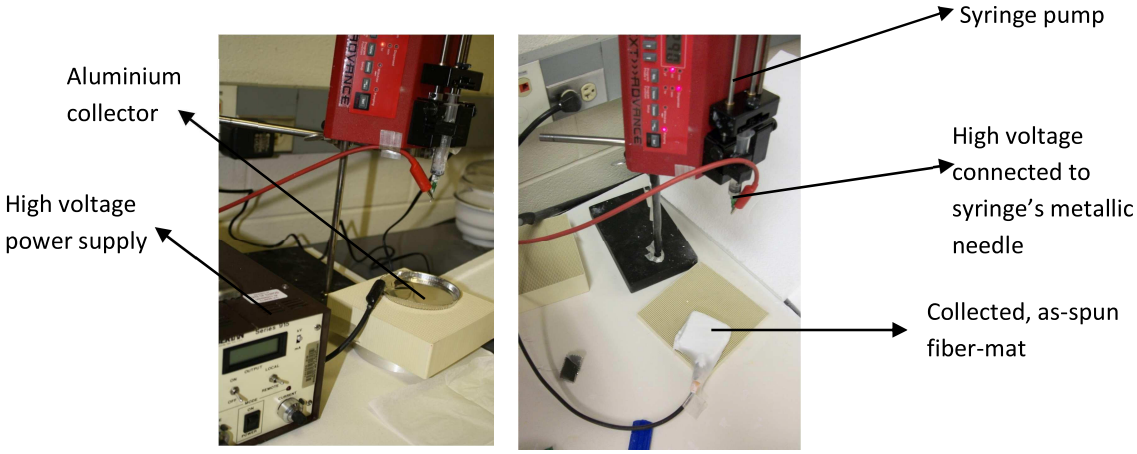

Figure-2.4: Pictures of the electrospinning setup label)

The composite inorganic-organic fiber mats (referred to as green or as-spun fibers) thus obtained were vacuum dried for 3hrs at 110^{o}C. Afterwards, they were moved to a furnace and subsequently heated to 340^{o}C at a rate of 4^{o}C/min. Fiber mats were kept at that temperature for 2hrs to remove the polymer and/or any other organic components. Thereafter, the temperature was raised at 2^{o}C/min to 600^{o}C. The fibers were sintered at 600^{o}C for 4hrs in air.

Fig-2.6 presents the complete process in the form a simplified flow chart. Depending upon the ratio of Zn to Ti in the precursor solution, fiber mats with different composition were obtained.

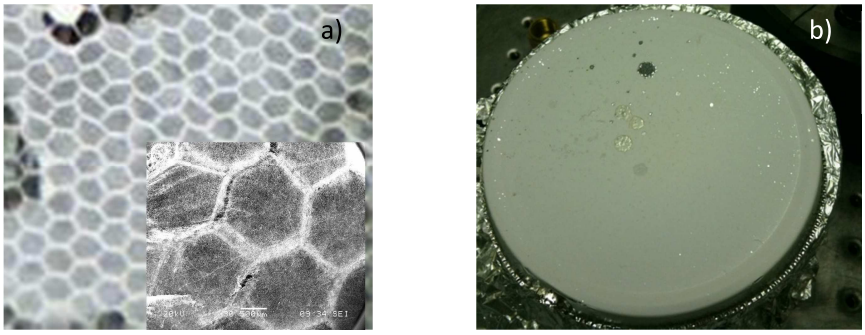

Figure-2.5: Different collector geometries were used: a) aluminium mesh, b) aluminium plate

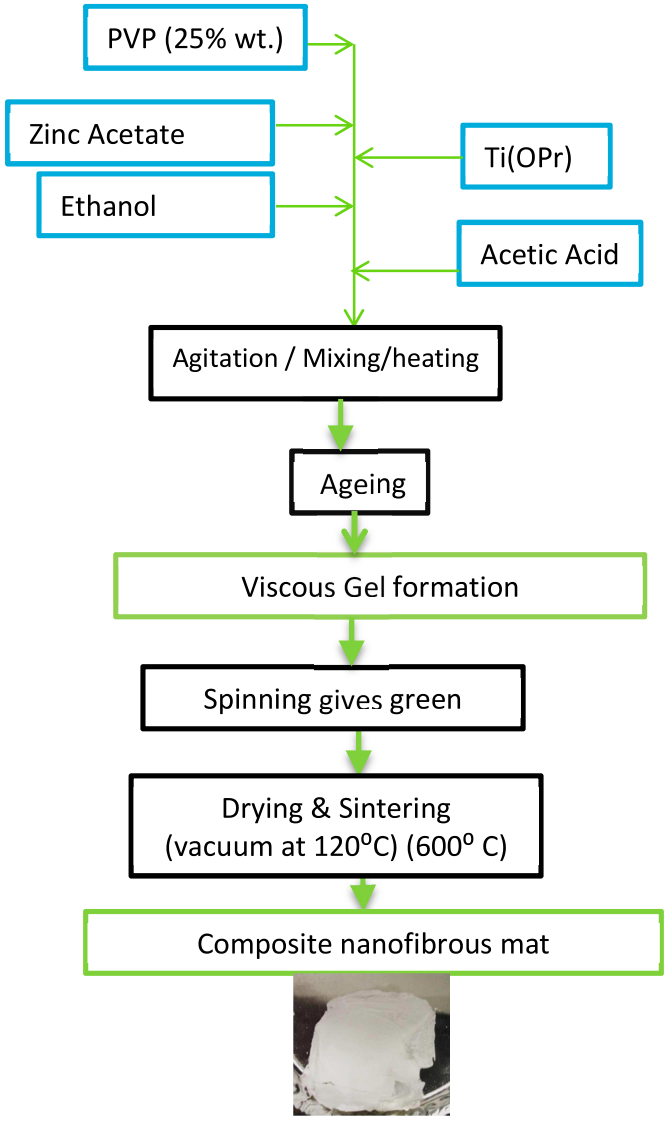

Figure-2.6: Flow chart depicting the step-by-step procedure undertaken during the synthesis of zinc titanate fiber-mats

The as-spun and sintered fiber mat (heat treated at 600 ^{o}C) are shown in Fig-2.7

Figure-2.7: Electrospun Zinc Titanate fibers (Sample-2): **a)** As-spun fiber-mat, **b)** Fiber-mat after sintering at 600°C

2.4. Results from material characterization of the fresh sorbent

2.4.1. X-Ray diffraction analysis

In order to identify the different crystalline phases present in the sintered fibers, technique of X-Ray Diffraction was used. An XRD instrument (X'pert MPD Pro, Philips®) with Cu Kα radiation (λ = 1.54 Å) was used for this analysis. The XRD spectrum generated by one such fiber mat (Sample-1) is shown in Fig-2.8. All the major peaks were identified and assigned to the corresponding crystal phases in accordance with JCPDS database.

The major phases identified in one of the sample were: $ZnTiO_3$ (Ecandrewsite), ZnO (Zincite), TiO_2 (Rutile, Anatase) and minimal amount of Zn_2TiO_4. Inset in Fig-2.8 also shows the relative amount of different crystalline phases identified in the Sample-1 (one of the calcined fibers mats). The relative amount of the different crystalline phases present in a given fiber mat sample (weight basis) were obtained by quantitative analysis of profile-fitted peaks (using a software called MDI-Jade®).

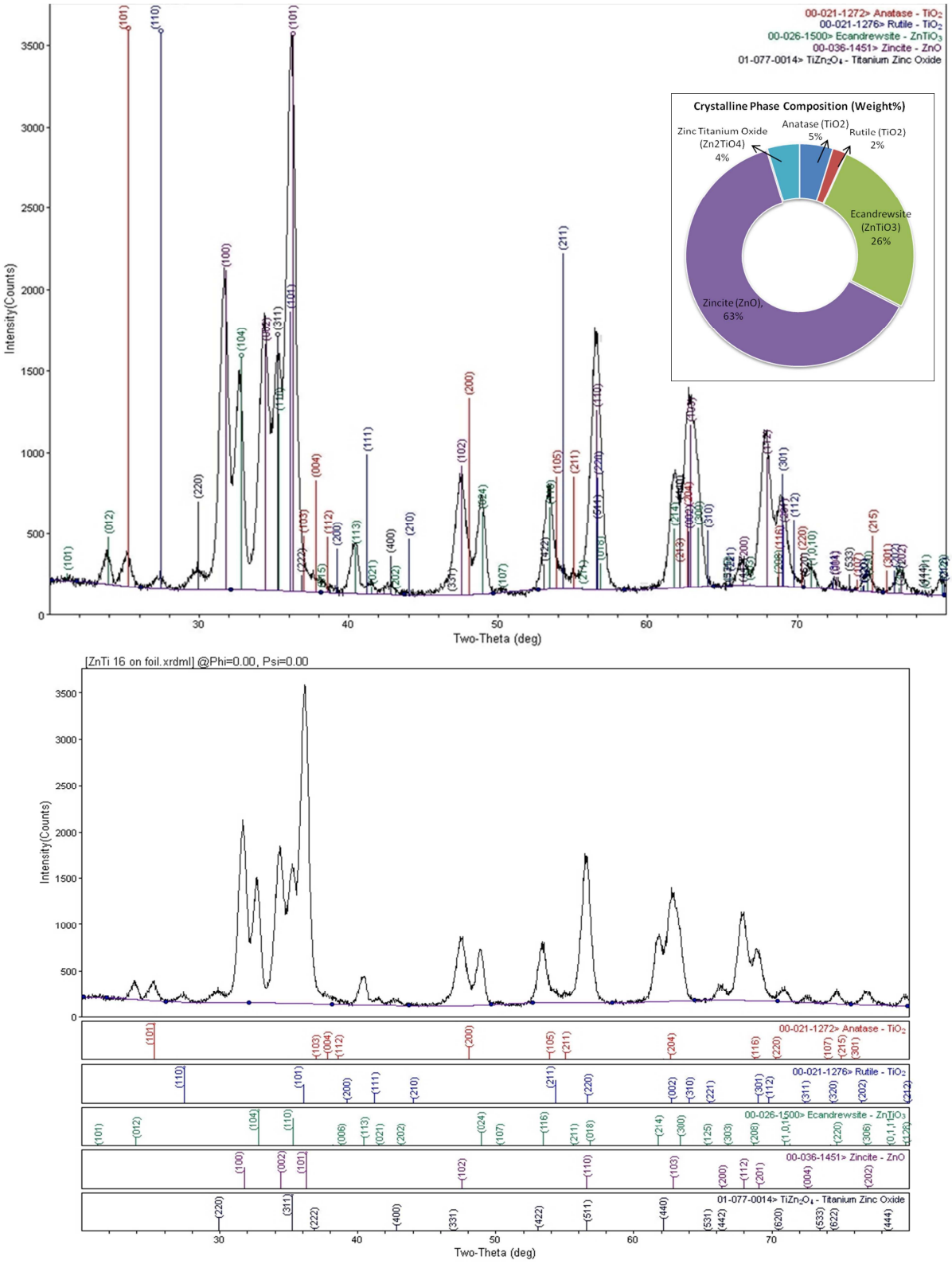

Figure-2.8: X-ray diffraction pattern of ZnO-TiO_2 nanofibers for **Sample-1**. Inset (top) also shows the composition of the different crystalline phases in Sample-1 estimated by analyzing the profile-fitted peaks

The d-spacing for some of the atomic planes and the corresponding grain size for the different crystal structures are given in Table-2.2.

Table-2.2: The d-spacing and grain size for some of the atomic planes of different phases (Sample-1)

Chemical compound/phase (plane)	d-spacing (nm)	grain size (nm)
$ZnTiO_3$ (012)	0.372	15.0
TiO2 anatase (101)	0.353	13.0
TiO2 rutile (110)	0.326	10.9
Zn_2TiO_4 (220)	0.299	9.0
ZnO (100)	0.282	13.1
$ZnTiO_3$ (104)	0.273	15.1
ZnO (112)	0.138	11.6

Fiber mats with different compositions (Zn-to-Ti ratio) were synthesized. In order to illustrate the effect of composition on the occurrence of crystalline phases, characterization results from a second sample (Sample-2a) are also discussed here. Fig-2.9 compares the crystalline phase compositions (weight percentage) for the two different mats**:** Sample-1 & Sample-2a. Figure-2.10 & 2.11 compares the changes in the peak intensities of the two samples which has been caused by the differences in the crystalline composition of the samples. These two fiber-mats were selected as the model samples for studying the effect of crystalline composition on the sorbent's performance (Ch-3 & Ch-4). Table-2.3 compares the Zn-to-Ti ratio (atomic percentage) and other important characteristics of these two samples (fresh, unsulfided).

Table-2.3: Comparison of the texture-related properties of two different samples (fresh)

Sorbent (Fresh)	Zn-to-Ti atomic ratio	Surface Area, α_0 (m^2/g)	Mean Fiber diameter (nm)	Avg. grain size (nm)
Sample-1	**3.69**	151.7	435	12.53
Sample-2a	**1.17**	90.1	714	15.82

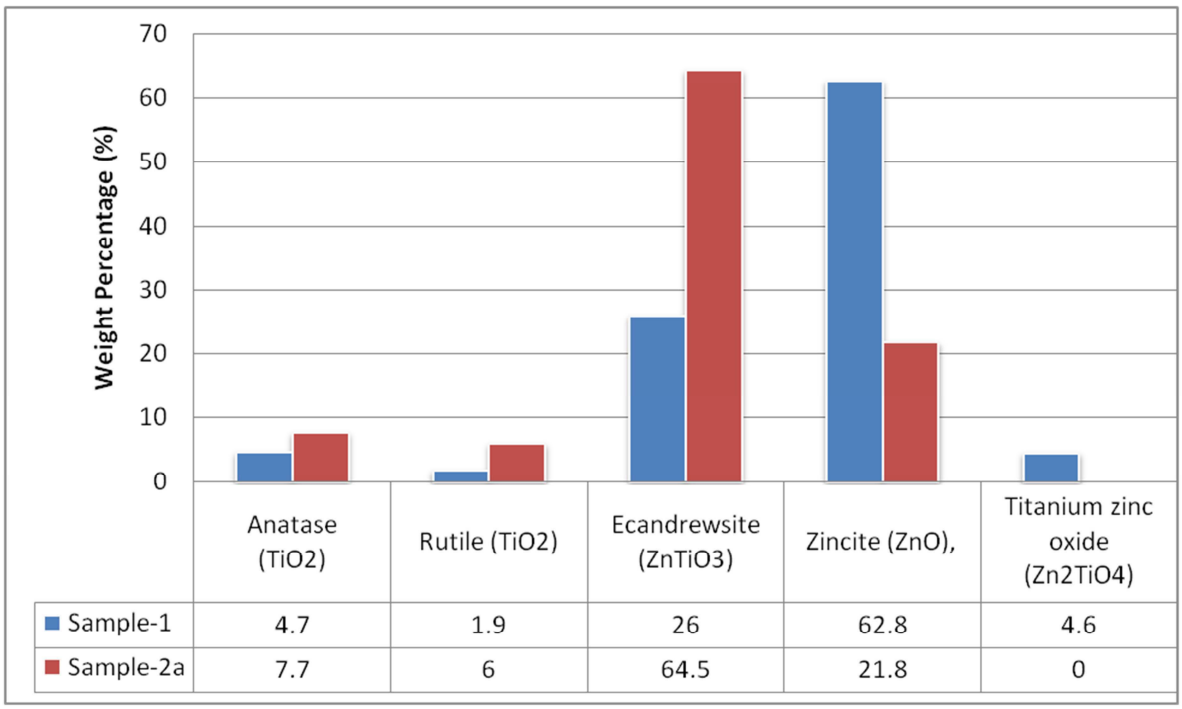

Figure-2.9: Comparison of the composition of two different fresh samples (weight%)

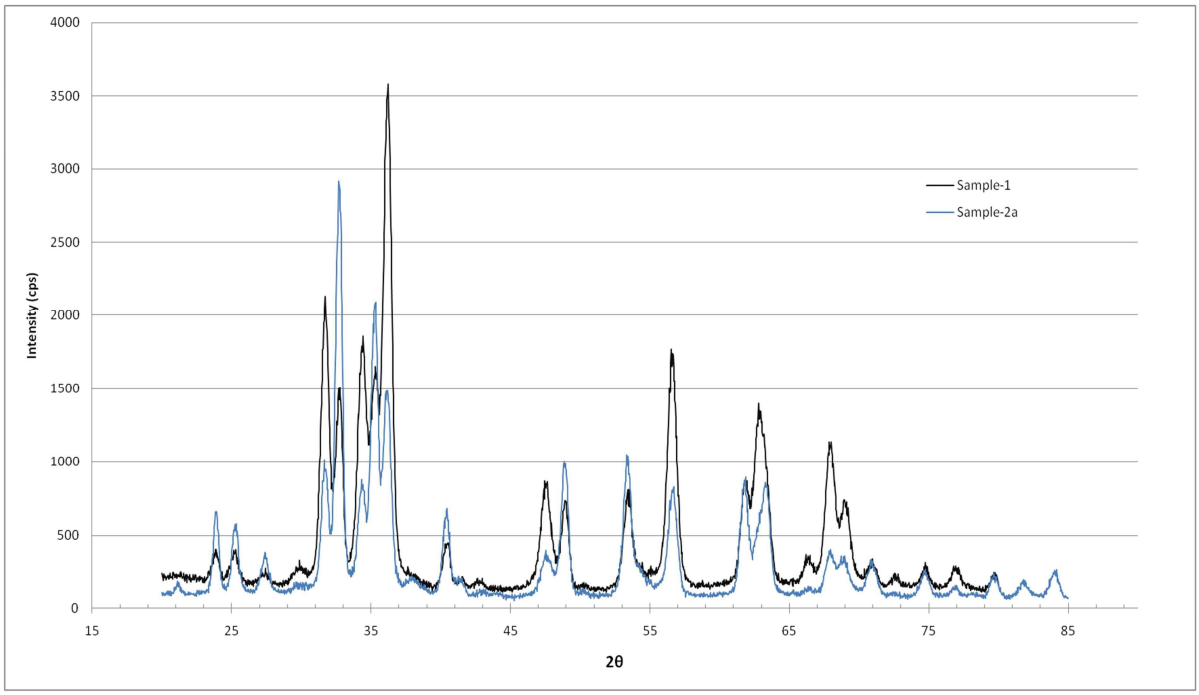

Figure-2.10: X-ray diffraction pattern of ZnO- TiO_2 nanofibers for Sample-1 (black curve) and Sample-2a (blue curve)

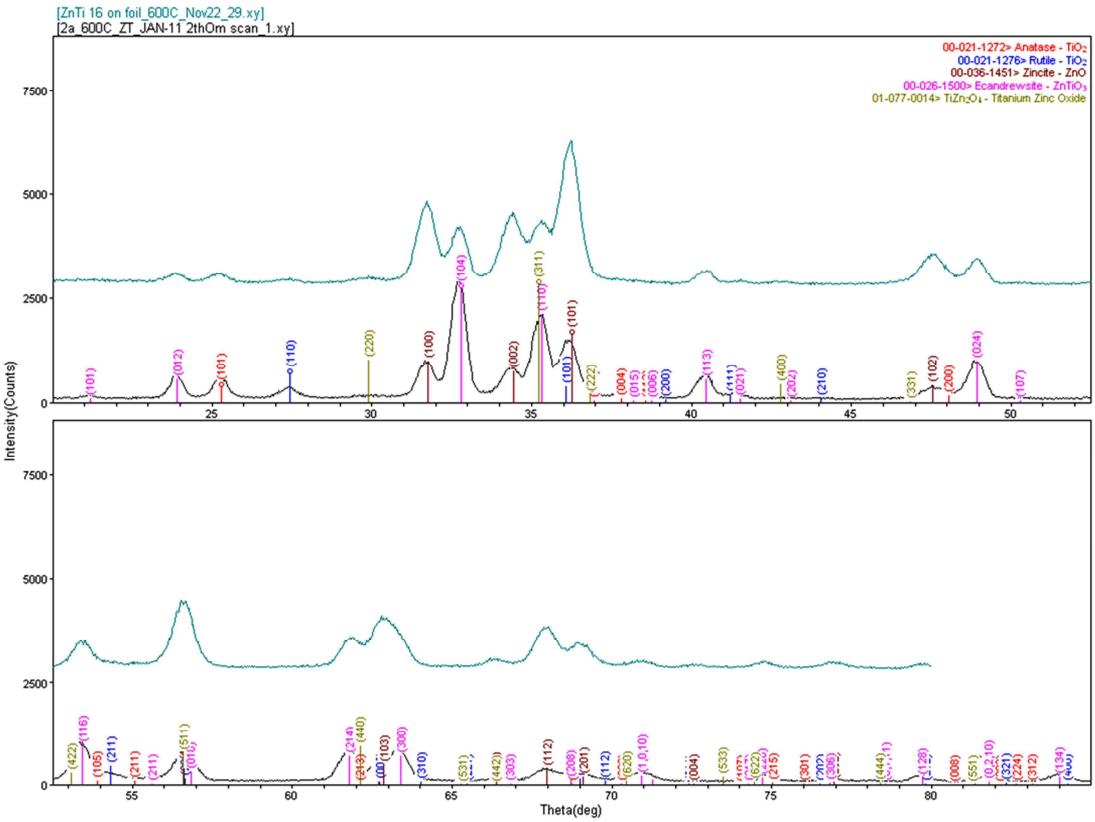

Figure-2.11: X-ray diffraction pattern for Sample-1 (teal) and Sample-2a (black) with peaks identified

Effect of sintering temperature on composition of crystalline phases.

The effect of sintering temperature was examined by performing XRD analysis on two samples, both prepared from the same precursor solution, but heat-treated at two different temperatures: one at 600 ^{o}C and the other at 700^{o}C. Fig-2.12-a shows the XRD spectra obtained for these two samples. One observation that can easily be made from the comparison is the absence of peaks corresponding ZnO phase in the sample that was sintered at 700^{o}C. As can be seen from the compositional analysis of Fig-2.12-b (carried out by analyzing profile-fitted peaks in the MDI-Jade® software), all zinc occurs in the mixed metal oxide form with zinc titanate (Ecandrewsite, ZnTiO3) as the dominant phase. In addition, there is free titania (mainly in rutile phase). These phase compositions differ considerably from the prediction of the bulk phase diagram (Sec-2.2), which suggests presence of ZnO along with other Zinc titanate phases for the given composition (Zn-to-Ti ratio ≈ 3.69 or Ti molar percentage ≈ 21.5%). SEM pictures helped in resolving the discrepancy: Figure 2.12-c depicts the SEM of the 700^{o}C sample.

Appearance of isolated clusters besides the expected fibrous morphology points to the possible segregation of a certain phase. Energy-Dispersive X-Ray analysis (EDX) analysis suggests presence of zinc-rich phase. So, one possible explanation is that the there must have been free Zn present, possibly due to lack of sufficient oxygen in the furnace. Since zinc metal tends to volatilize at temperatures above 600^{o}C, it steadily got lost during 4 hr sintering operation. Most of it managed to escape but some of it was able to condense back and react with Titanium to form aggregates as seen in the images from SEM (Fig- 2.12-c). This may have happened during the later stages of sintering operation when temperature was being reduced.

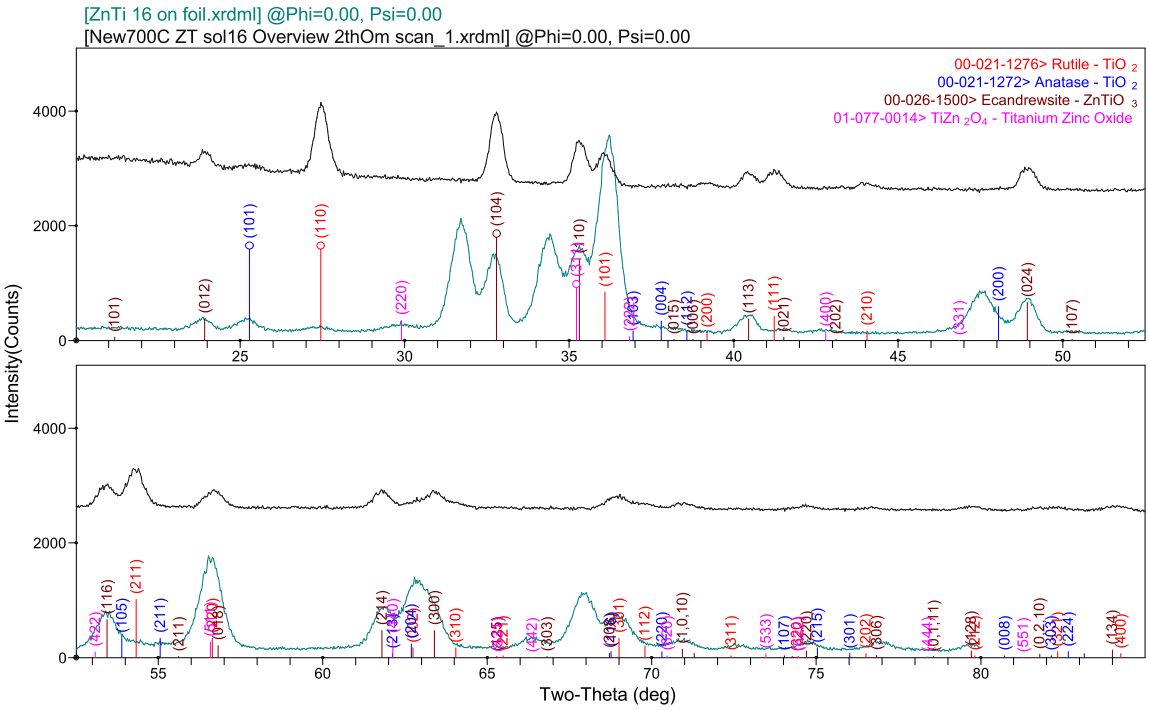

Figure-2.12(a): X-ray diffraction pattern for two samples sintered at different temperature (same starting composition): **Black** (top) – 700C, **Teal** (bottom) – 600^{o}C

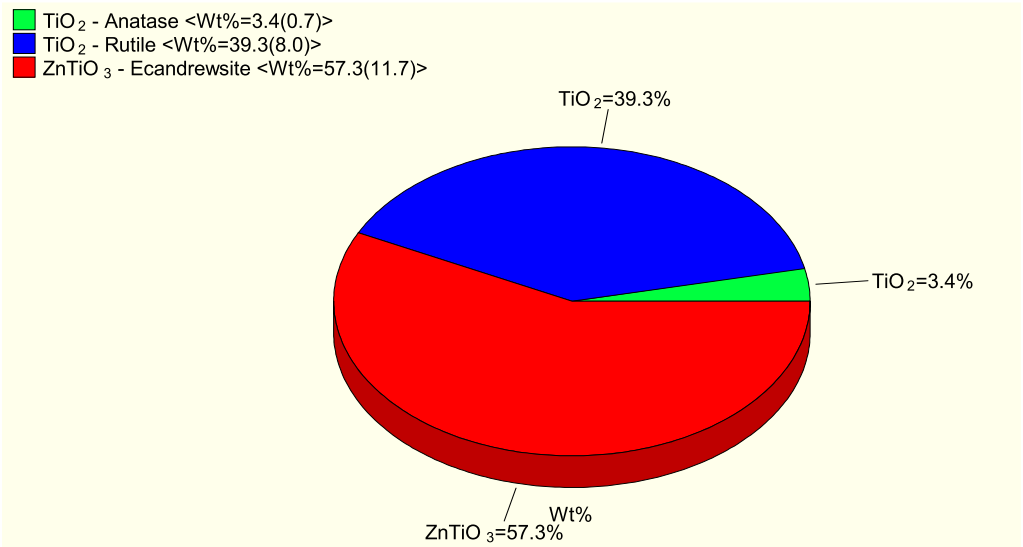

Figure-2.12(b): Quantitative analysis from profile-fitted peaks in the XRD spectra of sample sintered at 700^{o}C

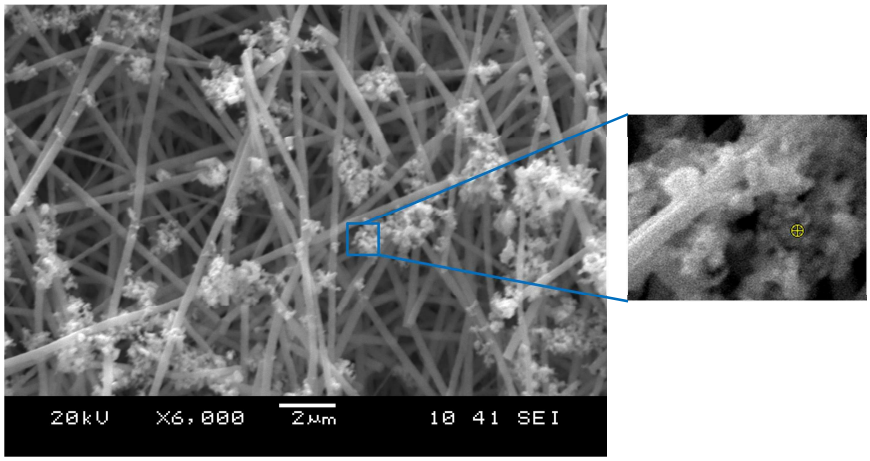

Element	Atomic%
O	58.72
Ti	17.47
Zn	23.81

Figure-2.12(c): SEM-EDX analysis of the sample sintered at 700^{o}C

2.4.2. Fresh sorbent characterization using scanning electron microscopy (SEM)

Surface morphology of the fiber-mats was studied using the technique of Scanning Electron Microscopy (SEM). A JEOL 6060LV® instrument was used for this purpose. Fig- 2.13 shows the SEM image of the calcined fibers obtained from Sample-1 & 2a (each sintered at 600^{o}C, but differ in compositions in crystalline phase, see Fig-2.9). Also shown in the figure is the fiber size distribution corresponding to the selected samples. An image analysis software (Image-J®) was used to estimate the size distribution.

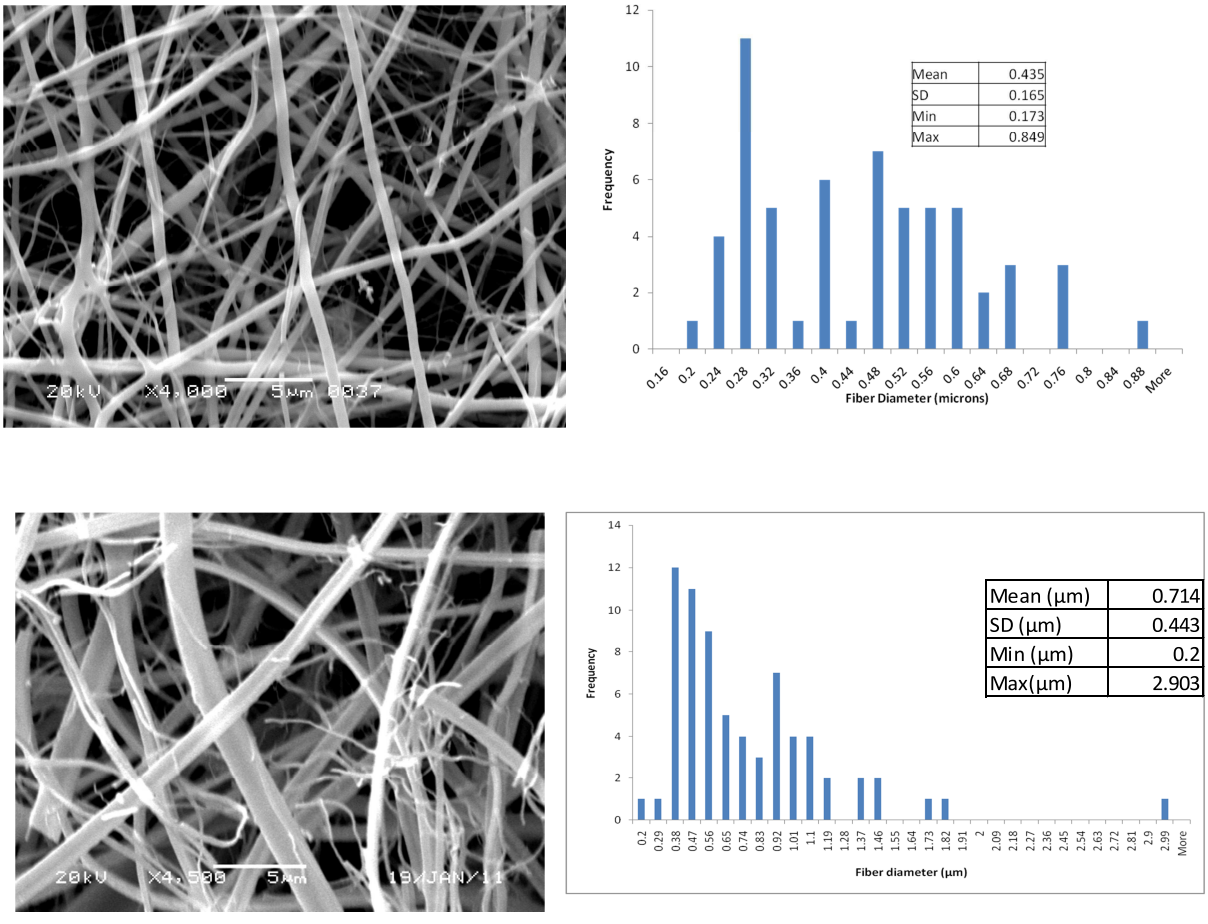

Figure-2.13: SEM of Zinc Titanate fiber mats: Sample-1(top), Sample-2a (bottom)

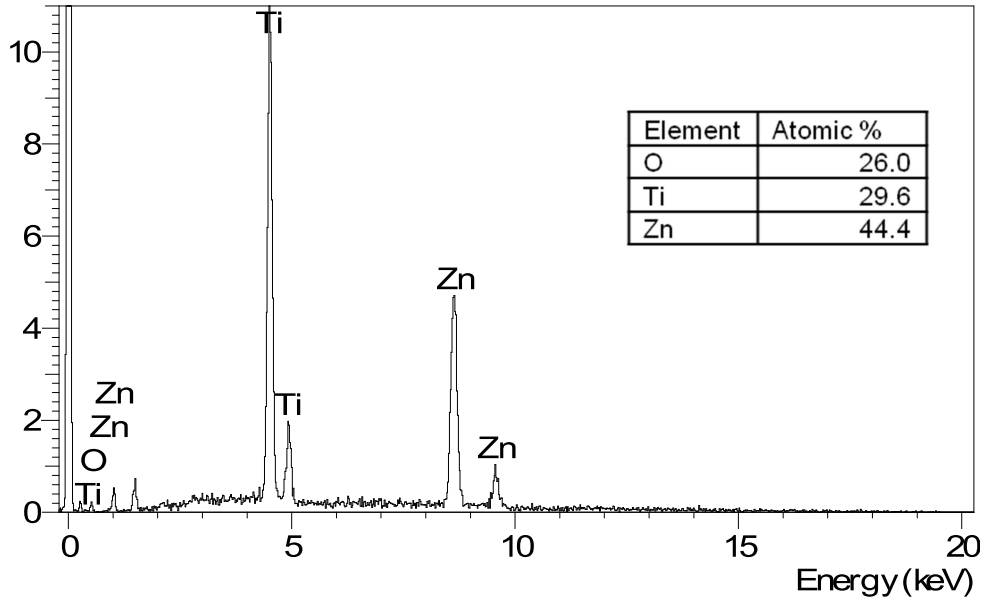

Figure-2.14: EDX spectra of Zinc Titanate fiber mat (Sample-2a)

Energy-Dispersive X-Ray analysis (EDX) was also conducted for quantitative estimation of the elemental composition of the portion of the sample being imaged. The setup for EDX was integrated with the SEM instrument. Fig- 2.14 shows the spectra obtained for Sample-2a along with the atomic composition for a selected region of the image.

It was found that the addition of an inorganic binder (like lithium polysilicate) helped in obtaining more uniform fiber size (Figure-2.15).

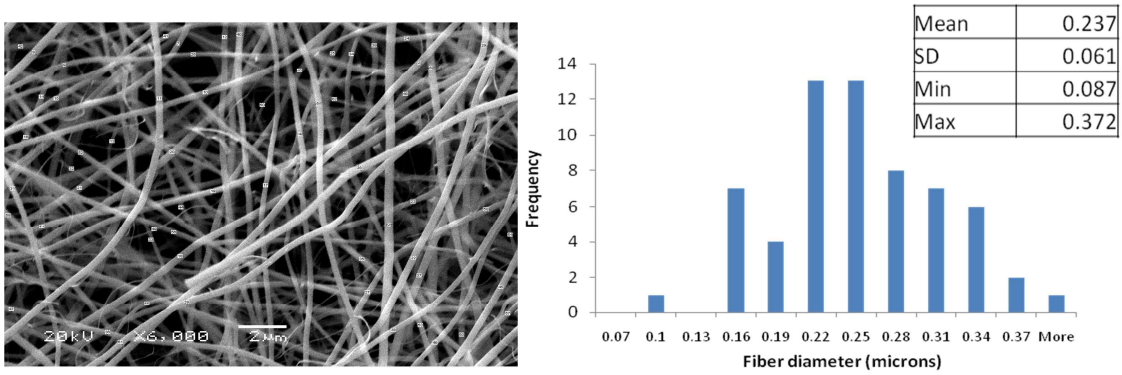

Figure-2.15: Zinc Titanate fiber mat with lithium polysilicate

2.4.3. Surface area measurements

BET specific surface area (α_0) of the sintered fibers was measured using a surface area analyzer (Quantachrome, Nova 2200 Series). It was found to be 151.7 m^2/g for Sample-1 and 90.1 m^2/g for Sample-2a.

2.4.4. Sample characterization using transmission electron microscopy (TEM)

Uniformity of distribution of the different crystalline phases present within an individual fiber was investigated using TEM. Unlike an image produced by a SEM, in which the contrast is mainly due to the surface topology of the specimen, the contrast appearing in an image generated by a TEM is due to the differences in the local densities which occur due to the presence of different crystalline phases. Different phases, with varying atomic densities and electrostatic potentials, affect the transmission of the electrons to various extents; this difference then lends contrast to the image. Figure-2.16 shows the TEM image of a fiber from a fresh sorbent (Sample-1).

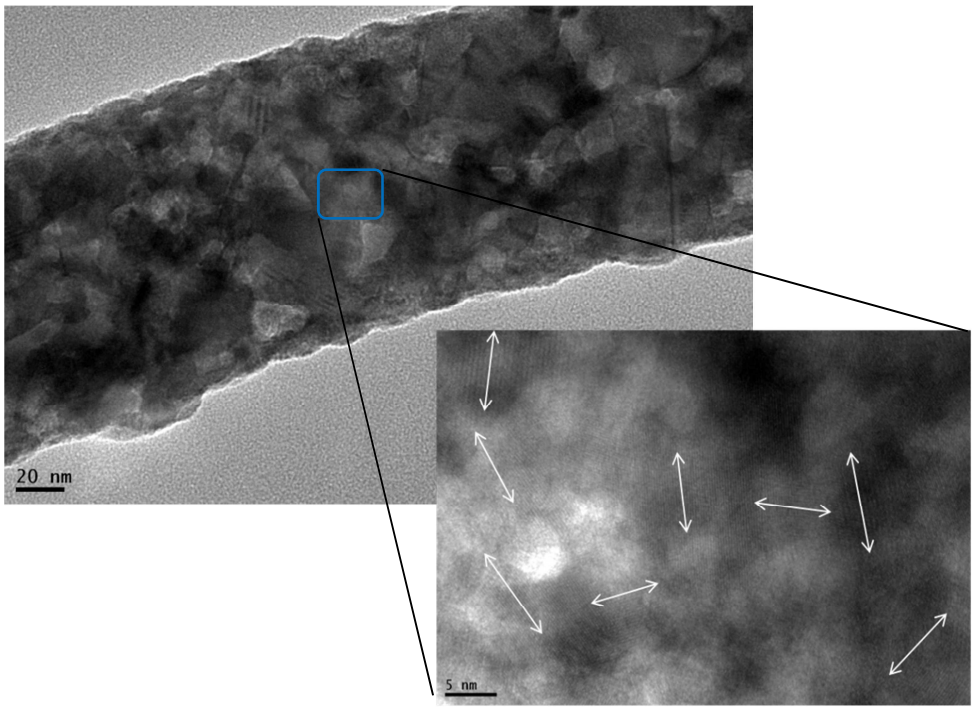

Figure-2.16: TEM image of a Zinc-titanate fiber from Sample-1 (Arrows in the inset indicate orientations of the atomic planes in different crystallites)

It can be clearly seen that the fiber consists of many different crystallites of varying sizes and orientations. Such polycrystalline nature was confirmed by XRD (as discussed earlier in Sec.-2.4.1). In addition, the individual crystallite size was found to lie within the range of 8 – 15 nm.

Figure-2.17 shows selected area electron diffraction (SAED) pattern obtained using TEM's dark field mode. Every bright spot in the image corresponds to the diffraction caused by a particular family of planes with a unique orientation (some bright spots may be present due to the higher order diffractions caused by the same actual plane-families). The diffraction pattern further confirms polycrystalline nature of the fibers.

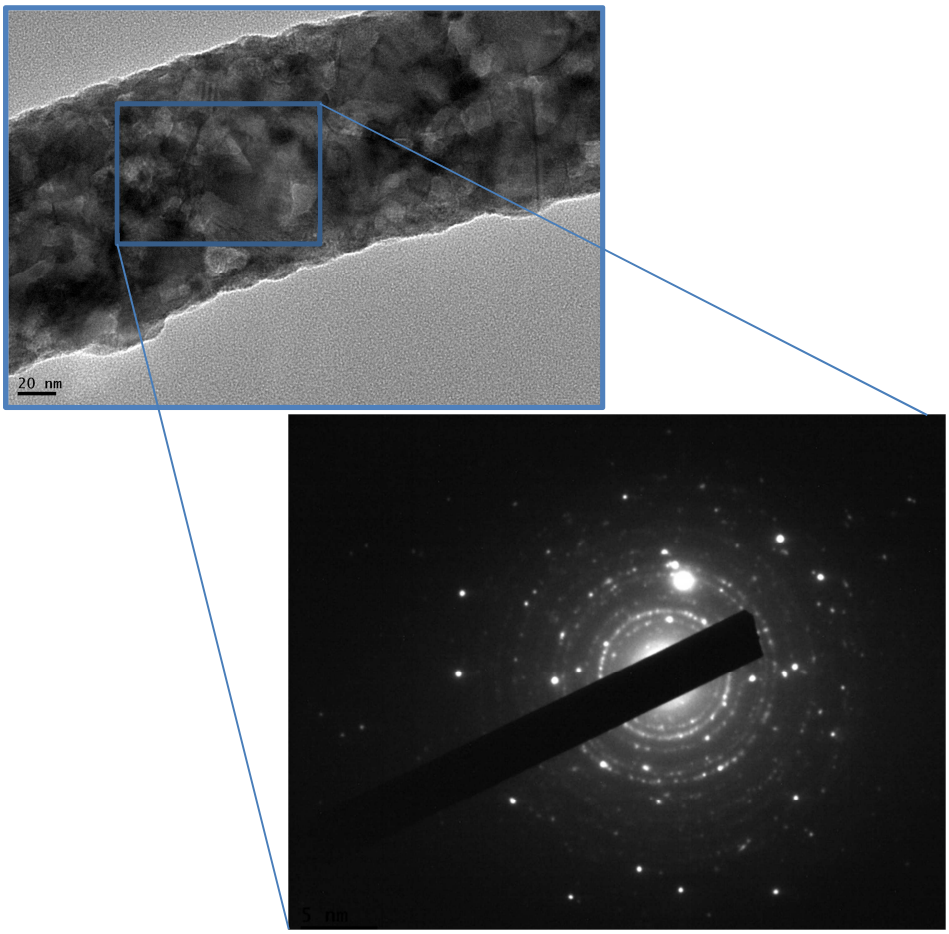

Figure-2.17: Selected area electron diffraction (SAED) pattern obtained using TEM confirms the polycrystalline nature

2.5. Conclusions

- The electrospun fibers, obtained after the heat-treatment (post-sintering), are multi-phase and polycrystalline in nature.
- The fiber diameter ranges from 165 nm to 830 nm. Use of inorganic binders can help in reducing the spread in the fiber diameter.
- At least two different phases of Zinc titanate, namely perovskite zinc meta-titanate ($ZnTiO_3$) and spinel zinc orthotitanate (Zn_2TiO_4), can be present in the calcined electrospun fibers which have been prepared using the sol-gel based process with zinc acetate and titanium isopropoxide as the ceramic precursors.
- Any zinc or titanium, present in excess of stoichiometric quantity, ends up as zinc oxide or titanium oxide respectively. But if sintering is being carried out at higher temperatures (greater than 600^oC), any free zinc tends to get lost rapidly (before solid-solid or gas-solid reaction can occur) due to its highly volatile nature and pure zinc oxide may not be present in the product mixture. As a result, mixed metal oxide phase ($ZnTiO_3$) may again become the major crystalline component (for starting Zn/Ti > 3).
- The crystallites formed within a fiber are within 8 – 15 nm in size.

Chapter-3

Reduction kinetics of nano-composite Zn-Ti-O fiber-mats

3.1. Introduction

For any applications involving desulfurization via metal oxides, reduction reaction occurs simultaneously along with the sulfidation reaction due to the presence of gases like H_2 and CO in the inlet gas mixture. Most of the metal oxides tend to get reduced to their lower oxides form (Fe_2O_3 to FeO) or to their metal form (ZnO to Zn), which if volatile can contribute to a steady loss of sorbent weight. Early work on hot gas desulfurization (Harrison & Atimtay, 1998; Lew et al., 1989), have confirmed that the lower oxide forms, for majority of the oxides, have inferior sulfidation thermodynamics and sluggish kinetics (only exception reported was by Wang & Stephanopoulos (2005) who found that Ce_2O_3 is thermodynamically more suitable than its higher oxidation-state form - CeO_2). This kind of sorbent deactivation is one of the primary reasons why pure metal oxides have such a short lifetime and their regeneration is commercially unattractive or is limited to few cycles only. Zinc oxide, popular for its favorable sulfidation thermodynamics but most prone to reduction and subsequent volatilization, was immediately a candidate for this research. At high temperatures (> 500^{o}C) and in presence of reducing gases like hydrogen, zinc oxide gets converted to zinc metal by undergoing the following reduction reaction:

$$ZnO_{(s)} + H_{2_{(g)}} \Leftrightarrow Zn_{(g)} + H_2O_{(g)}$$

Zinc metal, liquid above 419^{o}C, is highly volatile at the high temperatures of a typical hot gas cleaning operation. Employing zinc or other transition metal oxides as reusable adsorbents

requires their use in a manner that offers maximum possible resistance to the reduction reaction without affecting oxide's sulfur removal efficiency.

Many attempts have been made in this direction. Early in the research area of high temperature coal-gas cleaning (Flytzani-Stephanopoulas, 1986; Lew et al., 1989), it was realized that the addition of foreign atoms / molecules in metal oxides made them more resilient to reduction. In particular, Lew (1991) found that the addition of titania (TiO_2) to zinc oxide led to significant decrease in the rate of reduction (H_2 gas being the reducing agent). It was found that the titania tends to stabilize ZnO by formation of mixed metal oxide with perovskite or spinel crystal structures, thereby, limiting the sorbent loss that occurs due to formation of $Zn_{(g)}$. It was also confirmed by Baird et al., (1992) that mixed metal oxides, which were produced by coprecipitation of other transition metals with zinc oxide, tend to produce sorbents with higher specific surface area. But only zinc based sorbents that contained titania showed the optimal adsorption performance. Mixed metal oxides like zinc ferrite, on exposure to reducing conditions, undergo decomposition into individual oxides which are then free to get reduced to their less active lower oxidation states (Fe_2O_3 to Fe_3O_4 and ZnO to Zn).

As discussed earlier, Lew et al. (1989, 1992) were one of the first to study the kinetics of Zn−Ti−O reduction. In the temperature range of 550−1050 °C, they found that Zn−Ti−O solids have a lower reduction rate than ZnO when reacted with H_2−N_2 gas mixtures. This decrease in reduction rate was attributed to the activation energies associated with the reaction. Activation energies for Zn−Ti−O and ZnO reduction were calculated at 37 and 24 kcal mol^{-1}, respectively. All the different phases of zinc titanate (Zn_2TiO_4, $ZnTiO_3$) were found to be indistinguishable in performance. In agreement with Lew et al., Pineda et al. (1997) found spectroscopic evidence that the addition of titanium increases the stability of ZnO against reduction through the formation of Zn_2TiO_4.

Although mixed zinc and titanium oxides were successfully tested for their ability to decrease sorbent's reduction tendency, many researchers have been finding deterioration in efficiency of zinc titanates in a cyclic operation. On the observation of weight loss of zinc

titanate samples during reduction, Lew et al. themselves hypothesized the deactivation of zinc-titanium based mixed sorbents to proceed via the following overall reaction:

$$Zn_xTi_yO_{x+2y(s)} + x.H_{2(g)} \Leftrightarrow x.Zn_{(g)} + x.H_2O_{(g)} + y.TiO_{2(s)}$$

Evidence of formation of zinc sulfate was also reported. Mojtahedi and Abbasian (1995) first proposed that deactivation of zinc titanate sorbents, apart from sulfate formation, might be due to migration and accumulation of elemental zinc on the surface of the sorbent during reduction reaction in a high temperature cyclic process (an alternative to the hypothesis of zinc loss due to volatilization alone). Although details about the sorbent preparation were not provided, such behavior can be attributed to the imperfect preparation method which may have led to presence of free zinc oxide due to incomplete zinc titanate formation. Provided Zn-to-Ti ratio (≈ 1.5) was within stoichiometric limits, this can happen when using bulk sorbent preparation methods that involve solid-solid mixing. Sorbent preparation methods involving techniques like co-precipitation or sol-gel have been shown to produce more homogenous and higher surface area sorbents (Chang et al., 2002). This is most likely due to the fact that such methods involve network-forming at a molecular level (Sec-2.2).

Apart from reduction of zinc oxide and subsequent deactivation caused by the migration and deposition of elemental zinc onto the sorbent surface, other reasons that may lead to gradual decline in efficiency of zinc titanate sorbents include sintering and consequent loss in surface area caused by the repeated use in high temperature processing conditions. In order to minimize this loss in surface area due to sintering (and also zinc loss due to vaporization), there is a tendency to lower the operational temperatures below 500°C. Operation in such medium temperature range would not only take care of the above the above-mentioned concerns but would also avoid difficulties in operation and stability issues associated with high temperatures at the industrial scale (e.g. valve performance, see Sec-2.1). However, for bulk sorbents, regeneration temperature cannot be reduced beyond a certain limit due to the risk of formation of non-regenerable zinc sulfate. In addition, it has been shown that the sulfur removal capability of zinc based bulk sorbents gets affected if the operating temperature is below 600°C (Harrison, 1998). In particular, when being used at mid-high temperatures, zinc

based sorbents reportedly suffered from decreased sulfidation reactivity leading to lower adsorption capacity.

3.2. Motivation

Thus, it seems necessary that in order to prevent deactivation of zinc based sorbents, one need to look beyond reduction in operating temperatures alone. One option that has been most popular is modification in composition. As stated previously, when considering zinc based mixed metal oxides, zinc titanates have been shown to be the best option in several studies. However, as reported by many researchers (Lew et al., 1992; Mojtahedi and Abbasian, 1995; Park, N-K. et al., 2010), even with mixed zinc and titania oxides, the reduction reaction still progresses. Mixed zinc-titanium oxides, in their bulk form, at best can only slow down the reduction reaction the extent of which depends upon crystalline phase composition and the operating temperature. The fact that they still tend to suffer from deactivation caused by reduction corroborates the need for improvement. Some research groups investigated the effect of addition of dopants on the performance of zinc-titania based sorbents. For instance, Jun et al. (2001) examined cobalt oxide-doped zinc titanate and found it to have higher sulfur sorption capacity and better regenerability than undoped zinc titanate. They justified this observation by proposing that the addition of cobalt in zinc titanate matrix led to formation of complex spinel structures that minimized the volume expansion and contraction during sulfidation and regeneration. The authors, in that particular study, did not report any experiments that investigated modified zinc titanates' resistance to reduction. However, recently, a publication from a different group concluded that the pellet based *modified* zinc titanate sorbents (with Cobalt oxide as one of the dopants along with NiO) also suffer from deactivation. It was stressed that this deactivation was being caused not by vaporization loss of zinc, but due to migration and subsequent surface accumulation of elemental zinc produced as a result of reduction (Park, N-K. et al., 2010).

Thus, it seems that the challenge of developing regenerable zinc based sorbents still persists and is largely determined by sorbents' potential to resist reduction. The major goal continues to be the development of regenerable sulfur sorbents that can sustain reactivity and adsorption capacity in a multicycle operation in a mid-high temperature range (500 – 650^{o}C). At present, the way forward seems to be a path that investigates alternatives further than the modification of sorbent's chemical composition alone. One of the main objectives of the present work is to examine the possibility of a geometry/morphology/structure induced properties which can contribute to improved sorbent performance, in particular, by preventing sintering and imparting sorbent with resistance to deactivation caused by undesired reduction. Investigation of the proposed fiber-mat morphology, consisting of composite zinc-titania nanofibers, for their response to reducing atmosphere is the topic of this chapter. The motivation for testing such sorbent morphology arises from its potential to provide enhanced dispersion of the two metal oxides in the form of nanocomposites, improved pore structure (bimodal distribution, see Chapter-2), and the large surface area which is resistant to sintering due to the high aspect ratio offered by its fibrous morphology. In addition, because of the large density of active sites associated with such polycrystalline nanocomposites, use of nanostructured sorbents may also imply higher reactivity than the bulk sorbents due to the possibly large value of the frequency factor (associated with more active sites), making it possible for the sorbents to retain adequate reactivity even at lower than typical operating temperatures (thus minimizing the zinc losses associated with vaporization).

It is sufficiently clear from above discussion that the information obtained from the investigation of sorbents' reduction kinetics is crucial in determining its suitability to serve as a high temperature sorbent for sulfur removal. The aim of this chapter, therefore, is to experimentally examine the response of this alternative sorbent morphology of zinc titanate fiber-mats to a controlled reducing environment. If an evidence of reduction or resistance to reduction is found, different possible reasons will be examined and an attempt will be made to provide a mechanism by monitoring the chemical reactivity accompanied by concurrent measurement of the physical & chemical changes that are occurring in the sorbent properties.

3.3. Experimental estimation of reduction kinetics

3.3.1. Temperature controlled reduction using Thermo-Gravimetric Analyzer (TGA)

The technique of Temperature programmed Gravimetric Analysis (TGA) was used to investigate the sorbent response in the presence of reducing environment. Sample-1 and Sample-2a were selected for these experiments. The preparation and the composition of each of these sorbents have been previously discussed in detail (see Chapter-2). Table-3.1 briefly provides the values of some of the physical properties along with the corresponding zinc-to-titanium atomic ratio associated with each of the two samples (as-spun).

Table-3.1: Comparison of the properties of two different samples (fresh)

Sorbent (Fresh)	Zn-to-Ti atomic ratio*	Surface Area, α_0 (m^2/g)	Mean Fiber diameter (nm)	Avg. grain size (nm)
Sample-1	**3.69**	151.7	435	12.53
Sample-2a	**1.17**	90.1	714	15.82

*Obtained from the quantitative analysis done using the profile fitted peaks of the XRD spectra.

The samples were analyzed using a thermo-gravimetric balance (DuPont 951 TGA) with a platinum sample holder (pan-shaped). The instrument had a custom-made quartz furnace tube with an accompanying sidearm for introducing corrosive gases (for carrying out sulfidation, see Ch-4). In order to keep the instrument electronics free of the corrosive gases, a constant flow of nitrogen was introduced for purging via the standard gas inlet provided on the instrument.

For these experiments, a gas stream containing hydrogen/nitrogen mixture was used. Since zinc oxide reduction is known to be faster in hydrogen than carbon monoxide (Grunze & Hirschwald, 1974), using hydrogen in our experiments provides the reduction rates that causes maximum zinc loss possible during conditioning of the biomass-derived syngas. The total flow rate in the sample area was 200 mL/min with 160 mL/min nitrogen flowing through the

electronics area. Just prior to the sample, balance 40 mL/min of the desired gas was introduced so that the net concentration of H_2 inside the chamber is 4% by volume.

The instrument was being operated as an isothermal differential reactor. A small, known quantity of fibers ($W_0 \approx$ 12.5 - 14 mg) was used. The temperature was raised to the desired temperature (400^{o}C, 500^{o}C or 600^{o}C) at the rate of 15^{o}C/min. During ramp-heating, only N_2 was flowing through the balance. Once the selected temperature was attained, H_2 containing gas stream was introduced. The net flow rate was maintained at 200 mL/min by using a gas mass flow meter integrated with the TGA's temperature controller. The reaction was allowed to proceed for approximately 100 minutes.

Figure-3.1 compares the instrument output, weight change vs. time, for the two samples. As can be seen, Sample-2a did not suffer any significant weight loss. On the other hand, Sample-1 underwent substantial weight change. This difference in response to reducing atmosphere can be attributed to the difference in the phase compositions of the two samples due to different initial Zn-to-Ti atomic ratios. The essential difference in composition arises from the higher overall concentration of mixed / complex metal oxides (zinc titanates) as present in Sample-2a. In contrast, Sample-1, having Zn-to-Ti ratio of approximately 3.7, has a lot more free or uncombined zinc oxide (as compared to Sample-2a's Zn-to-Ti ratio of approx. 1.2, see Table-3.1). Most likely it is this uncombined zinc oxide that contributed the observed weight change: as discussed earlier, zinc oxide, in presence of hydrogen, must have got reduced to zinc metal, which would easily volatilize at the elevated operating temperature of the reaction (600^{o}C) causing the weight loss as measured by the thermo-gravimetric analyzer.

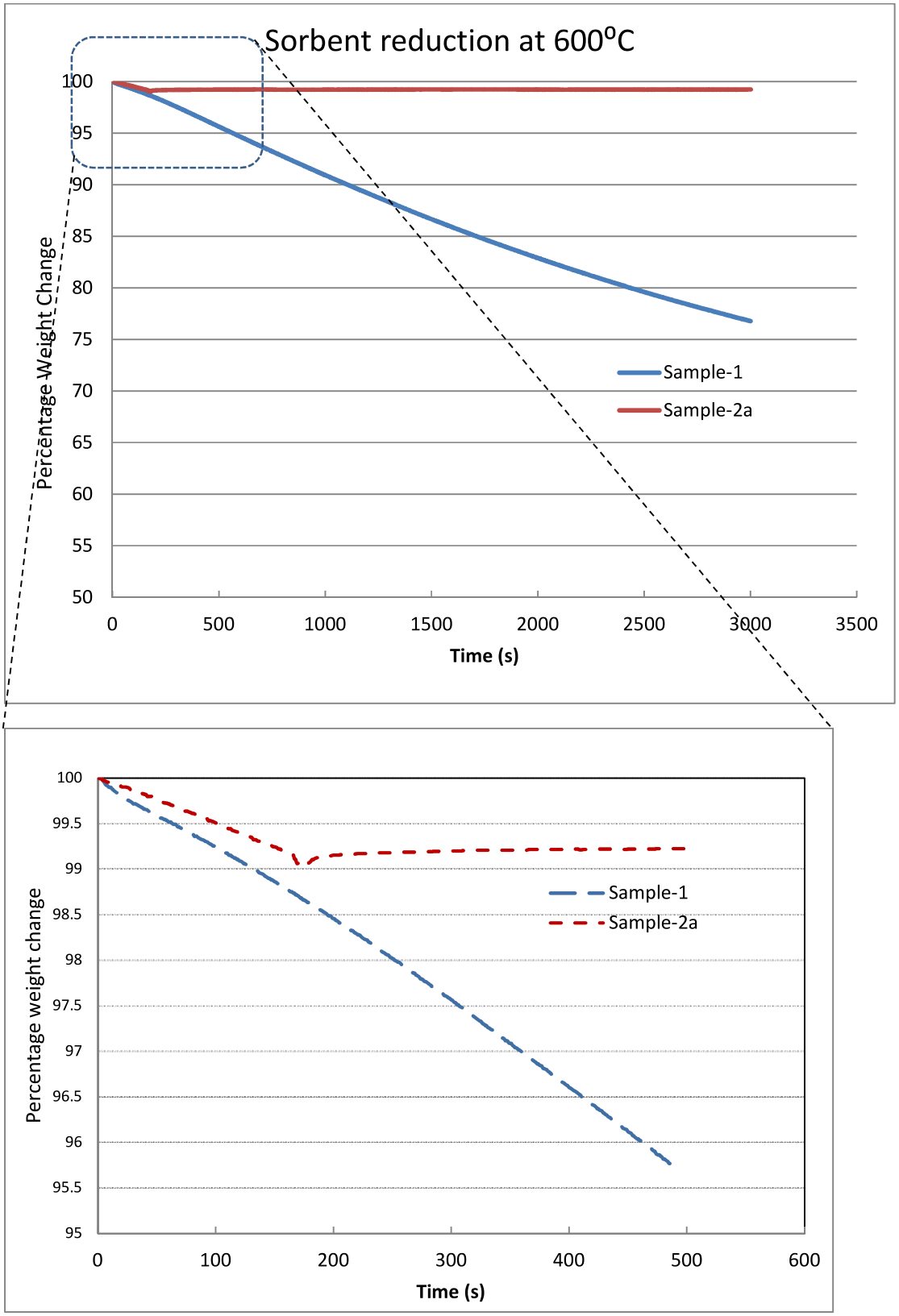

Figure-3.1: Comparison of the response of the two different zinc titanate samples when subjected to reduction reaction at 600°C.

Sample-2a experienced only a small change in weight due to much smaller concentration of free zinc oxide. As soon as all the uncombined zinc got lost, further loss in weight stopped almost immediately. From this point onwards, almost no weight loss was observed, as indicated by the horizontal portion of the curve. Thus, it appears that, contrary to the literature on bulk zinc titanates (Lew et al., 1992; Mojtahedi and Abbasian, 1995; Park, N-K. et al., 2010), results from the present experiments indicate that the zinc titanate, in its nanocomposite fibrous morphology, did not undergo any observable reduction. One possible explanation could be the enhanced dispersion of the two metal oxides due to the nanomixing that may have occurred due to the presence of nanometer sized grains (see Table-2.2). This would have furthered the mixed metal oxide's resistance to decomposition into the individual metal oxides, resulting in negligible weight loss during the reduction reaction.

3.3.2. Data analysis for estimation of kinetics

The weight loss suffered by Sample-1 was studied in more detail. Figure-3.2 shows the change in weight of Sample-1 plotted against time. All the weight loss measured by the instrument was assumed to be caused by the reduction of zinc oxide followed by the vaporization of elemental zinc product. Titania (TiO_2), in these operating conditions, has been shown to be non-reducible (Lew et al., 1992). This was confirmed by the fact that on post-reduction, no change in the sample color was observed. If titania would have undergone reduction, the sample must have turned grayish-blue in color due to the formation of the reduced product - Ti_3O_5.

The weight change due to elemental zinc loss was assumed to be coming entirely from the free zinc oxide present in the sample. The net decrease in weight was ascribed to the following reaction:

$$ZnO_{(s)} + H_{2(g)} \Leftrightarrow Zn_{(g)} + H_2O_{(g)}$$

The initial rate of reduction reaction is defined as following:

$$R_0 = \frac{(dW/dt)_0}{A_0 \cdot M_{ZnO}}$$

Where

$(dW/dt)_0$ = initial rate of change in the sample weight (attributed to the loss of elemental Zinc ($Zn_{(g)}$) and oxygen atom taken up in $H_2O_{(g)}$)

A_0 = Total area of the sorbent at t = 0 ($A_0 = W_0 * \alpha_0$)

M_{ZnO} = Molecular weight of Zinc Oxide = 81.4 g/g-mol

At 600^oC, the value of initial reduction rate for Sample-1 was calculated and found to be:

$$R_0 = 4.29E-07 \frac{moles}{\min.m^2}$$

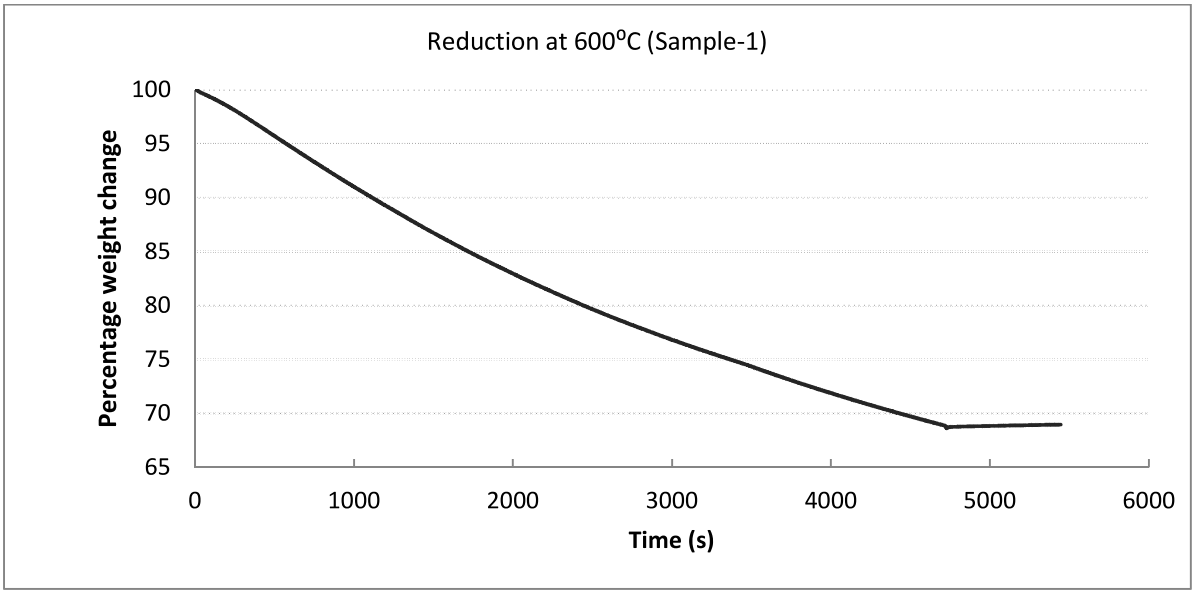

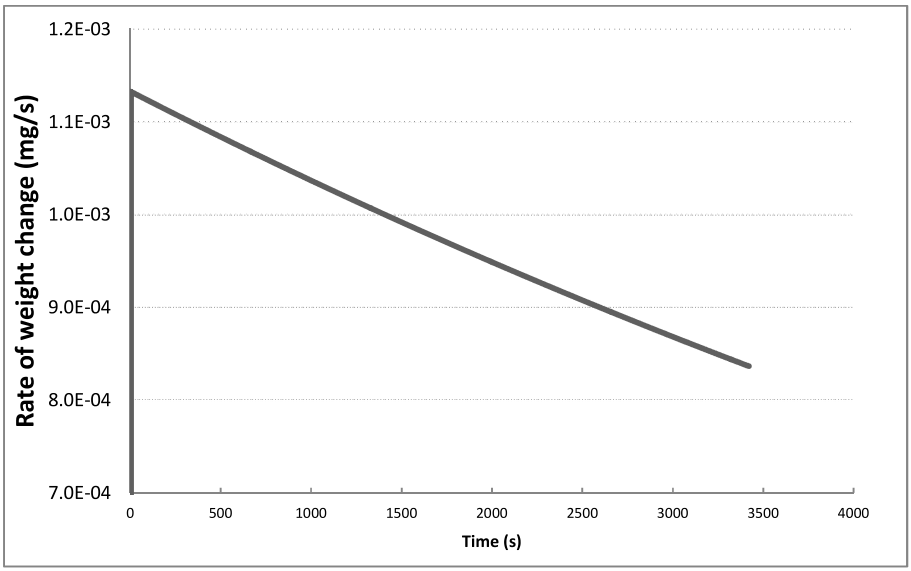

Figure-3.2: Top - Weight changes accompanying reduction reaction for Sample-1 at 600°C. Bottom - Corresponding rate of weight change with time derived by first fitting a curve to the weight change vs. time plot and then taking its time derivative and plotting it against time

Conversion (X) was defined as:

$$X(t) = \frac{W_0 - W_t}{W_0 - W_f}$$

Where,

W_0 = Initial sample weight

W_f = Sample weight after reduction

W_t = Sample weight at an intermediate time *t*

Fig.-3.3 depicts the how the conversion varied with time during the reduction of Sample-1.

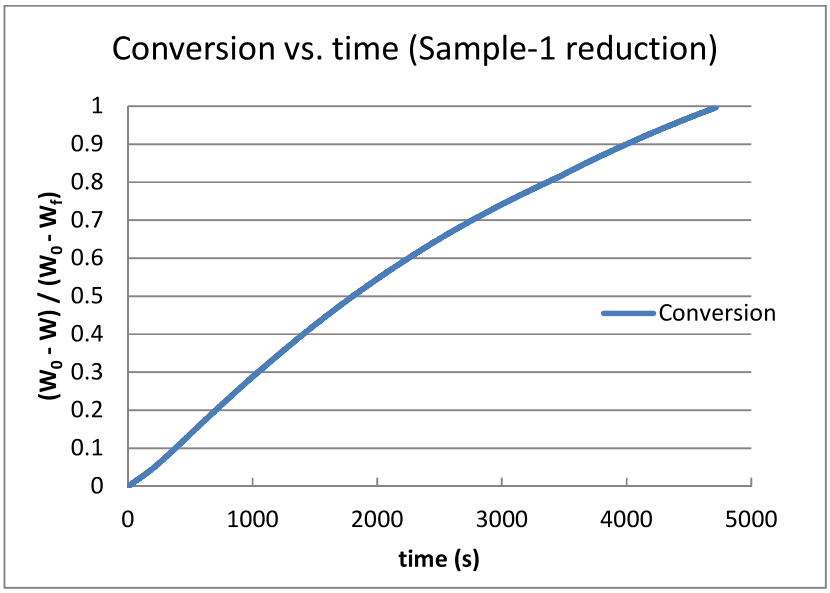

Figure-3.3: Variation of conversion for the reduction reaction for Sample-1 at 600^{o}C.

Results from the analysis for Sample-1 are presented in Table-3.2

Table-3.2: Estimation of initial reduction rate

Sorbent	Zn-to-Ti atomic ratio (x/y)	Sp. Surface Area, α_0 (m^2/g)	W_0 (mg)	Initial Rate of reduction, R_0 (moles/min/m^2)
Sample-1	3.69	151.7	12.82	4.29E-07
Sample-2a	1.17	90.7	15.18	3.34E-07

Table-3.3, for the same testing temperature of 600^{o}C, compares the initial rate of reduction of nanofibrous zinc titanate against the bulk zinc titanates as investigated by Lew et al., 1992. Although, the H2 content of the reducing gas stream used Lew et al. was different (10%), it was considered reasonable to do the comparison since the initial reduction rate is considered to be a much stronger function of temperature than that of the concentration of a gas reactant which contributes a reaction order that is less than or equal to one. Initial rate of reduction will also depend upon the starting Zn-to-Ti ratio present in the samples of the two studies. Higher the value i.e. larger zinc content in the sample is supposed to cause faster reaction rate (but the effect is still not as comparable to the effect of temperature, which was same as in the experiments performed by Lew et al.) Since the ratio was higher for the sample used in this study (3.69 as compared 3 in the literature), it should have led to higher initial rate of reduction and faster loss of elemental zinc. Instead, it was found that the reduction rate of nanofibrous samples used in this study were actually two orders of magnitude smaller than the initial rate of reduction as reported in the earlier study. The reduction rate was found to be 4.29E-07 Moles/min/m^2 as compared to the value of 3.61E-05 Moles/min/cm^2, which was reported by Lew et al. (1992).

Table-3.3: Estimation of initial reduction rate

Sorbent	**Zn-to-Ti atomic ratio (x/y)**	**Initial Rate of reduction, R_0 (moles/min/m^2)**
Sample-1 (zinc titanate fibers)	3.69	4.29E-07
Literature* (bulk Zinc titanate)	3.0	4.21E-05
Sample-2a (zinc titanate fibers)	1.17	3.34E-07
Literature* (bulk Zinc titanate)	1.0	3.10E-05

To explain this result, one need to look at the role played by a composite sorbent's microstructure and surface morphology. Polycrystalline nanofibrous mats, with high density of nanometer sized grains (≈ 10 - 15nm), seems to be causing much better dispersion of titanium, which is responsible for lowering the reduction rate. One possible reason could be that this improved dispersion of titania (unreacted or produced during the decomposition of zinc titanate) is eliminating larger number of sites for hydrogen dissociation more effectively than that is possible for the bulk sorbents. In addition, Lew et al. (1989) postulated that slow rate of reduction can be attributed to the titania's tendency to surround the active zinc components, which increases the diffusional resistance, making the escape of elemental zinc difficult. A set of reduction experiments occurring at different temperatures have been planned as a part of the future work for estimating the activation energy and reduction mechanism associated with the proposed sorbent structure.

3.3.3. Regime analysis and proposed reaction model for reduction

In order to understand how the reduction reaction proceeds, different reaction models developed for non-catalytic gas-solid reaction were attempted. Shrinking-particle model, described by Levenspiel (1999), was found to be the best fit for the zinc oxide reduction reaction that involves accompanying mass losses in the form of vaporization of the product (elemental zinc). In this model, particle shrinks during the reaction and finally disappears, which is distinct from the more popular shrinking-core model, in which the size of the particle tends to remain the same since the product stays and tends to form a growing "ash" layer around the still unreacted core (eventually the core goes away completely to the products, while the overall particle size remains unchanged).

The overall mechanism, in the shrinking-particle model, involves both the gas phase transport and the chemical reaction kinetics. It can be divided into these three steps:

(1) the gaseous reactant's diffusion (H_2 in the present case) through the gas boundary layer (film diffusion) surrounding the particle;

(2) the gas-solid interfacial chemical reaction at the surface; and

(3) gaseous product ($Zn_{(g)}$ or $H_2O_{(g)}$) diffusion through the gas film to the exterior into the main gas stream.

Although, this model assumes the absence of temperature gradients and consequent heat transfer across the solid-gas boundary layer, it has been shown to realistically represent the reduction of ZnO in reducing atmospheres such as in the presence of CO and H_2 (Steinfeld et al., 1995). One other source of discrepancy may arise if a slow reaction proceeds with a diffuse-reaction front instead of the sharp reaction front as assumed by the model. But since the zinc oxide reduction reaction has been shown to reasonably fast, it is expected to proceed with relatively sharp reaction front.

Depending upon the operating conditions and sorbent geometry and morphology, any of the above mentioned regimes could be the rate-controlling. For Sample-1, the shape of the experimentally obtained conversion vs. time curve (Fig.- 3.3) is indicative of the possibility that the rate is apparently controlled by the gas film diffusion in the Stokes regime (Levenspiel, 1999). The model involves deriving an equation describing how the conversion (fractional disappearance) varies with time (X vs. t) as the reaction proceeds. When the overall reaction is controlled by the gas film diffusion, the X-t relation can be derived by assuming that the rate of disappearance of the solid is proportional to the rate of arrival of gas species i.e. the flux of solid's disappearance is proportional to the flux of incoming gas; equating the two gives:

$$-\frac{1}{A_{ex}}\frac{dN_{ZnO}}{dt} = bk_g C_{H_2 g} \qquad (3.1)$$

where

N_{ZnO} = number of moles of zinc oxide (moles)

A_{ex} = external surface area of the fiber-mat sample (m^2)

$C_{H_2 g}$ = Concentration of H_2 in the bulk gas phase (mol/m^3)

k_g = Mass transfer coefficient of the gas film ($m^3/m^2.s$)

b = stoichiometric coefficient in a gas-solid reaction: $A_g + bB_s \rightarrow pP_g$ (b = 1 in the present case)

Assuming the sample to behave as a spherical particle of effective initial radius of R_0, (and R at a time t > 0) and ρ_s being the molar density of zinc oxide in the sample, then at some time t:

$$dN_{ZnO} = \rho_m . dV = \rho_m . 4\prod R^2 dR \quad (3.2)$$

$$A_{ex} = 4\prod R^2 \quad (3.3)$$

Mass transfer coefficient a gas component (with mole fraction y) is given by the following equation (Froessling, 1938):

$$\frac{k_g d_p y}{\mathscr{D}} = 2 + 0.6(\mathrm{Sc})^{1/3}(\mathrm{Re})^{1/2} = 2 + 0.6\left(\frac{\mu}{\rho\mathscr{D}}\right)^{1/3}\left(\frac{d_p u \rho}{\mu}\right)^{1/2}$$

where $\mathscr{D}$ (elsewhere labeled as D)= molecular diffusion coefficient in the gas phase (m^2/s)

d_p = effective sample diameter=2.R,

$\boldsymbol{\mu}$ = gas phase dynamic viscosity,

ρ= *mass density of the gas phase*

y = mole fraction of H_2 in gas phase

For stokes regime, RHS of the above empirical relation reduces to a constant = 2, which on solving for k_g gives the following approximation:

$$k_g \approx \frac{2D}{d_p} = \frac{D}{R} \quad (3.4)$$

Inserting the equations 3.2, 3.3 and 3.4 in 3.1, reduces 3.1 to the following equation:

$$-\rho_m \frac{dR}{dt} = b.\frac{D}{R} C_{H_2\,g} = \frac{D}{R} C_{H_2\,g} \quad (3.5)$$

which on integrating gives the following relation

$$t = \frac{\rho_s R_0^2}{2C_{H_2 g}\, D}\left(1 - \left(\frac{R}{R_0}\right)^2\right) \tag{3.6}$$

Also, sample being represented by a spherical particle with some initial effective diameter R0 and R at time t > 0, conversion can be defined as following:

$$X(t) = \frac{R_0^3 - R^3}{R_0^3} \tag{3.7}$$

which on rearranging gives:

$$\left(1 - \left(\frac{R}{R_0}\right)^2\right) = \left(1 - (1 - X)^{2/3}\right) \tag{3.8}$$

Thus, equation 3.6 can be rewritten as following:

$$t = \tau\left(1 - (1 - X)^{2/3}\right) \tag{3.9}$$

where $\tau = \frac{\rho_s R_0^2}{2C_{H_2 g}\, D}$ = constant at a given temperature.

Experimentally observed conversion (as a function of time) was converted into the expression: $(1 - (1–X)^{2/3})$ and was plotted against time, as shown Fig-3.4. The closely followed linear relation between the two, as predicted by the model, is an indication of the validity of the model.

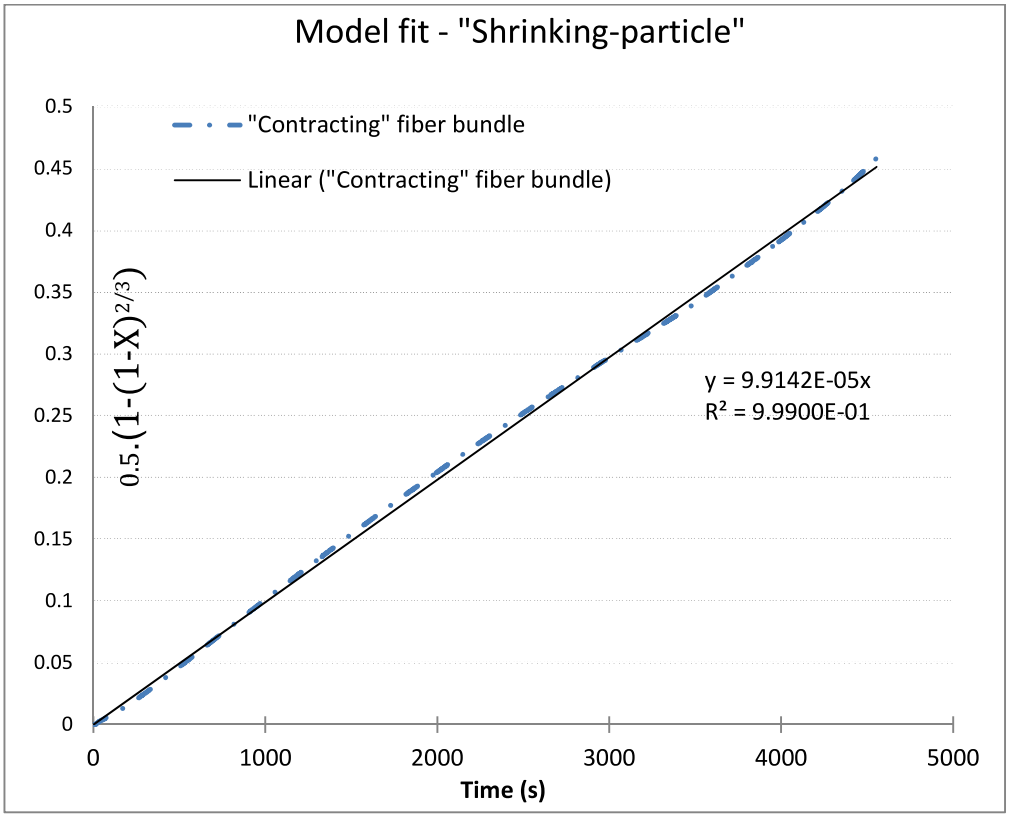

Figure-3.4: Test for confirming the shrinking-particle model with gas film diffusion control – good validity

Although, the shrinking-particle model is a good fit, the result should be extrapolated only for the reactor conditions and configurations which have the associated flow regimes that facilitate gas film-diffusion step as the primary rate controlling step. For instance, film diffusion through stagnant gas is likely to be of large influence if the fiber-mats were to be used in a stacked configuration, resembling a packed-bed design with its accompanying reaction conditions. In other conditions, such resistance would be negligible as is the case of fluidized bed reactor, which promotes conditions of high gas velocity with respect to the solid reactant.

Another assumption worth-noting is that the above model was found to be a good fit to the data obtained from the reduction experiments that were carried out on a sample containing high free zinc oxide (Sample-1). Thus, the applicability of the model should therefore be limited to solid adsorbents in which free zinc oxide contribute a major fraction (more than ≈

50% by weight). Zinc based sorbents with mixed metal oxides, in particular zinc titanates, as the major components may exhibit a different behavior. In particular, zinc titanates, in which the other metal oxide (i.e. TiO_2) is thermally and chemically more stable, may deviate considerably from the film-diffusion controlled shrinking-particle model. This is because a small zinc loss that is possible, may occur without any shrinking in sample size since the non-reduced titania (a product if zinc titanate gets reduced) still preserves the sorbent's overall size (possibly with increased porosity). This growing layer of titania may in fact provide another layer of resistance to the gas transport and may very well become the controlling step. Thus, this core-shell structure / condition, with zinc tiatante at the core and free titania as the shell, may adhere to another type of gas-solid reaction model, known in the literature as the Shrinking-Core model (Levenspiel, 1999). This model will be discussed in more detail in the next chapter (Ch-4).

3.4. Conclusions and Summary

- Nanocomposites (zinc + titanium oxides) were found to possess much higher resistance to the deactivation caused by the reduction. The effect was particularly strong if the zinc-to-titanium ratio was closer to one.
- Different compositions of the mixed oxide sorbent exhibited different regimes as controlling during the reduction reaction. More zinc content in the sorbent implied that the overall reaction rate was controlled by the gas-film diffusion step.
- Product layer diffusion step becomes rate controlling if there is comparable zinc-to-titanium content (as in Sample -2a). In such sample, shrinking-core mechanism can be seen in operation in which inert product layer grows as the active core shrinks. This is distinct from the shrinking – particle mechanism (as seen in sorbents with higher zinc content), in which the main product is not solid (Zinc vapors) and the reaction proceeds as the entire sorbent unit starts shrinking in size.
- The weight loss was attributed to the free zinc oxide. The sorbent with higher mixed metal oxide content was found to be almost immune to reduction.
- No conclusive evidence of surface accumulation of elemental zinc was found

Chapter-4

Sulfidation & regeneration of Zn-Ti-O fiber-mats

4.1. Introduction and Motivation

Over the past two decades, development of mixed or promoted metal oxides as high temperature multi-cycle sulfur adsorbents has been an active area of research. Quite early on this area it was realized that for syngas desulfurization process to be economical and operational, sorbents that can be used repeatedly over many cycles, instead of the more prevalent "once-through guard beds" of metal oxides, need to be developed. However, for a sorbent to last multiple cycles, in addition to its favorable sulfur removal thermodynamics, it should also possess the necessary mechanical properties of high attrition resistance and ability to withstand high temperature conditions. Thus, as described in the literature, many researchers tested their sorbents for certain set of properties as a measure of potential success in a multi-cycle operation. These desirable properties were summarized by Cheah et al. (2009) as follows:

(1) Large sulfur adsorption capacity. This helps in reducing the overall costs involved by decreasing both the sorbent quantity and process equipment size.
(2) Fast adsorption kinetics (for the sorbent-H_2S reaction).
(3) Improved mechanical properties – Ability to resist spalling and other structure-related changes during a high temperature operation.

(4) Resistance to chemically induced deactivation caused mainly by reduction in an environment containing hydrogen, carbon monoxide, steam etc.

(5) Regenerable through a suitable pathway while maintaining efficient sulfur sorption capacity during repeated sulfidation-regeneration cycles.

Bulk of the research in the field of sulfur sorbent development has been focused mainly on improving the chemical properties, either by modifying the composition of the popular transition metal oxides sorbents (developing mixed metal oxides like zinc ferrites (Kobayashi et al., 2002), zinc titanates (Lew et al., 1992) or by incorporating precious metals like nickel, cobalt in the conventional metal oxides (Jun et al., 2001)) or by investigating unconventional metal oxides like lanthanum / cerium oxides (Wang & Stephanopoulos, 2005). Promising progress has been made, for instance, use of zinc titanates have led to the development of better solid adsorbents that have been shown to be more resistant to deactivation caused by the reduction. In order to compensate for the decreased capacity of zinc titanates (due to incorporation of inert titania, the theoretical sulfur capacity gets reduced from 33% (by wt.) in ZnO to 23% in Zn_2TiO_4), use of nickel & cobalt as promoters for zinc-titania based sorbents was investigated by Jun et al. (2001). They found it to have higher sulfur sorption capacity (particularly at 480 °C) than the undoped zinc titanates. Wang et al. (2005) successfully used rare-earth metal oxides as sour gas adsorbents for cleaning the inlet gas of SOFCs (Solid Oxide Fuel Cells). It was found that these rare-earth metal oxides do not suffer from the reduction-induced loss of activity and associated metal volatilization, the problem which has weighed down many single transition metal oxides. This makes CeO_2 and La_2O_3 a good candidate for sulfur removal operations requiring very high temperatures (700°C to 1000°C).

But in order to make the use of metal oxides economical, they must be able to demonstrate adequate performance in a multi-cycle operation. In spite of the above mentioned advances in sorbent chemistry, metal oxide based adsorbents have only shown limited success when dealing with cyclic sulfidation/regeneration, primarily because of the inadequate structural and mechanical properties. Poor durability, spalling, loss of mechanical integrity and loss of surface area in subsequent operations are some of the problems associated with metal

oxides when being used as regenerable sorbents. Compositional modifications as mentioned above (promoted metal oxides) can help in extending the sorbent lifetime (Jun et al., 2001), however, this may not prove to be very economical way of doing so because of the inclusion of costly promoters (Ni, Co), which limits the scalability of the operation. For the case of rare-earth metal oxides, although cerium and lanthanum oxides have shown to be much more stable at high temperatures as compared to the transitional metal oxides, the reactivity of individual cerium (IV) oxide has been reported to be considerably low (Dooley et al., 2011). Doping it with lanthanum oxide may improve reactivity but it significantly diminishes the sorbent ability to regenerate. Clearly, more work needs to be done before rare-earth metal oxides can be successfully used as regenerable sulfur sorbents.

Furthermore, it seems that the major research thrust, for some years now, has shifted on developing the sorbents for operations requiring gas cleaning at mid-high temperature ranges ($350^{o}C$ - $600^{o}C$), different from the earlier trend of carrying out at the gas cleaning operation at high temperatures ($600^{o}C$ – $800^{o}C$). This change in approach has come about by the realization of the fact that at an industry scale, the overall thermal efficiency gains of carrying out desulfurization above 550°C may not be sufficient to justify the cleaning operation at such high temperatures (Slimane & Abbasian, 2000). With technical feasibility (like valve operation at high temperatures) and the process efficiency being the two constraining factors, a lower overall process cost is attained when the desulfurization temperature range is between 350–600°C. As this temperature range is increasingly becoming popular, some of the concerns associated with the zinc-titanate-based sorbents, like reduction and subsequent loss of metal by vaporization, get relieved to some extent. However, this also implies reduction in the reactivity of the zinc titanates sorbents due to the reduced temperature as reported several times in literature. Lew et al. (1992) themselves showed that the addition of titania to zinc oxide is accompanied by the reduction in chemical reactivity of the mixed metal oxide, especially when operating at lower temperatures.

Consequently, if zinc titanates, one of the most successful desulfurizing sorbents yet developed, are continued to be used as adsorbents for the moderate temperature range gas

cleaning operations, new ways have to be found to make it reactive enough at these lower temperatures. As discussed earlier, compositional – based changes in the sorbents have only led to a limited success. As a way forward, it will be worthwhile exploring methods other than chemical and compositional modifications for the development of mid-high temperature sorbents which are easily regenerable.

Among the different approaches developed for countering the damaging effects of cyclic regeneration, an approach that has not got much attention is the development of desirable structure & morphology-induced features and functionalities in the sorbent. It is well known that the efficiency of an adsorbent depend not only on its composition but also on the physical properties of the adsorbent, like the specific surface area, individual grain size, pore structure, active site distribution etc. If a certain sorbent architecture or morphology allows the preservation of these features during a cyclic operation and also provides some level of control of these properties, then integration of such capability with the material's inherent favorable thermodynamics and kinetics can lead to a sorbent that is potentially more equipped to withstand the conditions of repeated regeneration. However, the conventional bulk scale sorbents may not allow for the full utilization of the benefits that arise from the control of the features like grain size, microstructure and associated sorbent morphology. In fact many problems associated with the cyclic operation, like progressive sorbent underutilization (due to excessive product layer diffusion resistance, see Fig-2.1), can be linked to the bulk nature of the sorbents. The approach, therefore, should be to come up with a sorbent architecture that facilitates the full-utilization of the benefits associated with such control of structural features.

Nanostructuring, i.e. sizing and shaping the sorbent structure at the nanoscale, is a way of achieving such sorbent architecture. However, it should be noted that a mere reduction in the sorbent's size may not be the best approach; for instance, sorbent in the form of nanopowders tend to aggregate in general and sinter at high temperatures, resulting in mass transfer resistances and loss of surface area similar to the case of bulk sorbents. However, nanostructures with high aspect ratio, like 1-d nanofibers, can remain isolated; thus, potentially providing a more suitable framework for carrying out frequent cyclic sulfidation-regeneration

operation. These high aspect ratio nanoscale structures can not only retain the properties from their bulk form such as favorable thermodynamics, chemical affinity etc., but they also tend to develop useful properties due to highly anisotropic geometry and confined grain size. Because of the confinement of the grain size and short contacting time, nanofibers will tend to limit the large volume changes and accompanying grain boundary collisions which are typical during repeated sulfidation/regeneration. Thus, it is expected that the use of nanostructured sorbent will not only lead to high specific surface area and improved mass transfer, it can also lead to an improved mechanical behavior during high temperature cyclic operation.

Highly porous fiber mats made up of electrospun nanofibrous metal oxides may help in providing such a sorbent architecture. Due to the polycrystalline nature of these nanocomposites, there will be a high density of defects (active sites) and grain boundaries. Also, with fibers' nanometer sized grains, the specific surface area increases. All this may help in lowering the energy barrier i.e. the activation energy needed for the reaction to occur. It will be worthwhile to investigate if such structurally-enhanced fiber mats of zinc titanate help in increasing the overall reactivity to an extent that would compensate the decrease in reactivity caused by the moderate temperature operation.

As discussed earlier (Ch-2, Sec-2.1), sorbent design and overall architecture provided by such nanofibrous mats may also facilitate sorbent regenerability.

4.2. Background on sulfidation of zinc oxide / zinc titanate

Gibson and Harrison (1980) applied grain model to predict the extent of the sulfidation reaction between zinc oxide and H_2S between the temperature range of 375^oC and 800^oC. They found that at or below 600^oC, the reaction stopped well before the total zinc oxide conversion was obtained, primarily due to the formation of a growing non-porous zinc sulfide layer around the zinc oxide pellet. Modeling of the results with the grain model suggested that the primary limitation to reaction rate on both Zn−Ti−O and ZnO is diffusion through a ZnS product layer.

Lew et al. (1992) found that between 400 and 700 °C, the reaction order with respect to hydrogen sulfide was one for both Zn−Ti−O and ZnO sorbents. They also showed that the activation energies for sulfidation were similar (≈ 9−10 kcal/mol), indicating that the sulfidation mechanism on these two types of solids is likely the same. However, for sorbents containing more than 25 mol% Ti, the initial sulfidation rate of Zn−Ti−O sorbents was 1.5−2 times slower than that of ZnO, suggesting the frequency factor in the rate expression for Zn−Ti−O is smaller, that is, there are fewer reaction sites on Zn−Ti−O than ZnO. The smaller number of reaction sites on Zn−Ti−O was presumed to be due to nonreactive titanium on the surface.

Siriwardane et al. (1994) studied molybdenum-containing zinc titanate sorbents. During sulfidation and regeneration, they found evidence of sulfate formation and sorbent spalling. Sorbent degradation was attributed to the incidence of substantial changes in the sorbent structure due to the large volume difference between sulfate and oxide. In addition, they also found that when regeneration was conducted at 649−760°C, there was incomplete reformation of the titanate structure, and that the degree of incomplete reformation increased (amount of pure TiO_2 increased) with an increasing number of sulfidation and regeneration cycles.

Some researchers reported modification of Zn−Ti based materials further with other oxides. Sasaoka et al. (1999) modified 50% ZnO-TiO_2 with 5−10% ZrO_2 and found that it improved the reactivity during sulfidation and regeneration. Authors hypothesized that addition of ZrO_2 improved the pore structure and helped to maintain a large surface area after regeneration.

Wang et al. (2005) showed that by using very high gas velocities or short contact times with the sorbent during the sulfidation / regeneration steps, deactivation of the sorbent due to structural degradation can be prevented. They also found that the use of rare-earth metal oxides like lanthanum and cerium oxide can possess favorable thermodynamic of zinc oxide based sorbents.

4.2.1. Objectives

One of the primary objectives of this chapter is to investigate the changes in the physical structure and the chemical composition of the fibrous zinc titanates when subjected to sulfidation and regeneration at mid-high temperature range. Specifically, the specimens will be evaluated for the changes in the fiber morphology as well as for the presence of sulfidation / regeneration products like zinc sulfide, zinc sulfate and different crystalline phases of zinc titanate. For evaluating these characteristics, techniques like XRD, XPS, SEM, EDX & TEM will be used.

Kinetics of the sulfidation and regeneration will be analyzed using the technique of thermo-gravimetric analysis. Activation energy associated with the sulfidation reaction will be evaluated by performing the reaction at different temperatures. Regime analysis will be carried out to identify the rate controlling step in the gas-solid reaction between the H_2S and the zinc oxide based sorbents. This will be done by first fitting the kinetic data to the different gas-solid non-catalytic reaction models, each with a different rate controlling step, followed by a comparison of the goodness of the fit.

The relationship between the microstructure of the fibrous zinc titanates and the sulfidation/ regeneration kinetics will also be discussed. The findings may help to estimate some important aspects of the reaction that have not got much attention from other investigators, for instance, the understanding of the relationship between the grain size/grain boundary density and the sorbent performance may help in estimating the extent to which sorbent regeneration is surface sensitive.

4.3. Experimental setup and procedure

For analyzing the kinetics of the sulfidation reaction between H_2S and the fibrous samples of zinc titanate, a Thermo-gravimetric analyzer (TGA) was used. Some known amount of specimen (W_0, in mgs) was placed in the sample-holder. The specimens (Sample-1 & Sample-2a, see Ch-2 for the synthesis and Table-3.1 for the measured physical properties) used in the sulfidation experiments were pre-exposed to 4% H_2 for a fixed duration (typically for 90 mins). A

gas stream containing 1% H_2S (by volume) in nitrogen was used as the gaseous reactant. This concentration of H_2S is much higher than the value typically present in the raw syngas mixture obtained from the biomass gasification (~ 50 – 600ppmv). This was intentionally done to speed up the reaction. The flow rate of the gas was fixed at 200 ml/min using the mass flow controllers. The reaction between the samples and H_2S was allowed to proceed isothermally at a pre-determined temperature. The samples were heated at a rate of 15 °C/min from the room temperature to the pre-assigned reaction temperature. The duration of each sulfidation reaction, at a given temperature, was fixed. After the reaction, the samples were allowed to cool down to the room temperature before performing the material characterization. During the heating and cooling segments, only the nitrogen gas was flowing. Table-4.1 summarizes the operating conditions used.

Table-4.1: Operating conditions used in the TGA

	Sulfidation conditions		**flow**
Sample1/2	Room Temp. to Reaction temperature (suppose 600^{o}C)	Heating at 15^{o}C/min (with **N_2**)	0.2 LPM
	Pre-reduction at 600^{o}C	Prereduction with 4% **H_2 gas** for 90 mins	0.2 LPM
	Sulfidation at 600^{o}C	Gas switchover to 1% **H_2S** gas mixture reaction proceeds for another 100 mins	0.2 LPM
	Cooling in inert atmosphere	Gas switchover to N2	0.2 LPM

4.4. Results and analysis for sorbent sulfidation

4.4.1. Sulfidation kinetics

For Sample-2a, Figure- 4.1 shows the specimen's weight change when being reacted with H_2S at 600^{o}C. It also shows the rate at which the weight is changing. This will give us the initial rate of reaction.

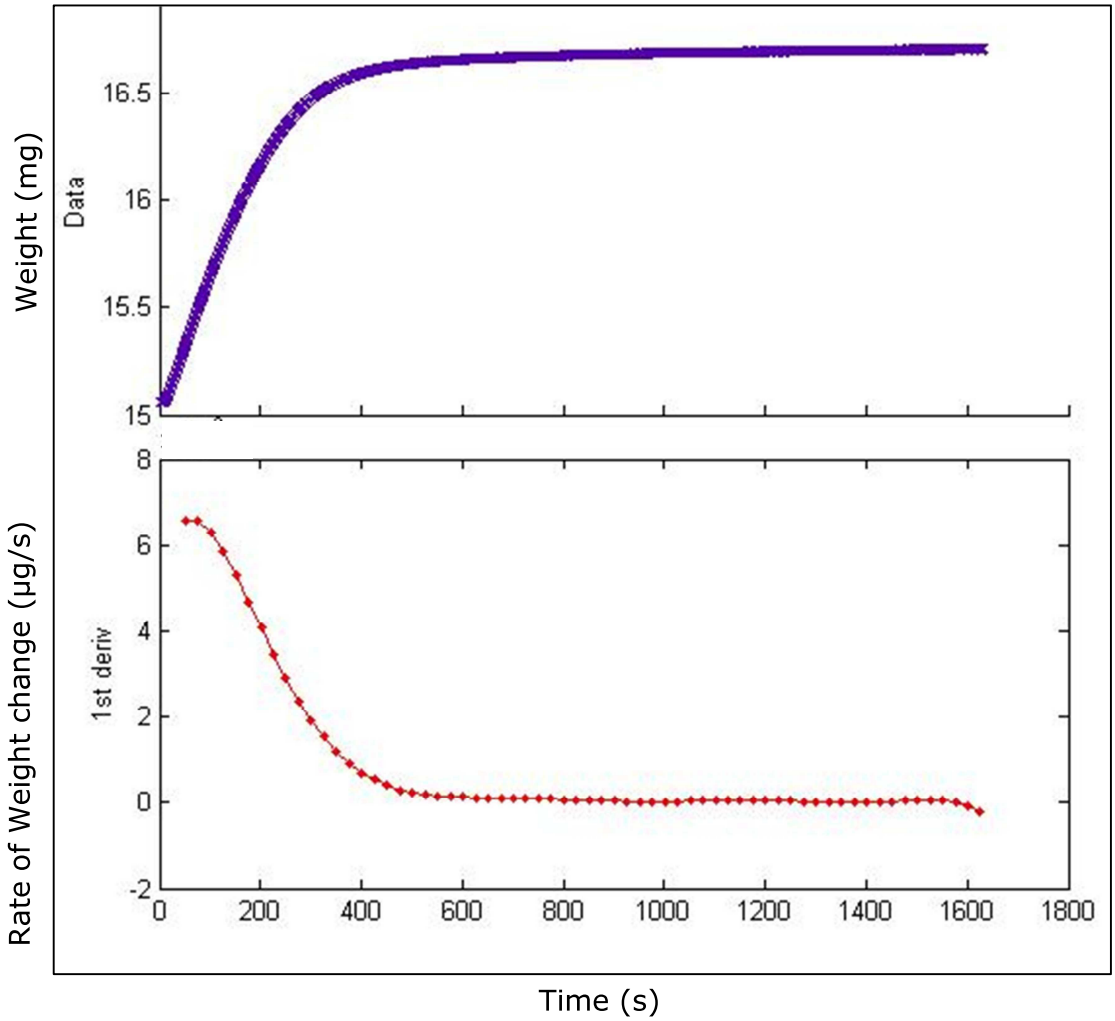

Figure-4.1: Weight change (top) along with rate of weight change (bottom) for Sample-2a during the sulfidation reaction (at 600^{o}C)

Following is the *overall* reaction that was assumed to be responsible for the observed weight gain:

$$Zn_xTi_yO_{x+2y_{(s)}} + x.H_2S_{(g)} \Leftrightarrow x.ZnS_{(S)} + x.H_2O_{(g)} + y.TiO_{2(s)}$$

The product Zinc sulfide being heavier than the zinc oxide component of the zinc titanate, a net increase in weight occurs. For the given operating temperature range, titania was assumed to be inert and would not react with H_2S (Lew et al., 1992).

Initial sulfidation reaction rate was defined as moles of zinc oxide converted per unit time per unit area:

$$R_0 = \frac{(dW/dt)_0}{A_0 \cdot (M_{ZnS} - M_{ZnO})}$$

Where

$(dW/dt)_0$ = initial rate of change in the sample weight (in g/min)

A_0 = Total area of the sorbent (in m^2) at t = 0 ($A_0 = W_0 * \alpha_0$)

M_{ZnO} $M_{ZnS,}$ = Molecular weight of Zinc Oxide = 81.4 g/g-mol, Zinc Sulfide = 97.47/g-mol

Table-4.2: Initial sulfidation rates at 600^oC

Specimen name	Initial rate of weight gain $(dw/dt)_o$	α_o (m^2/g)	W_o (mg)	Initial rate of sulfidation moles/min/m^2
Sample-1	4.24 µg/s	151.7	8.86	1.18E-05
Sample-2a	7.13 µg/s	90.1	15.14	1.94E-05

Table- 4.2 compares the initial sulfidation rate, as calculated for the Sample-1 and Sample-2a (both pre-reduced). At 600^{o}C, the value of initial sulfidation rate for Sample-2a was calculated and found to be: 1.94E-05 moles/min/m^2. For Sample-1, it was found to be 1.18E -06 moles/min/m^2. As expected, the sulfidation rates for the two samples were not very different. The initial sulfidation rate is known to be only a weak function of the specimen's Zn-to-Ti ratio. Different samples with different phases of zinc titanate have been shown to exhibit sulfidation rate of the same order, independent of the Zn-to-Ti ratio (Lew et al., 1992). It should be noted, however, that both the samples in our experiment were pre-reduced and weren't reacted with hydrogen and hydrogen sulfide simultaneously, as done by Lew et al. (1992). Although, the use of pre-reduced samples is more precise in simulating the actual reaction conditions, it will be interesting to see if this trend persists when using fresh samples.

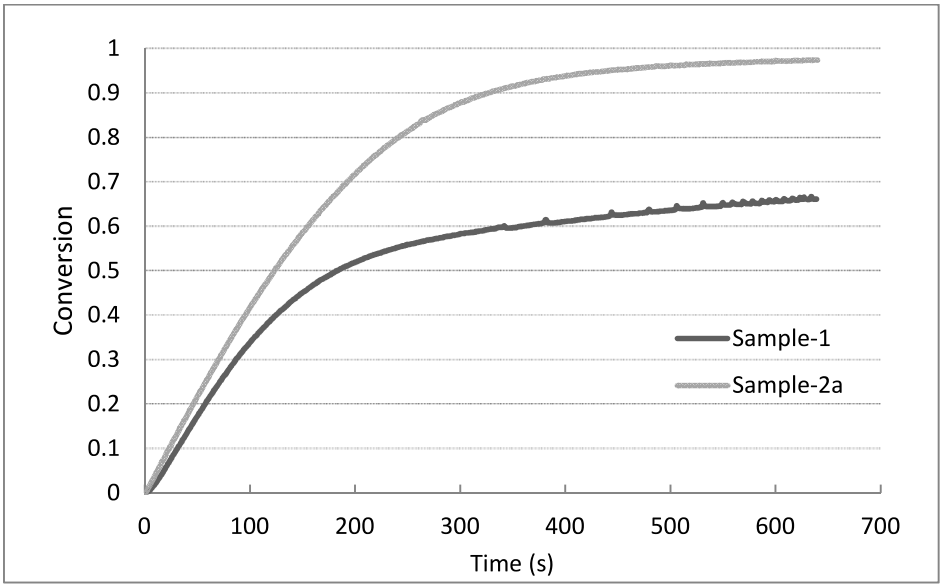

Figure-4.2: Conversion vs. time for Sample-1 & Sample-2a during the sulfidation reaction (at 600^{o}C)

Conversion (X) was defined as following:

$$X(t) = \frac{W(t) - W_o}{W_f - W_o}$$

Where

W_0 = Initial sample weight

W (t) = Sample weight at a time *t*

W_f = Sample weight after the sulfidation reaction

Fig-4.2 shows the conversion, as it varies with time during the sulfidation reaction, for Sample-1 & Sample-2a. Although, for both the samples, the initial sulfidation rates were not very different, Sample-2a clearly performed better than Sample-1 if desulfurization is monitored over a longer time (as can be seen from the Fig-4.2). For a given time interval after from the beginning, Sample-2a converted more hydrogen sulfide than Sample-1, and at a faster rate. Rate of weight gain, dw/dt, (indicator of sulfidation rate), as it varies with time for Sample-1 and Sample-2a, has also been compared in Fig-4.3.

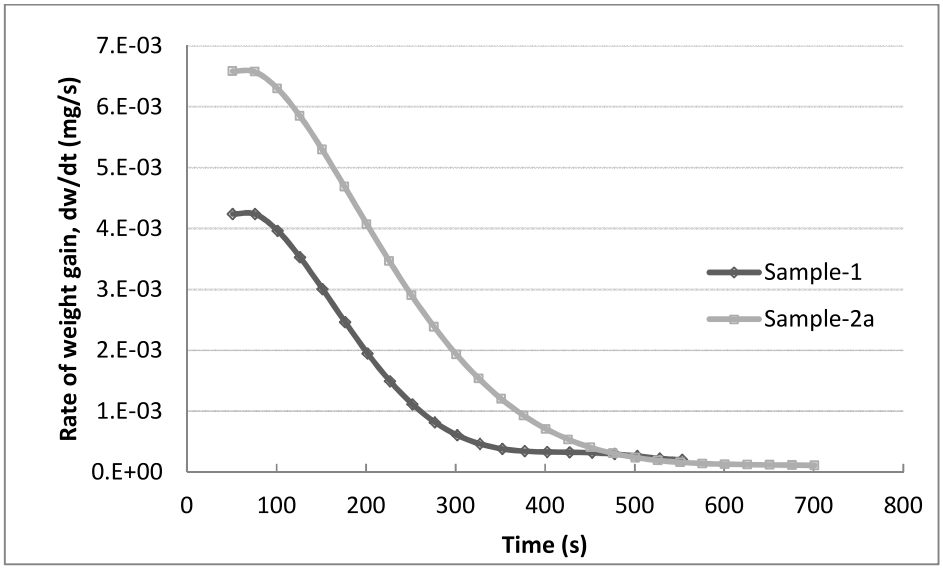

Figure-4.3: Complete Conversion vs. time for Sample-2a during the sulfidation reaction (at 600^{o}C)

Since, Sampe-2a has shown good resistance to the deactivation caused by sorbent reduction (see Ch-3) and now has also shown to be more effective and faster than Sample-1 in terms of removing hydrogen sulfide, it is believed that the composition of Sample-2a will be more acceptable in terms of actual application and hence, it was chosen for further kinetics related investigation and modeling purposes.

4.4.2. Modeling & regime analysis for the rate-controlling step

A non-catalytic gas-solid reaction of the form: $A_g + bB_s \rightarrow cC_g + dD_s$, presumably proceeds via 4 distinct steps: (1) Diffusion of gaseous reactant (A) through the gas-film: from the bulk gas stream to the surface of the outer solid product layer (gas-film diffusion),

(2) Diffusion of reactant gas through the growing layer of solid product (D),

(3) The gas-solid chemical reaction at the surface of the reactant core (B),

(4) Finally, the diffusion of the gaseous product (C) through the product layer and the gas film into the bulk gas stream.

Typically, one of these steps is relatively much slower than the other three. The overall rate of the reaction is then determined by this step, which is distinct from the inherent reaction rate. In order to determine which step is rate-controlling, different mathematical relations called as reaction models, each derived by assuming a specific step as rate-controlling, are then applied to the reaction data and the goodness of the fit is evaluated. If a particular model fits the data well, then the step taken to be the rate-controlling in the model is assumed as the one that will influence the progress of the overall reaction process more than the others.

Model Development

In literature, the reaction between ZnO and H_2S, a noncatalytic gas–solid reaction, has been modeled using various methods. Two of the most frequently used are the unreacted-shrinking-core model and the grain model. Shrinking-core model (Levenspiel, 1999) assumes that the reaction occurs at a sharp interface that divides the reacted outer shell (product “ash”) and the non-reacted core of the solid. This model is most suitable to highly non-porous solid reactants. Grain model, on the other hand, is more popular for modeling reactions between porous solids and gas (Gibson and Harrison, 1980; Huiling et al., 2002; Sohn & Szekely, 1972). This model assumes the solid sorbent to be composed of a large number of fine grains. Inbetween these grains are the macropores, through which the gas has to diffuse to reach the various grains. Each grain, however, still reacts according to the unreacted core model. Since, the grain model

incorporates the structural properties (such as grain size, grain shape, porosity, etc.) of the solid reactants; it can help in estimating the associated structural changes that occur as the reaction progresses. However, this makes the model mathematically more complex. In order to obtain the overall conversion for the reaction and the time varying concentration of the reactants, a set of simultaneous differential equations need to be solved. By making few assumptions, like assuming the gass-solid reaction in consideration being isothermal and first order-reaction system (true for the H_2S reaction order), Sohn & Szekely simplified the model and went on to obtain an approximate solution in which the structural changes on reaction could be neglected without adversely affecting the model's ability to predict the reaction extent (i.e. conversion (X)). It was shown that the extent of reaction (X) of a porous solid could be related to time (t) by the approximate solution:

$$t = P.\{F_r(X)\} + Q.\{F_d(X)\}$$

where

$$P = \frac{\rho_m . r_{g_o}}{k_r . C_{A_0}}$$

$$Q = \frac{\rho_m . R_i^2}{6 . D . C_{A_0}}$$

{ k_r = chemical reaction rate constant, D = diffusion coefficient (both follow Arrhenius dependence on temperature, $k_r = k_0.\exp(-E_{ar}/RT)$, $D = D_0.\exp(-E_{ad}/RT)$, ρ_m = molar density of ZnO in sorbent (mol/l), C_{A0} = Concentration of gaseous reactant H_2S in bulk phase (mol/l), r_{go} = mean grain radius, R_i = initial sorbent radius }.

If we assume the fibrous sorbent in the present case to have a spherically equivalent radius of R_i and being made up of grains with initial mean radius of r_{go}, then $F_r(X)$ and $F_d(x)$ can be derived to have the following expressions:

$$F_r(X) = \left(1 - (1 - X)^{1/3}\right)$$

$$F_d(X) = \left(1 - 3.(1 - X)^{2/3} + 2.(1 - X)\right)$$

These expressions can be derived in a similar way in which the Eq. (3.9) was derived in Chapter-3 by using the unreacted-core model with a specific step as rate controlling. Asymptotic analysis of this approximate solution (Huiling et al., 2002) leads to further simplification: a reaction system that is being purely controlled by the chemical reaction step can then be described by the following relation:

$$t = P.\ \{ F_r(X) \}$$

And a system that is being purely controlled by the product layer diffusion step can be described by the following relation:

$$t = Q.\ \{ F_d(X) \}$$

Sohn–Szekely's approximation equations were limited for the particular reaction system that was being studied and was not appropriate for the study of H_2S removal by ZnO. Only when the overall rate was controlled by chemical reaction of the grain was the model applicable. In order to provide the best fit to experiment data, the approximation of the grain model was improved. The refinement was called the equivalent grain model. The equivalent grain model, which took account of the grain diffusion, was more practical, and has been successfully used to describe this reaction system (Huiling et al., 2002).

The equivalent grain model can be expressed as follows: In the region controlled by chemical reaction rate:

$$t = P.\ \{ F_r(X) \}$$

In the region controlled by product layer diffusion step, a correction term, Q_1 (with units of time), was added to the equation, indicating the contribution of chemical reaction in this region:

$$t = Q_1 + Q.\ \{ F_d(X) \}$$

In order to find which step is rate-controlling, $F_r(X)$ and $F_d(X)$ were plotted against time. Fig-4.4a and 4.4b provide these plots.

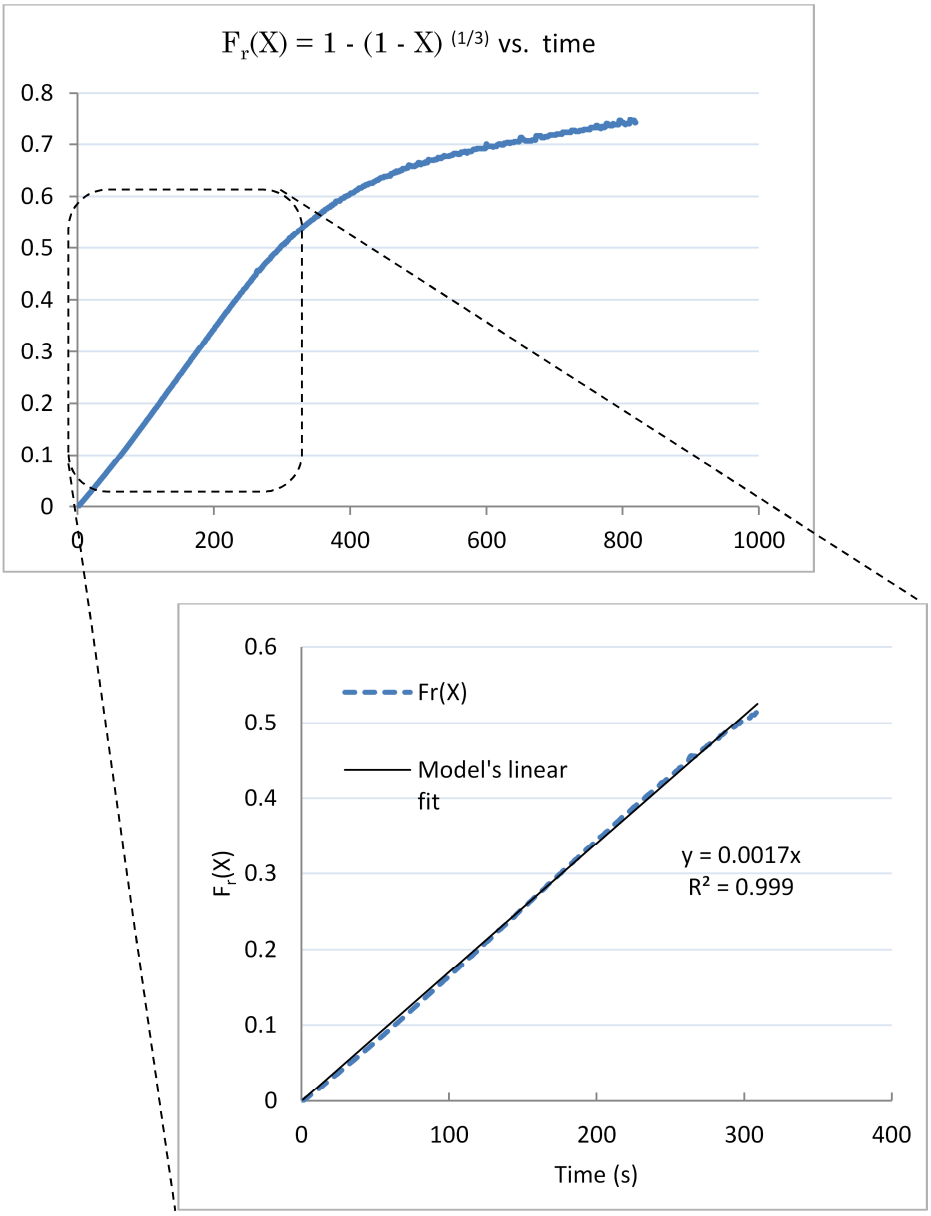

Figure-4.4a: $F_r(X)$ vs. time for Sample-2a

These plots suggest that during the initial stages, the overall rate of sulfidation was being controlled by the surface reaction rate, as inferred by the linear relationship between $F_r(X)$ and t. A deviation from the straight line towards the later stages indicates that the reaction entered the diffusion rate controlled region. The plot of $F_d(X)$ vs. t (Fig-4.4b) clearly shows an overall non-linear relationship. However, during the later stages (t > 500s), a linear behavior can be observed (as shown by red curve in the top portion of Fig-4.4b). The corrected

model. During the early stages, application of Equivalent Grain Model, which introduces a correction term to incorporate the effect of chemical reaction, fits the data only approximately (lower plot in Fig-4.4b) and a linear relationship is obtained which does not pass through the origin. The original grain model (without the intercept) for the relationship of $F_d(X)$ with time does not follow the relevant equation. Thus, the equivalent grain model is better option for describing the kinetic behavior of removal H_2S by ZnO.

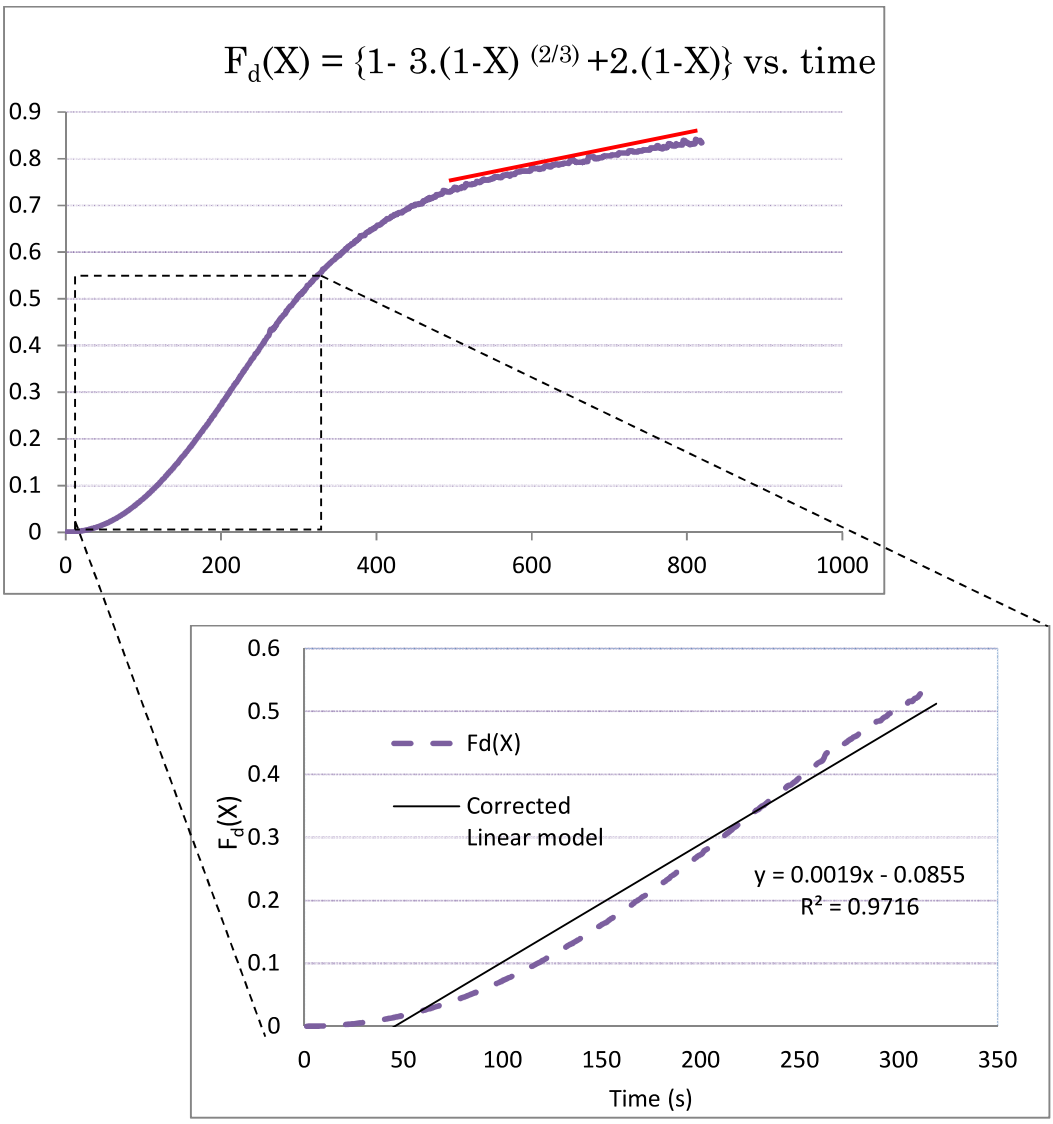

Figure-4.4b: $F_d(X)$ vs. time for Sample-2a

Many researchers in the past, who attempted to model the sulfidation reaction, found that the primary limitation to reaction rate on both Zn–Ti–O and ZnO is diffusion through a ZnS

product layer (Gibson & Harrison, 1980; Woods et al. 1990; Harrison, 1998). The result of the present study, that for nanofibrous adsorbent specimens the inherent chemical reaction is the rate-controlling step for a significant duration of the sulfidation process, is supportive of the central proposition in this work, which proposes that the sorbent morphology and its overall architecture play an important role in influencing the overall rate of the sulfur removal process. The fact that the product-layer diffusion is no longer the primary limitation and the inherently fast reaction kinetics of the reaction between ZnO and H_2S now determines the overall rate of the process, is a success for the proposed sorbent geometry. This knowledge can allow for the development of fast adsorption-based sulfur removal systems. Such fast adsorption processes have a potential to limit the occurrence of deep-sulfidation of the sorbents, thus avoiding the condition which usually leads to sorbent deactivation as in the case of bulk sorbents (Wang & Stephanopoulos, 2005).

For a given temperature, k_r and D can be calculated from the slope of the fitted line. For different temperatures, dependence of k_r (T) and D (T) on temperature can be determined, from which kinetic parameters like activation energy and pre-exponential factor, A_0 (or maximum diffusion coefficient D_0) can be found. Effect of temperature will be studied as a part of the future work. Estimation of kinetic parameters and comparison of the activation energies associated with the chemical reaction and the product layer diffusion will help in strengthening the above findings.

4.5. Post-sulfidation characterization results

4.5.1. SEM analysis

To examine the changes in the specimen's morphology after the sulfidation, SEM was used. Figures Fig-4.5 (Sample-1), Fig-4.6 (Sample-2a), Fig-4.7 (fiber size distribution, Sample-1), compare the sulfided specimens with the fresh samples. Although, the individual grains / crystallites in each case, were too small (~ 10 – 15nm from XRD) to be resolved by SEM (see TEM images in Ch-2), the overall fibrous morphology can be seen as well-preserved after sulfidation. The mean diameter does not appear to have been altered by much (see Fig-4.7). No

signs of spalling or fiber fragmentation are evident. However, in Fig-4.5 for Sample-1, a morphological feature in the sulfided specimen appears to be distinct from the fresh specimen: an array of non-uniformly distributed fibers supporting dendritic growth branching off from the parent fibers. Such appearance of hierarchical growth seems to be largely absent in the sulfided Sample-2a (Fig-4.6). Also, even in Sample-1, such features were not found to be present on all the fibers and appeared to occur sporadically. This may be suggestive of the fact that for such growth to occur, a specific set of local conditions must be at work. In literature, 1-D nanostructures of zinc oxide have been shown to exhibit such hierarchical structures (known as nanobranches, nano-combs, nano-saws) during the intended growth via processes like solid-vapor phase thermal sublimation (Zhong, 2004) electrodeposition (Xu et al., 2007), or wet chemical deposition (Zhang et al., 2007). In the present case, these nanobranches most likely consist of zinc sulfide, as confirmed later by EDX, XPS and XRD (See Sec-4.5.2, 4.5.3 & 4.5.4).

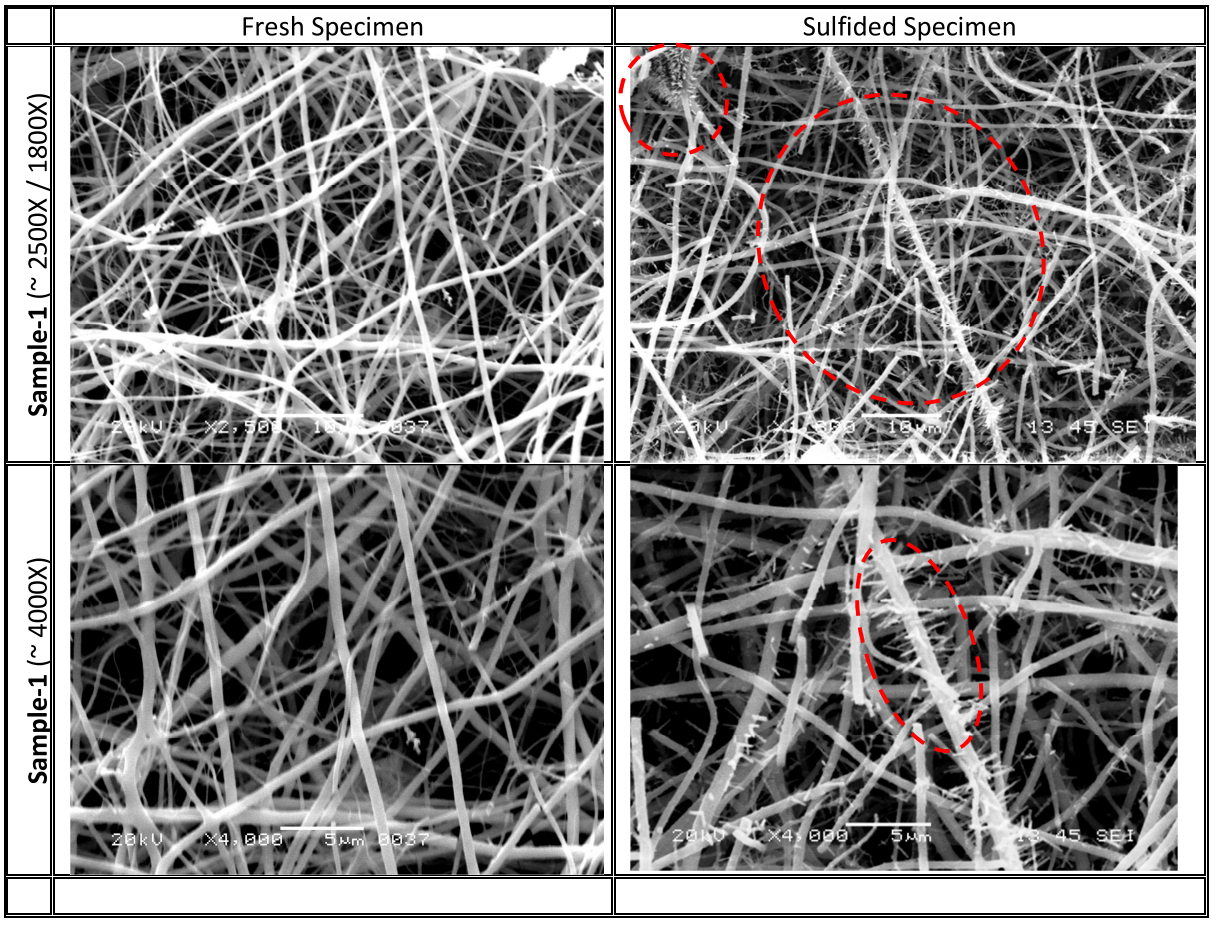

Figure-4.5: Comparison of surface morphology of **Sample-1**, before & after sulfidation (at 600^{o}C). Regions with hierarchical growth have been highlighted

Since, reduction and sulfidation were carried out (step-wise) in the same chamber, some of the residual volatilized zinc (produced as a result of reduction of free zinc oxide) could have led to a gas-vapor reaction between hydrogen sulfide and the volatilized zinc that probably led to formation of gas-phase zinc sulfide, which subsequently deposited anisotropically on some preferred locations over the fibers, resulting in the observed hierarchical growth pattern. The fact that such features were absent in Sample-2a, which was deficient in free zinc oxide and didn't undergo much reduction, reinforces this possibility. The mechanism would then be similar to hierarchical growth of zinc oxide via solid-vapor sublimation as discussed by Zhong (2004). Sulfidation of the parent fiber may have been going on simultaneously. It may be possible then that the polar surfaces of ZnS nanofibers could induce a preferred anisotropic-

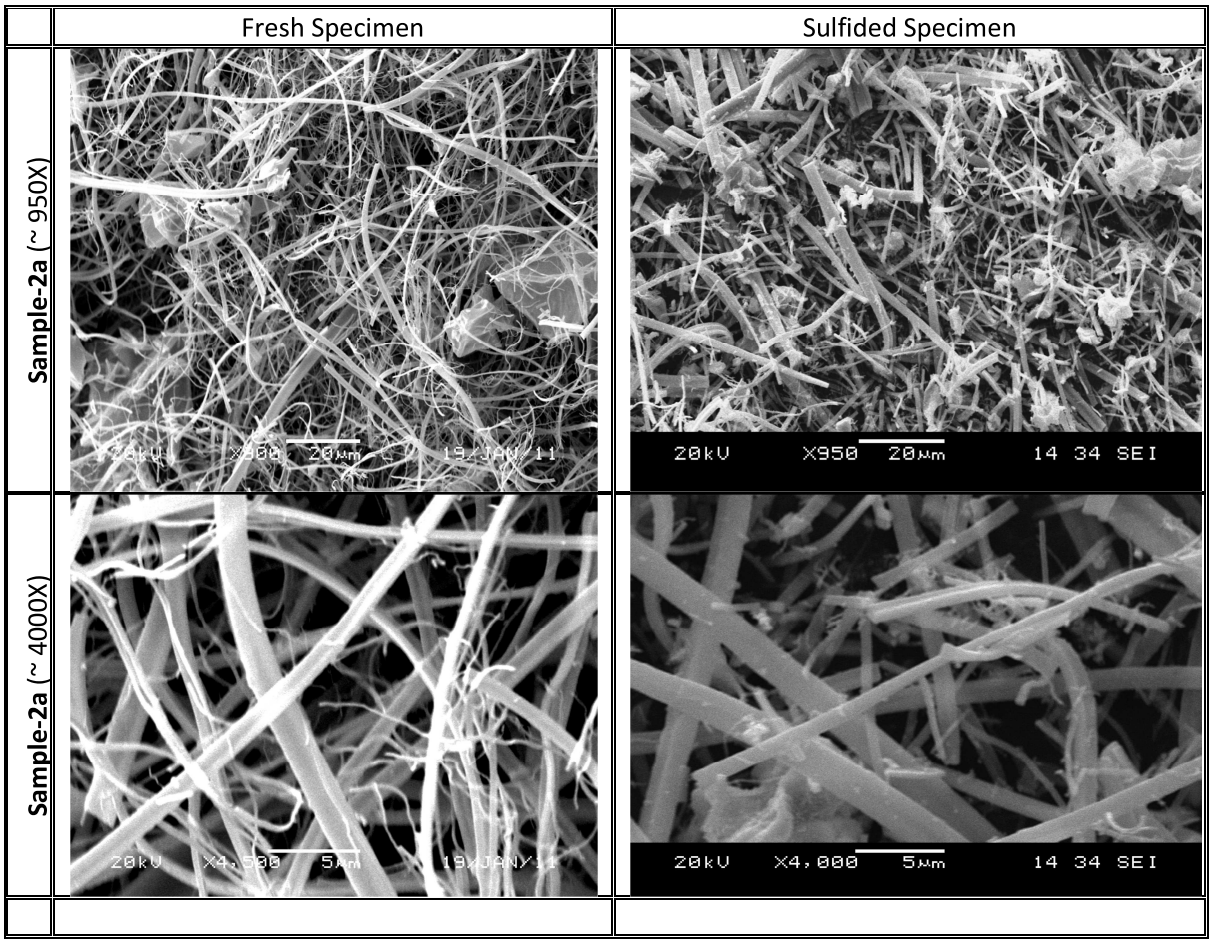

Figure-4.6: Comparison of surface morphology of **Sample-2a**, before & after sulfidation (at 600^{o}C)

growth of ZnO/ZnS nanobranches on the fiber surface. In addition, the local concentration of H_2S gas and Zn vapor may have decided the density and location of the. Thus, a combination of the polar surface of ZnS/ZnO and local gas-vapor concentration may have determined the observed growth of ZnS/ZnO hierarchical nanostructures. It will be interesting to develop and test this hypothesis more rigorously in a future study.

Such dendritic growth, during sulfidation of 1-D nanostructured zinc oxide, is very different from the reported growth patterns observed in bulk zinc oxides (for instance, pellet based ZnO, refer Fig-2.1), in which sulfidation proceeds primarily in a core-shell growth pattern with zinc sulfide (reaction product) forming a growing layer over a shrinking zinc oxide core. Since, the sulfidation reaction is inherently fast, this difference in growth patterns can be crucial in determining the overall reaction rate. Core-sheath growth would have inevitably lead to increased mass transfer resistance to the ongoing reaction, whereas, dendritic growth may actually facilitate the reaction by providing additional surfaces for the reaction to proceed without causing additional mass transfer resistance. This will lead to faster overall reaction allowing for faster regeneration operation, which in turn will avoid deep sorbent sulfidation and

Sulfided Sample-1 Size distribution (µm)	
Mean	0.482
SD	0.138
Min	0.201
Max	0.807

Fresh Sample-1 Size distribution (µm)	
Mean	0.435
SD	0.165
Min	0.173
Max	0.849

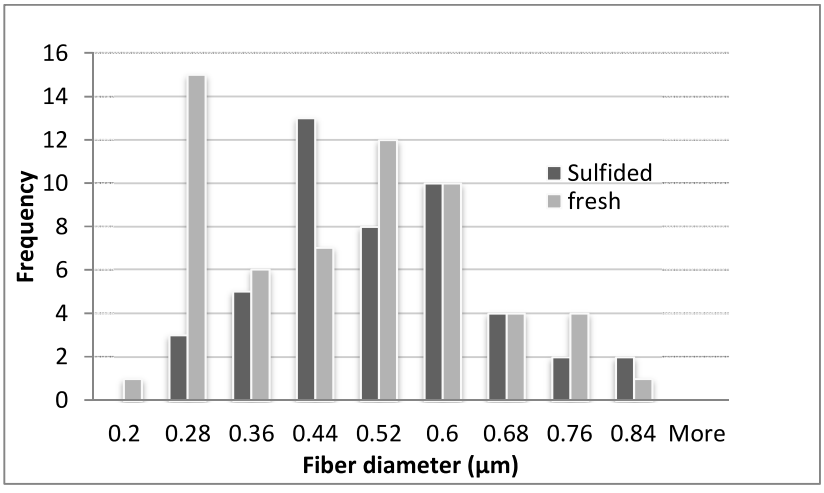

Figure-4.7: Comparison of fiber size distribution for Sample-1, before & after sulfidation (at 600^{o}C)

thus, extending sorbent's lifetime. This observation corroborates the proposed thesis of the current work which states that the 1-D nanostructured adsorbents, in the form of fibrous metal

oxides, may provide some distinct advantages during the gas-solid reaction, which, otherwise, are difficult to attain when working with the geometry & morphology of a bulk sorbent.

Ostermann et al. (2006) showed that it is possible to use electrospinning to grow nanofibers with controllable hierarchical structures. Growth of single-crystal V_2O_5 nanorods stemming from the composite nanofibers of V_2O_5 & TiO_2 was demonstrated. The size of the resulting V_2O_5 nanorods was shown to be controllable by varying the composition of the nanofibers and/or the calcination temperature. In the present study, if a way to control and increase the chances of obtaining specific polar planes of composite zinc titanates crystal as the fiber outer surfaces can be found, then it is possible to expect much larger occurrence of similar dendritic growth in such composite metal oxides as well. This can serve as an interesting area of study for the future work.

4.5.2. Results from EDX analysis

Fig-4.8 & 4.9 compares the EDX spectra, (before and after sulfidation) of Sample-1 & Sample-2a. Atomic compositions, corresponding to the observed local region, have also been included. A distinct sulfur peak, in the sulfided samples in both the cases, indicates formation of zinc sulfide. In order to confirm if the peak indeed corresponds to sulfide form of sulfer and not the sulfate form, XPS analysis was carried out, results of which have been included in one of the following sections.

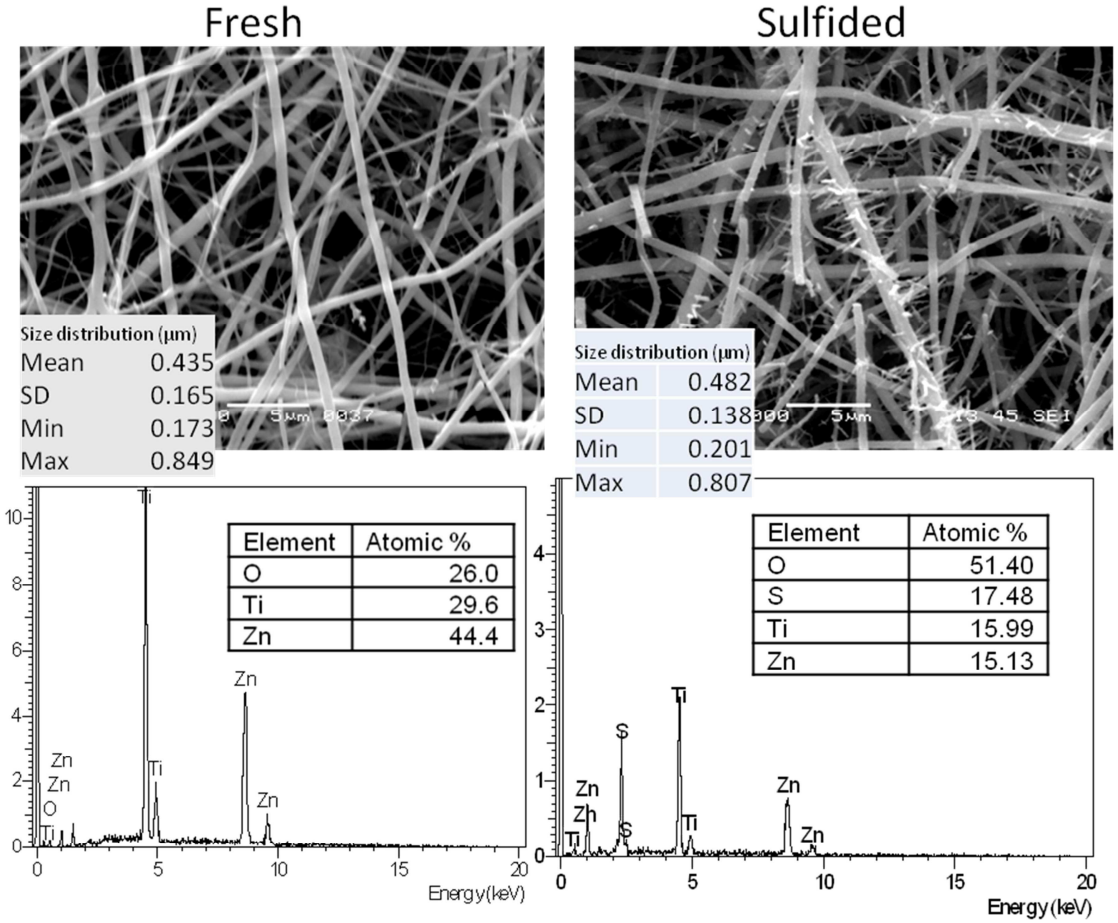

Figure-4.8: Comparison EDX spectra for **Sample-1**, before & after sulfidation (at 600^{o}C)

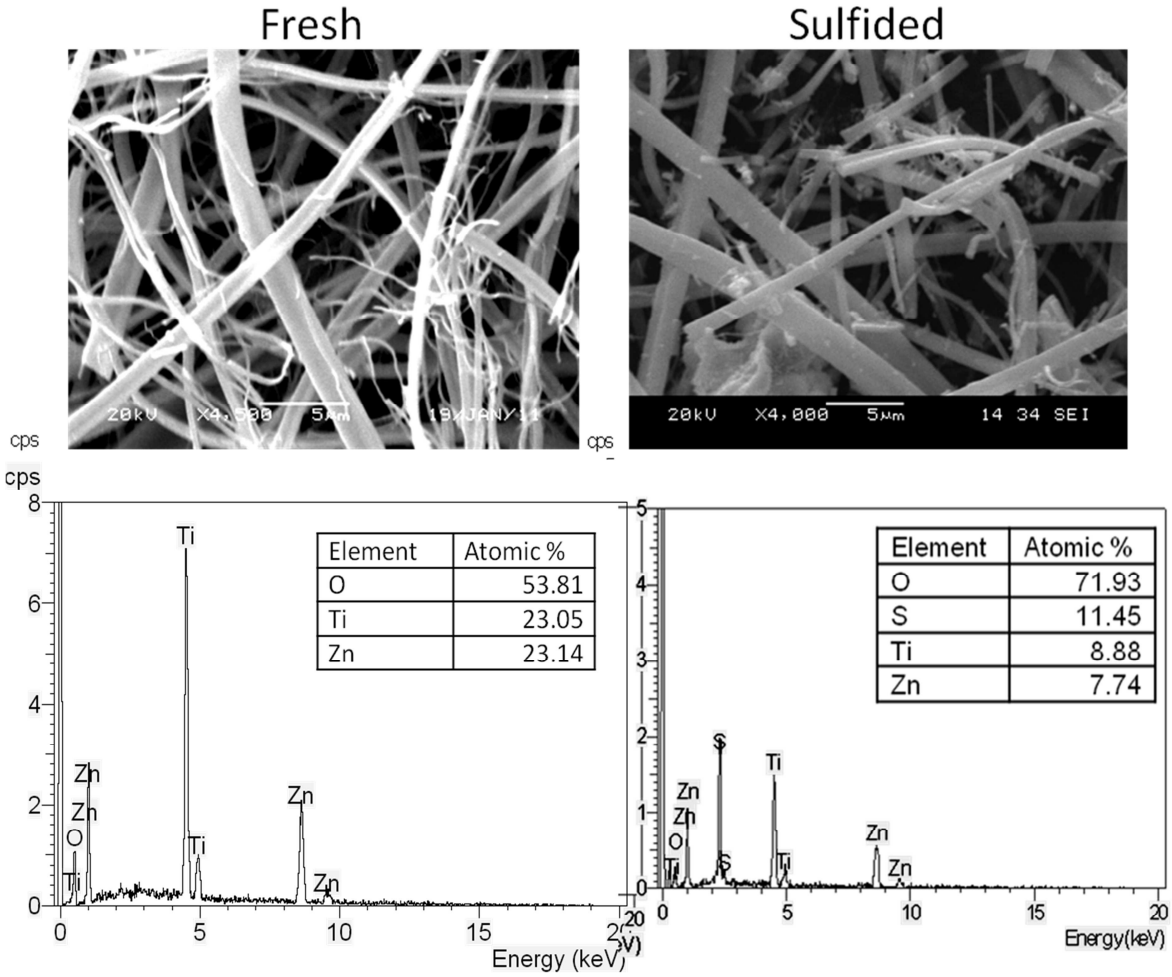

Figure-4.9: Comparison of EDX spectra for **Sample-2a,** before & after sulfidation (at 600^{o}C)

4.5.3. XPS analysis

In order to carry out more precise surface characterization of the fresh and sulfided samples, XPS analysis was carried out. In XPS, X-ray exposure leads to photoemission of electron which allows calculation of the associated binding energy characteristic to the element and its corresponding energy level. XPS can not only identify the elemental composition of the specimen, but can also determine the chemical or the oxidation state of the identified element (due to characteristic peak shifts from the standard element peak). This feature, in our case, can help in estimating the stoichiometry of different possible reaction products that would have formed on sulfidation.

The system used for this study (Kratos Axis Ultra) has a monochromatized Al Kα X-ray source of 15kV (~10mA). Instrument consists of separate specimen preparation/transfer and analysis chambers, typically operated at 5E-07 torr and 1E-09 torr respectively. The samples were loaded on to a motorized sample bar, the location of which can be varied using an external lever.

Fig-4.10 compares the overall survey spectra together with a quantitative estimate of the surface composition of the fresh against the sulfided specimens of Sample-2a. The elemental composition was estimated using O(1s), Ti(2p), Zn(2p) and S(2p) signatures. All the peaks were identified and assigned to their corresponding elements (Zn, Ti, O or S). Carbon peak appears since the specimens were mounted on a carbon tape (In fact, the carbon peak was used as a reference for assigning other peaks).

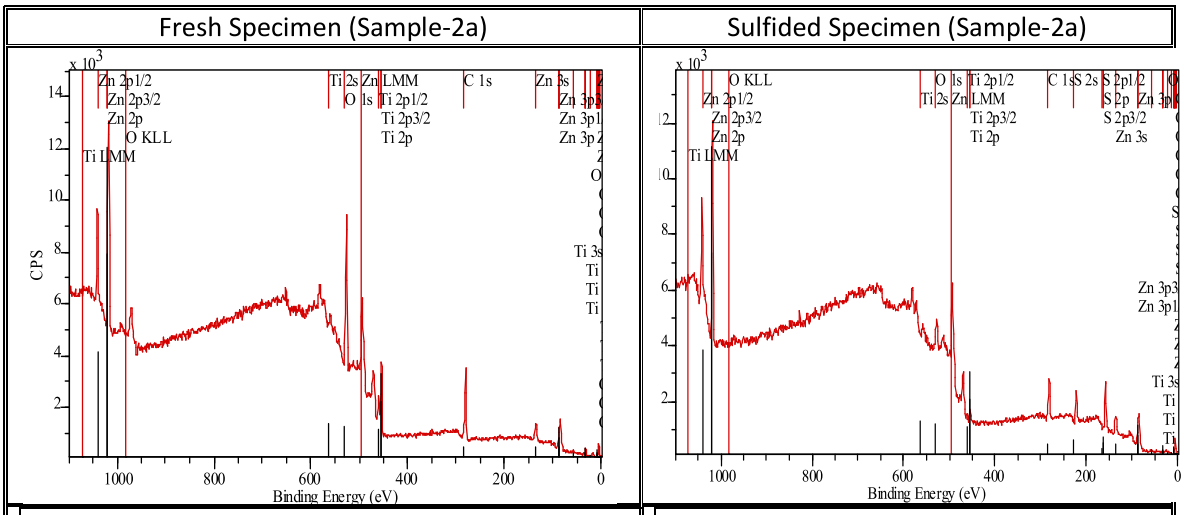

Atomic Concentration %				
Zn 2p	O 1s	Ti 2p	C 1s	S 2p
7.01	35.07	5.72	52.2	—

Atomic Concentration %				
Zn 2p	O 1s	Ti 2p	C 1s	S 2p
8.23	14.19	0.48	65.84	11.26

Figure-4.10: Comparison of XPS survey spectra for **Sample-2a,** before & after sulfidation (at 600^{o}C)

Each elemental peak was then resolved to verify if there is any chemical shift that may have been present. Fig-4.11 shows the resolved peaks for the different elements (Zn, Ti, O or S) along with the corresponding profile fitted curves (using 30% Gaussian / 7O%

Lorentzian peak shapes), which are characteristic of the oxidation states in which the elements are present.

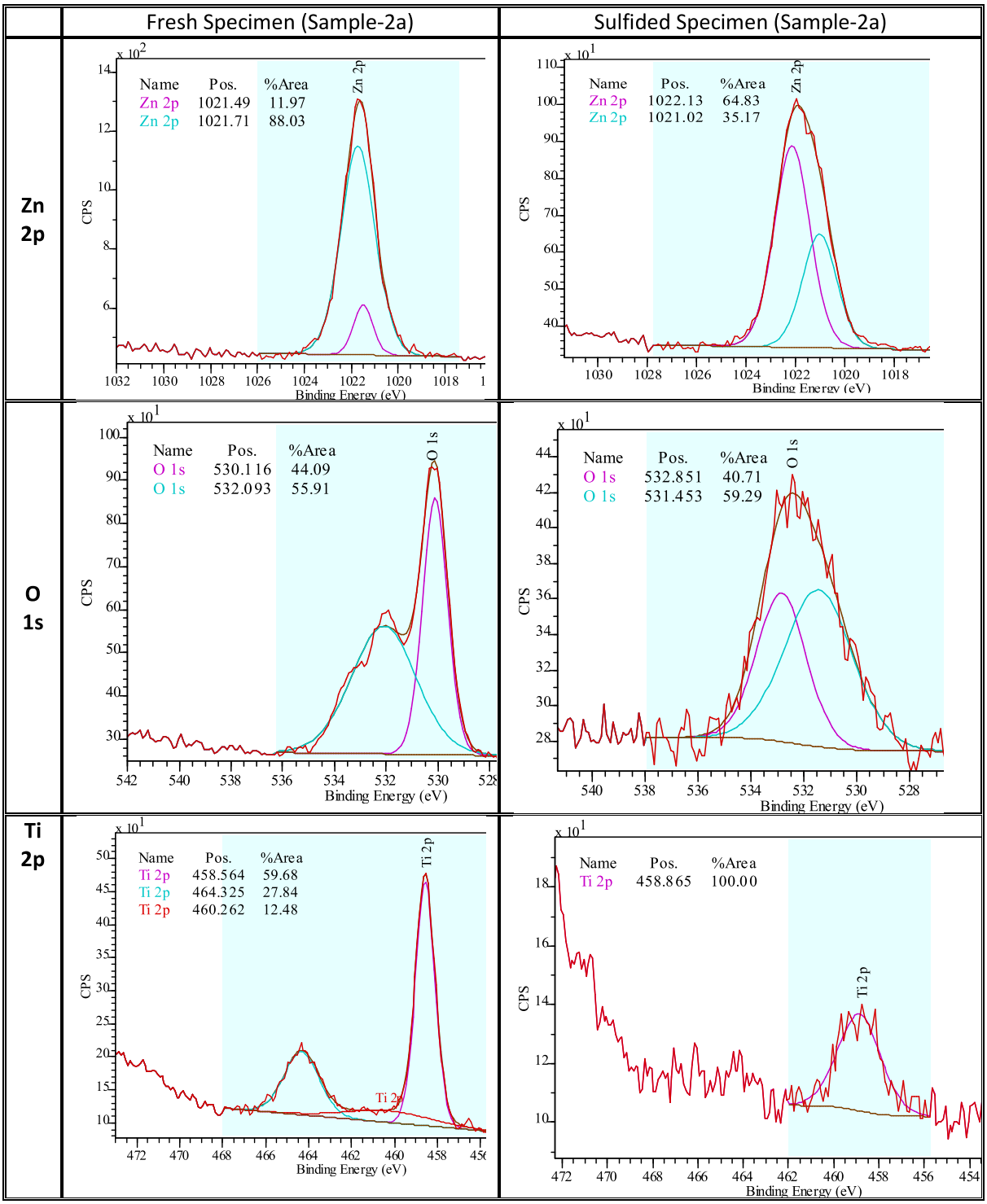

Figure-4.11(contd. on next page): Comparison of the individual elemental peaks, before & after sulfidation (Sample-2a)

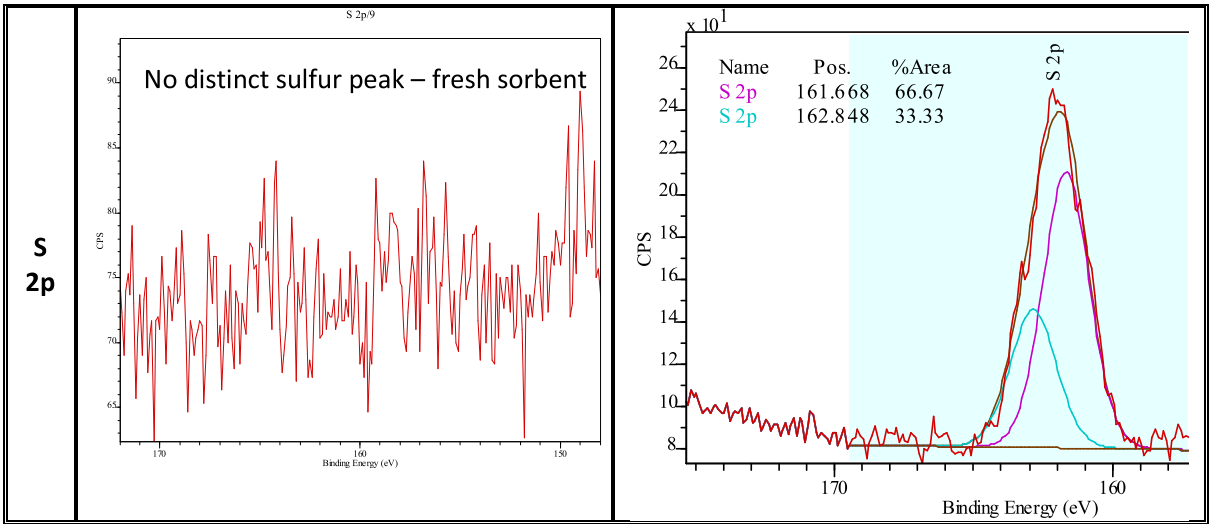

Figure-4.11 (cont.): Comparison of the individual elemental peaks, before & after sulfidation (at 600^{o}C, Sample-2a)

In order to identify the oxidation states of sulfur, the observed peaks in the sulfur spectral region were compared with those of the standard compounds (shown in Table – 4.3). Sulfur spectra were fitted with 30% Gaussian / 7O% Lorentzian peak shapes with spin-orbit peak intervals and area ratios of 1.18 eV and 2.00, respectively. Only one sulfur peak was observed (in the sulfided specimen). For clarity, its spin-orbit components have also been included. This peak (~161.67eV) correspond well with the standard sulfide peak (161.7eV), implying that the sulfur is present in its sulfide form. Absence of any significant intensity at around 168 - 170eV is indicative of the fact that no sulfates are present (as it is clear from the Table-4.2 that it will be hard to comment from the XPS data alone, whether the sulfide is from ZnS or TiS_2, although, thermodynamically, we know that at 600^{o}C formation of TiS_2 is not as favorable as the formation of ZnS. On the other hand, the current XPS data is reasonably convincing and sufficient for to ruling out presence of any sulfate in the sulfided specimen).

Table-4.3: Comparison of the observed elemental peaks with the standard* XPS data for the sulfided Sample-2a (at 600^{o}C)

Sulfided Specimen 600^{o}C	**Binding energies (eV)**					
	S 2p		**Zn 2p$_{3/2}$**		**Ti 2p$_{3/2}$**	
Compound	Standard*	Observed	Standard*	Observed	Standard	Observed
ZnS	161.7	161.67	1022.3	1022.13	—	—
$ZnSO_4$	169.0	none	1022.9	none	—	—
Ti(IV)S_2	161.5	161.67	—	—	458.50	458.87

*Siriwardane and Poston (1990)

Many researchers in the literature have reported the formation of zinc sulfate during the sulfidation step (Siriwardane & Poston, 1990; Harrison, 1998; Poston, 1996; Pineda et al., 1997). Sulfate formation, during the sulfidation step, is generally attributed to the release of oxygen during the phase separation of zinc titanate (supposed to occur during its reaction with H_2S, Lew et al., 1989). It is supposed to proceed via following route:

$$ZnO_{(from\ zinc\ titanate)} + H_2S \Leftrightarrow ZnS + H_2O_{(g)}$$

$$ZnS + 2O_2\ (from\ the\ oxygen\ release) \leftrightarrow ZnSO_4$$

One of the possible reasons for the observed absence of sulfate formation in the current study may be related to the possibility that during sulfidation, phase separation may still be occurring (due to observed titania as one of the products (Sec-4.5.4, Fig-4.13)); however, due to the nanostructured grains, metal atoms in the oxide bind with oxygen much strongly and no or minimal oxygen release happens. Since, there is no release of oxygen from the sorbent, linked to the formation of zinc sulfate (Siriwardane & Poston, 1990), zinc sulfide happens to be the major product of the sulfidation reaction. A more detailed analysis needs to be carried out to confirm this hypothesis.

Absence of formation of any sulfate compounds during the sulfidation of nanofibrous zinc titanate adsorbent is expected to improve the chances of carrying out complete regeneration. As discussed earlier, due to sulfates' poor reversibility, formation of compounds such as zinc sulfate is, to a large extent, has been held responsible for the incomplete regeneration of oxide based sorbents.

4.5.4. XRD analysis

XRD analysis was carried out to indentify the crystal structures and the corresponding composition of the sulfidation products. Same instrument and setup were used as in the case of fresh sorbent (described earlier in Chapter-2). Fig-4.12 shows the XRD spectrum of the sulfided Sample-1. It can be seen that, primarily, there were only two components in the sulfided sample: ZnS (wurtzite) and TiO_2 (rutile). Fig-4.13 gives a estimate of the relative amounts of these two products (weight percentage), obtained as a result of performing quantitative analysis on the XRD data by using profile-fitted curves.

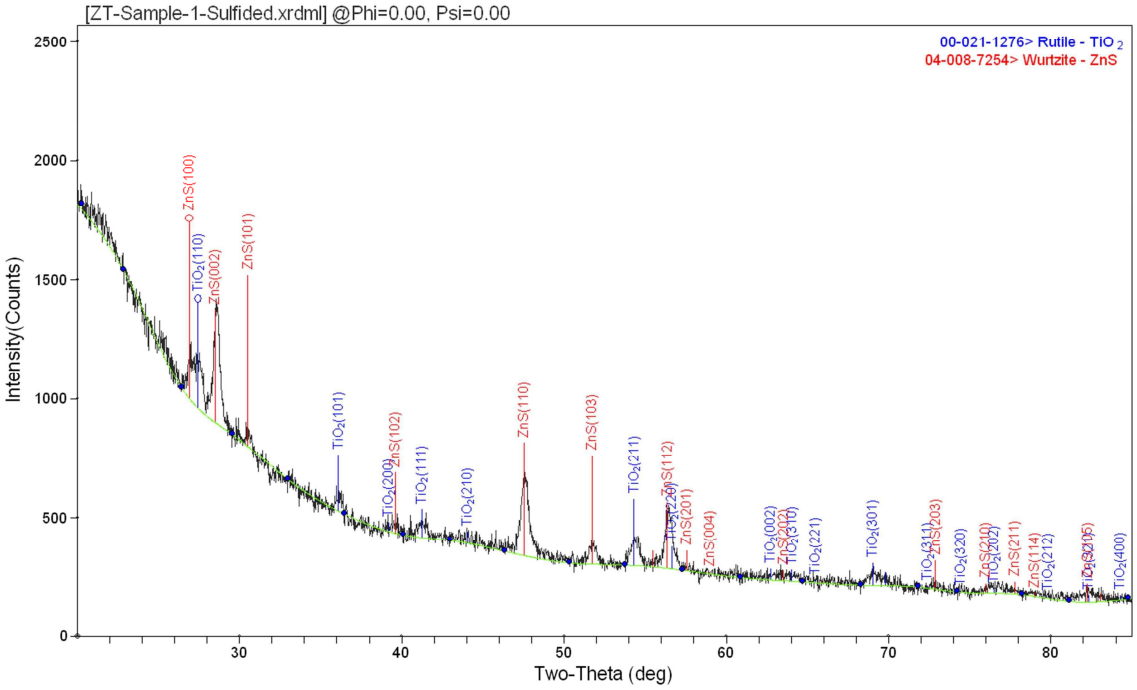

Figure-4.12: XRD spectrum of Sample-1 after sulfidation (at 600^{o}C)

(Note: The large hump observed near lower angles was caused by the glass substrate that was used to mount the specimen).

These results confirm our earlier postulate that most of the zinc oxide component of the specimen (here Sample-1), either the free ZnO or from mixed metal oxide, reacts with H2S, whereas titania remains inert. Lew et al., 1989 proposed that the zinc oxide from the mixed metal oxide component can react because the zinc titanate, on exposure to H2S, undergoes

phase separation into individual oxides before the sulfidation occurs. Although, this is generally regarded as a plausible mechanism, no direct experimental evidence has been found yet.

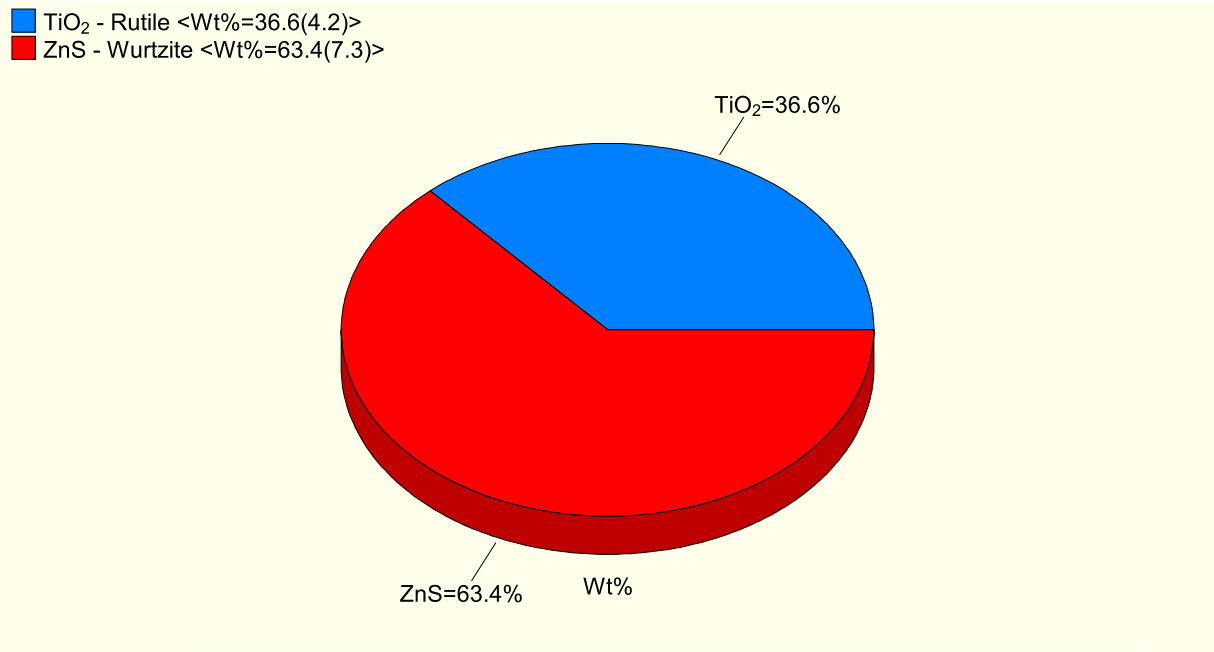

Figure-4.13: Quantitative analysis from the profile-fitted peaks (Sulfided Sample-1)

ZnS (Wurtzite)	Crystal structure identified by XRD on post-sulfided specimen (Sample-1) 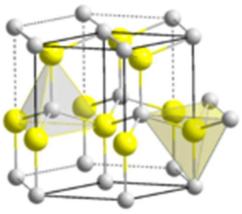	**ZnS Wurtzite: Hexagonal** **Cell Dimensions (Å):** a = 3.82, c = 6.2 **Axial Ratios:** a:c = 1:1.64
ZnS (Sphalerite)	Other possible crystal structure for ZnS (absent from the XRD spectrum) 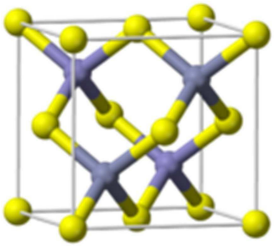	**ZnS Sphalerite: Cubic** **Cell Dimensions (Å):** a = 5.41, c=a **Axis ratios** a:c = 1:1

Figure-4.14: Different polymorphs of Zinc Sulfide (Images retrieved from http://en.wikipedia.org/wiki/Zinc_sulfide)

It is interesting to note that although zinc sulfide's cubic form (sphalerite) is known to be more stable form (below 1000^{o}C), it was its hexagonal form (wurtzite) which was identified as the major product (Fig-4.12 & 4.14). Yin and Bando (2005) described how the nanostructures (nanobelts in particular) can facilitate the formation of wurtzite phase which leads to an overall lower surface energy in the nanostructures. Formation of wurtzite phase is beneficial to sorbent regeneration. Schultze (1995) used thermogravimetric analysis to study the oxidation of phase-pure sphalerite and wurtzite forms of ZnS. It was found that the wurtzite tend to oxidize directly to zinc oxide whereas oxidation of sphalerite resulted in the formation of $ZnSO_4$ and $Zn_3O(SO_4)_2$. As discussed previously, formation of zinc sulfate, either during oxidation or sulfidation, is detrimental to a multi-cycle process as it contributes to progressive underutilization of the adsorbent. Formation of wurtzite form of zinc sulfide in the present study, thus, was seen as another potential advantage of using nanostructured sorbent morphology. In literature, phase analysis of the sulfidation products and its relation to sorbent structure has received comparatively much less attention. It will be helpful to do a future study to understand how the microstructure of the sorbent influences the formation of different sulfidation products. In literature, this aspect has not been given much attention.

4.6. Sorbent regeneration

4.6.1. Introduction

To make the use of a solid desulfurizing sorbent economical, it is important for it to be reusable, preferably over many cycles. Use of metal / mixed metal oxides as regenerable adsorbents, however, has seen only a limited success and that too has been limited only to a few-cycle operation. Several reasons have been identified for this inadequate regeneration potential of metal oxides. Before discussing these reasons, the process for regeneration will be discussed first.

Metal sulfides, the typical chemical state of metal oxides post-sulfidation, can be converted back to their oxide form most commonly by subjecting then to oxidation, either in

air, oxygen or steam typically at high temperatures (650^{o}C to 900^{o}C). Following is the overall reaction that takes place during sorbent oxidation:

$$M_x S_y + \frac{3}{2} y.O_2 \Leftrightarrow M_x O_y + y.SO_2$$

The above reaction is typical of sulfides of transition metals. Rare-earth metal oxides, like ceria or lanthanum oxide, typically form an oxysulfide on sulfidation (like Ce_2O_2S for the case of cerium) and the overall reaction that occurs during the oxidation of these sulfided rare-earth metal oxides is given as follows:

$$2M_2O_2\,S(s) + 2O_2(g) \Leftrightarrow 4MO_2(s) + S_2(g)$$

(Note: In the above reaction, metal (M) in the oxysulfide goes from 3+ valence state to 4+ state in oxide).

Major challenges associated with the regeneration process can be attributed to the following two causes: high temperature of the regeneration process and the progressive loss of chemical reactivity and the incomplete oxidation due to the increasing mass transfer resistance caused by the growing product layer. All of these reasons contribute to increasing underutilization and physical degradation of the sorbent. These factors become even more limiting for the case of mixed metal oxides which already contain an inert component (like TiO_2 in zinc titanates: $ZnTiO_3$, Zn_2TiO_4). In particular, Woods et al. (1990) showed that the zinc titanates, considered as the more efficient metal oxide based sorbents currently available, can be regenerated effectively only when the regeneration temperature exceeds 625^{o}C. There are many problems associated with the high temperature of the regeneration process. First, high temperature operation is responsible for the sintering of the sorbent i.e. sorbent tends to lose specific surface area due to the gradual grain growth caused by the high temperatures. Another reason for avoiding the high temperatures, as discussed previously, is due to the design limitations linked with an industrial scale operation, the design temperature of the desulfurizing unit, therefore, is typically fixed at a temperature below 600^{o}C (Jothimurugesan & Gangwal, 1998; Slimane et al., 2002). Higher temperature is known to interfere with the operation of valves which are being used in the process. Furthermore, regeneration of the bulk

sorbents is typically carried out at a temperature that is typically couple of hundred degrees higher than the sulfidation temperature. The key reason for bridging the gap between the sulfidation and regeneration is to minimize the thermal stresses that may develop in the sorbent due to the frequent cycling between the two operations. These temperatures quickly lead to spalling and mechanical disintegration of the sorbent.

Mechanical disintegration and surface area loss also leads to a loss of the active sites available for adsorption and reaction. This in turn leads to slower and incomplete oxidation. This results in the accumulation of the unconverted metal sulfide over the surface of the bulk sorbents. Such product layer growth is known to be associated with the increased diffusion resistances resulting in overall sluggish operation. More the product remains unoxidized, lesser is the number of active sites available during the regeneration reaction, which again end up increasing the portion of incompletely-oxidized sorbent — a cycle resulting in rapid deactivation of the sorbent.

In order to overcome these limitations associated with the regeneration of metal oxide based sorbent, many researchers attempted modification of the chemical make-up of the sorbent by introducing additional promoters. For instance, Jothimurugesan and Gangwal (1998) demonstrated that the co-precipitation of 5 wt % Ni and 5 wt % Co with zinc titanate (solid mixture of $ZnO{-}TiO_2$, 1.5:1) effectively reduced the regeneration temperature without significantly affecting sorbent's sulfur capacity. TGA and fixed-bed microreactor were used to determine performance of the regeneration process. Regeneration temperatures of as low as 475^oC were reported. Addition of 5 wt % Cu, a cheaper option, was found to be equally effective as 5 wt % Co + 5 wt % Ni in lowering the regeneration temperature, however, the Cu additive adversely affected the ability for H_2S removal in subsequent cycles. The reasons causing these changes were not completely understood. As pointed by Cheah et al. (2009) recently, the reduction in the regeneration temperature did not correlate with the pore volume or surface area of the sorbent.

Another option that has been mostly overlooked for improving the regeneration performance is the deliberate introduction of structure-induced functionalities in the adsorbent

instead of the more common method of introducing chemical additives. Investigation of different sorbent design morphologies (other than the popular pellet based design) with higher specific surface area, calculated modifications of the sorbent microstructure, adoption of a controllable sorbent synthesis methods for obtaining control over the internal pore structure and other possible methods that can lead to improved performance without any chemical modification can thought to be introducing structure-induced functionalities. Nanofibrous metal oxides, obtained from the electrospinning process, can come under this category of adsorbents.

Motivation

The motivation for using polycrystalline nanostructured sorbents is two-fold: first, the potential to sustain sufficient chemical reactivity at lower temperatures because of the nanofibers' higher specific surface area along with the increased number of active sites due to the larger number of crystal defects and the nanosized grains present in the polycrystalline sample; Second reason for investigating such adsorbents is the minimal mass transfer resistance offered at such scales.

4.6.2. Regeneration kinetics

The kinetics for the regeneration previously synthesized nanofibrous zinc titanate sorbents was evaluated by using the method of thermogravimetric analysis. The TGA instrument used in these experiments was a DuPont 951 with an option of using a corrosive reactive atmosphere (needed for the sulfidation step H_2S). The reaction progress was estimated by monitoring the weight changes of the sorbent sample as a function of time at a fixed temperature with the desired gas compositions (isothermal temperature). A known amount of sample was loaded on the sample holder. The temperature was raised to the desired reaction temperature at a constant rate (15 ^oC /min, either to 400^oC, 500^oC or 600^oC). Samples were first subjected to a reduction reaction with 4% H_2 (by vol.) in the N_2 gas stream for around 90 mins. This step was followed by sulfidation for 60 mins at the same temperature with a gas stream containing 1% H_2S in N_2. A portion of the sample was removed for characterization and the remaining portion was ramped back to the previous operating temperature. Finally, regeneration was carried out with 3% O_2 (rest N_2) for 70 mins at the same temperature. It is to be noted here that the oxidation temperature was kept same as the sulfidation temperature (it was either 400^oC or 500^oC or 600^oC).

Fig-4.15 shows the instrument output for Sample-2a (Fig-4.17 for Sample-1), change in weight vs. time, for the regeneration step at 600^oC. Weight loss was attributed to the steady formation of zinc oxide whose molar mass is less than the reactant zinc sulfide.

The initial rate of oxidation reaction was calculated based upon the moles of zinc oxide being formed per unit time per unit area. Mathematically, this was defined as following:

$$R_0 = \frac{\left|dW/dt\right|_0}{A_0 \cdot (M_{ZnS} - M_{ZnO})}$$

Where

$(dW/dt)_0$ = initial rate of change in the sample weight

A_0 = Total area of the sorbent at t = 0 ($A_0 = W_0 * \alpha_0$)

M_{ZnS} , M_{ZnO} = Molecular weight of zinc sulfide =97.47 g/g-mol, zinc oxide = 81.4 g/g-mol

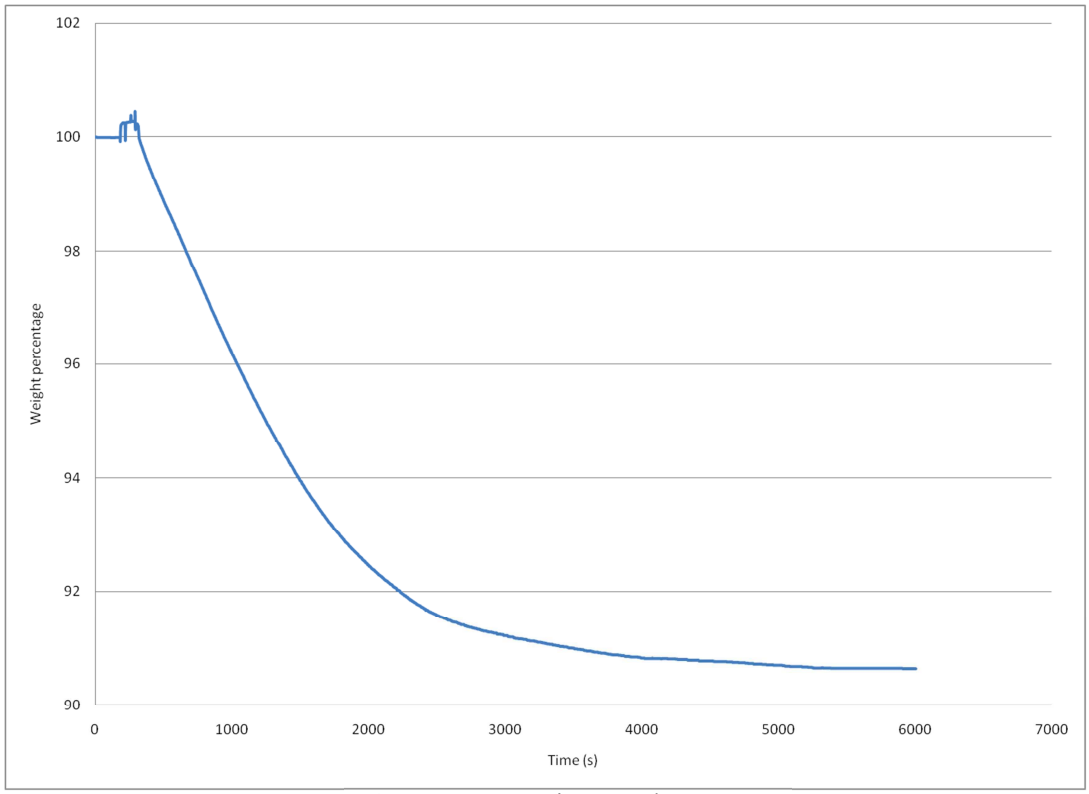

Figure-4.15: Sample-2a oxidation

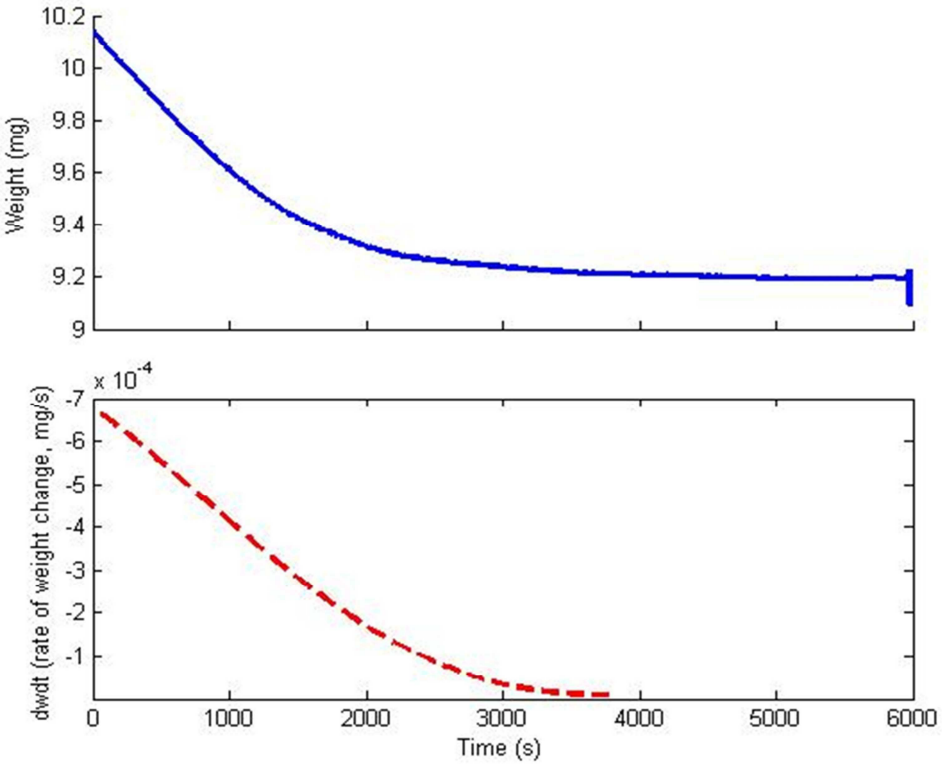

Figure-4.16: Rate of weight change (bottom curve) for Sample-2a oxidation at 600C

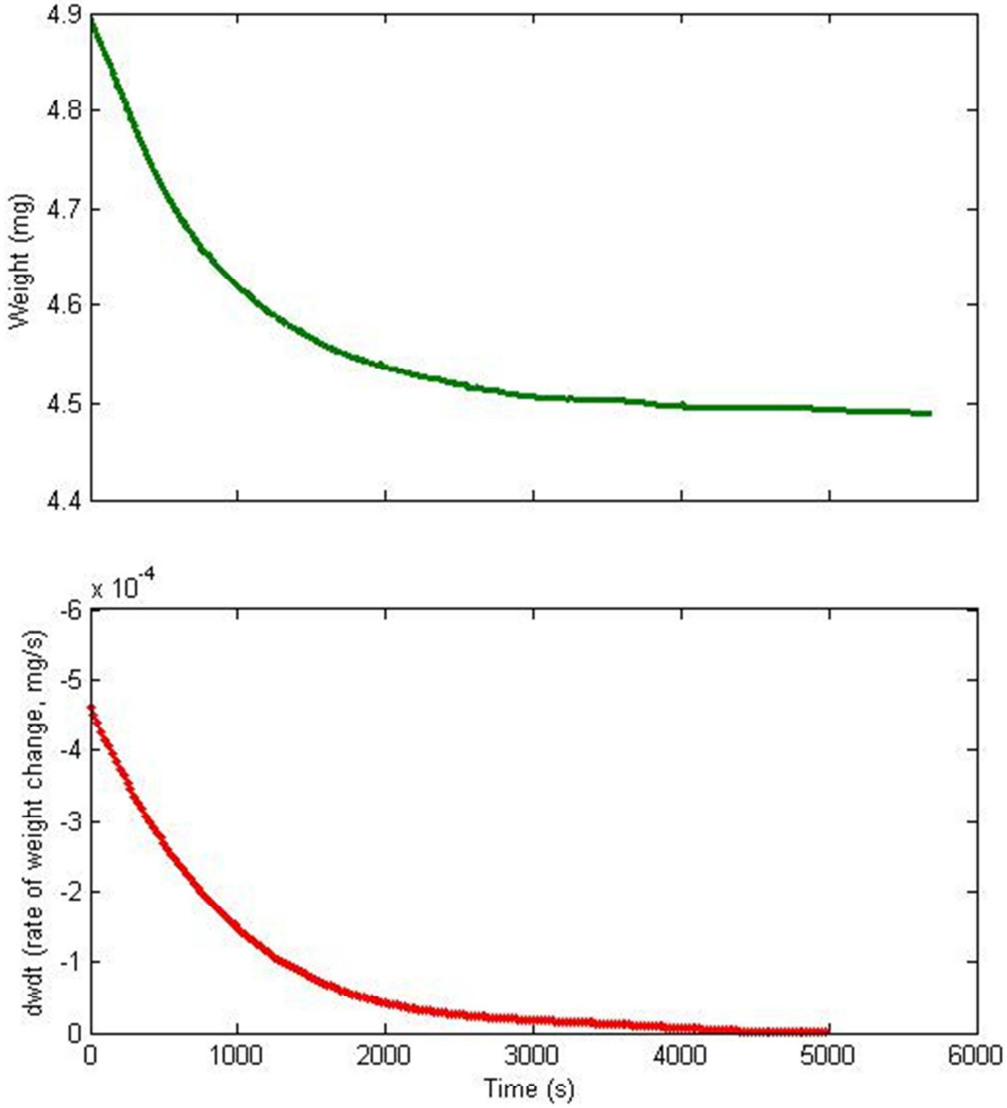

Figure-4.17: Rate of weight change (bottom curve) for Sample-1 oxidation at 600C

Initial rate of weight change $(dW/dt)_0$ was found by using the curve fitting tool (CFTOOL®) of Matlab® (Fig-4.16, 4.17). Table-4.4 calculates the initial oxidation rates for the sample-1 and sample-2a at 600^{o}C. The value of initial oxidation rate for Sample-2a was calculated and found to be 2.77x10^{-6}moles/min/m^{2}

Table-4.4: Initial oxidation rates at 600^{o}C

Specimen name	Initial rate of weight loss $(dw/dt)_o$	α_o (m^2/g)	W_o (mg)	Initial rate of regeneration at 600^{o}C (moles/min/m^2)
Sample-1	0.461 µg/s	151.7	4.89	2.32E-06
Sample-2a	0.677 µg/s	90.1	10.14	2.77E-06

Not only Sample-2a, a sorbent specimen rich in mixed metal oxide (mainly $ZnTiO_3$ with little free ZnO, net Zn-to-Ti ratio ≈ 1.1), was found to regenerate a little faster than Sample-1 (Zn-to-Ti ratio ≈ 3.7), it was also able to sustain higher rates for longer time duration, which leveled-off much later than the other sample, as can be seen from Fig-4.18. This may suggest a higher active site density in the mixed metal oxide sample. Many researchers studying bulk zinc based sorbents have typically found the opposite being true: simple oxides being more reactive than the mixed metal oxides (Lew et al., 1992; Jothimurugesan et al., 1998). A probable reason could be related to the possibility that when using sorbents with nanometer-sized grains, polycrystalline complex oxides like zinc titanate, may tend to offer more number of active sites and other associated surface defects than simple oxide specimens. In order to strengthen this reasoning, another set of experiments have been planned which will carry out the sulfidation & subsequent regeneration on the same sorbents which have not been pre-reduced, so as to make sure that the zinc content remains the same as in the fresh sorbent until the sulfidation begins. This may help in ruling out the possibility that Sample-2a's higher reactivity is not due to the possibility that it had higher zinc content by the time sulfidation started which could have happen since results of Chapter-3 showed that sample-1 suffered more zinc loss when compared to Sample-2a (although even then it seemed to have more zinc than Sample-2a). Nevertheless, it seems the sorbent nanostructuring does offer a good opportunity of solving the problem of lower reactivity associated with the mixed metal oxide based sorbents.

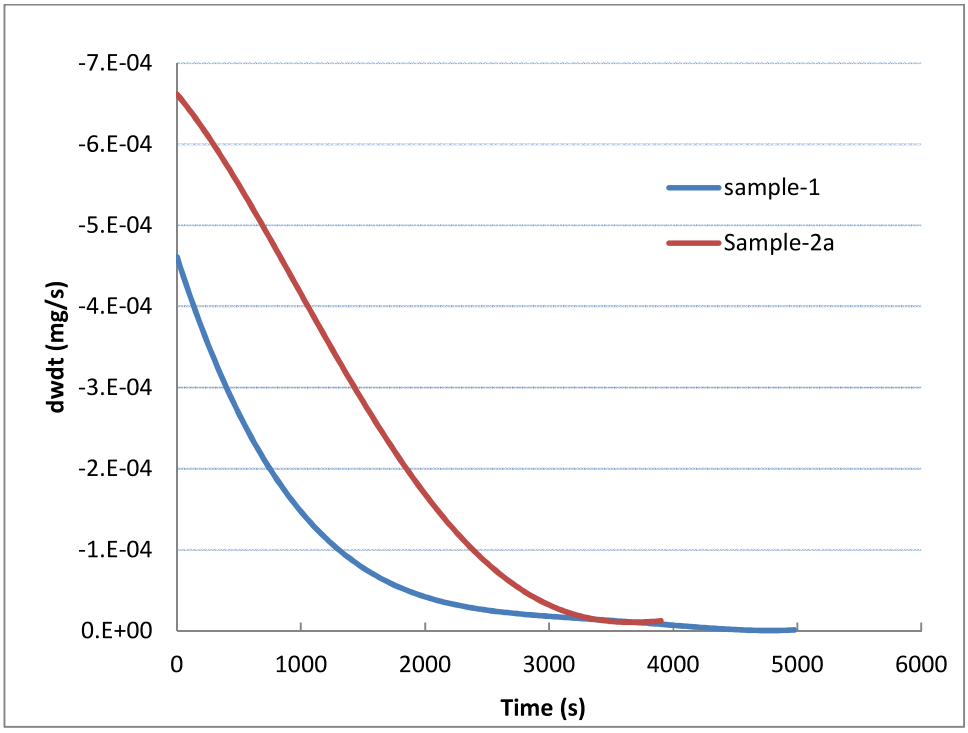

Table-4.18: Comparison of rate of weight loss between Sample-1 &2a, being regenerated at 600^{o}C

4.6.3. Post-regeneration image analysis using SEM & TEM

Fig-**4.19** (a & b) compares the SEM images of the regenerated fibers with the fibers in the fresh sorbent (Sample-1 & Sample-2a respetively). For Sample-1, it also shows the size distribution associated with each image. As it can be seen, much of the overall fiber morphology remains preserved post-regeneration. The fiber size distributions for the specimens (before-after) were found to be statistically similar to each other. The hierarchical growth, pervasive in the SEM images of the sulfided samples (though sporadic), could not be captured in the SEM images of the regenerated samples. It may be that these structures could grow only with a particular set of local conditions (combination of abrupt high local gas concentration over polar planes of the sulfide/oxide). As shown via a TEM image (**Fig-4.20**) of the regenerated specimen, branching was still going on. But using TEM it was hard to conclusively tell how widespread such branching was. In a follow-up work, it will be interesting

to see if the morphology is retained after a multi-cycle operation and to what extent, if at all, the initially observed hierarchical growth can be sustained over the subsequent cycles.

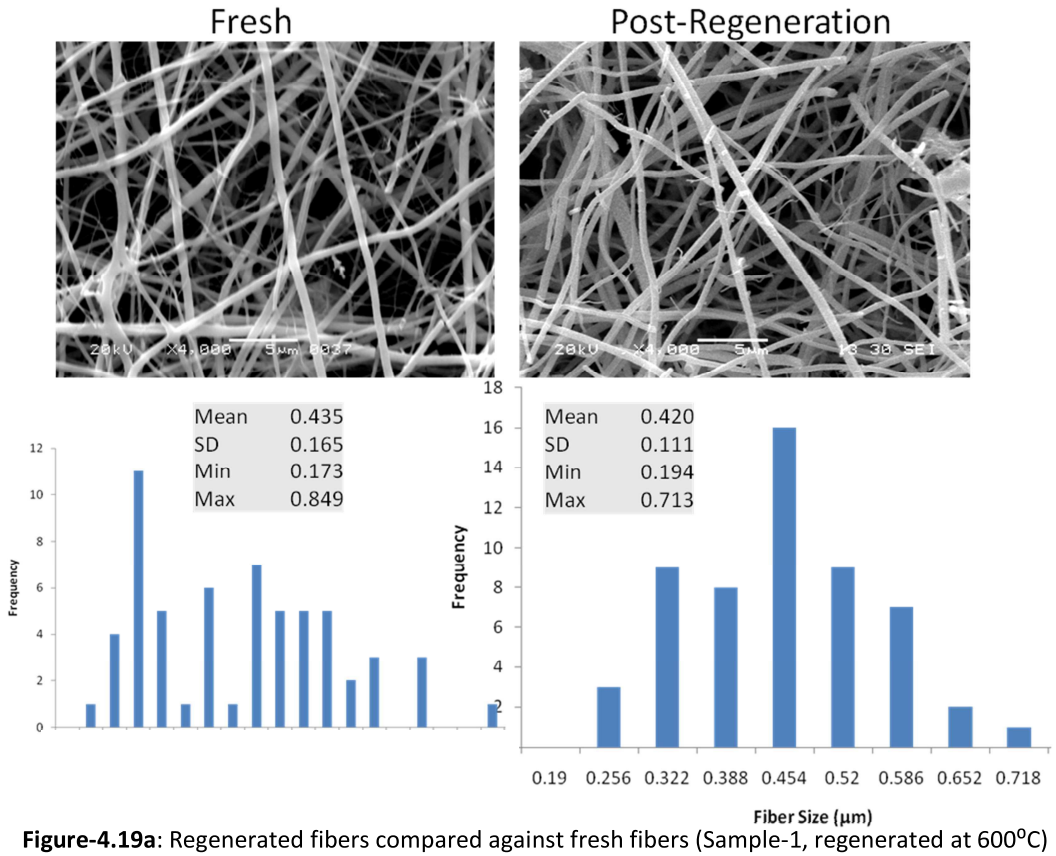

Figure-4.19a: Regenerated fibers compared against fresh fibers (Sample-1, regenerated at 600^{o}C)

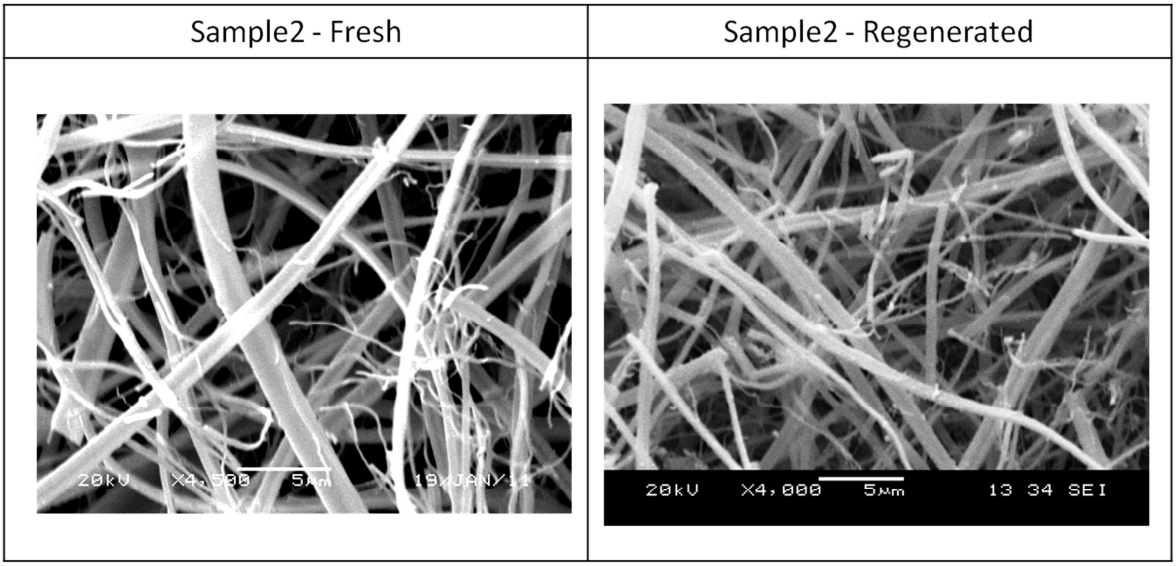

Figure-4.19b: Regenerated fibers compared against fresh fibers (Sample-2a, regenerated at 600^{o}C)

Fig-4.20 also shows the high resolution image of a “nano-branch”. Distribution of the different crystalline phases can be seen within this branch. As we know, contrast in an image generated by a TEM is due to the differences in the local densities which occur due to the presence of different crystalline phases. Different phases, with varying atomic densities and electrostatic potentials, affect the transmission of the electrons to various extents; this difference then lends contrast to the image. Figure**-4.21** directly compares the contrast of the fresh and the regenerated fibers. The difference in the two images is suggestive of the different ways in which the crystallite growth has occurred. In the fibers from the fresh sorbent, grain growth was occurring at high temperature during the long calcination step. For the case of fibers in the regenerated sample, the grain growth is attributed to the solid-vapor deposition and is dependent upon the kinetics of the gas-solid reaction (especially for the branched fibers).

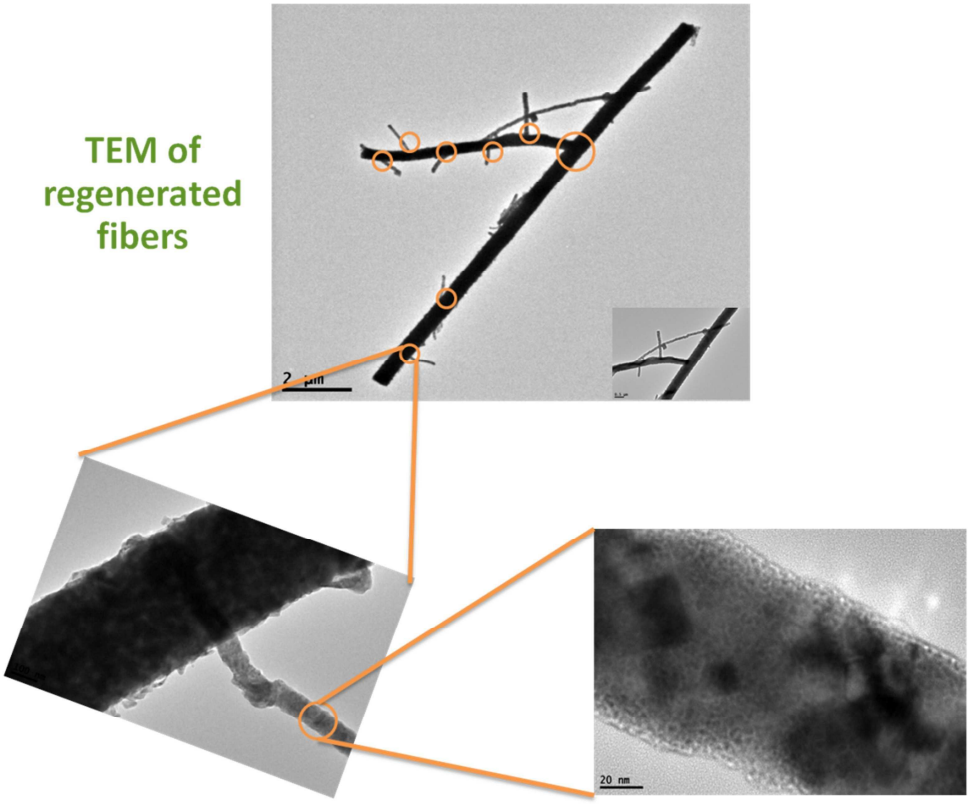

Figure-4.20: TEM images of the regenerated fibers (Sample-1, regenerated at 600^{o}C)

Fig-4.21 also compares the Selected Area Electron Diffraction (SAED) images for Sample-1. Each bright spot in a SAED image corresponds to a satisfied Bragg-diffraction condition from a particular set of crystal planes. Large number of bright spots with different distances (from the center point), confirm the polycrystallinity of the regenerated sample, as was in the case for the fresh sample. The differences in the SAED patterns of the two specimens suggest smaller inter-atomic plane spacing in the nanobranches.

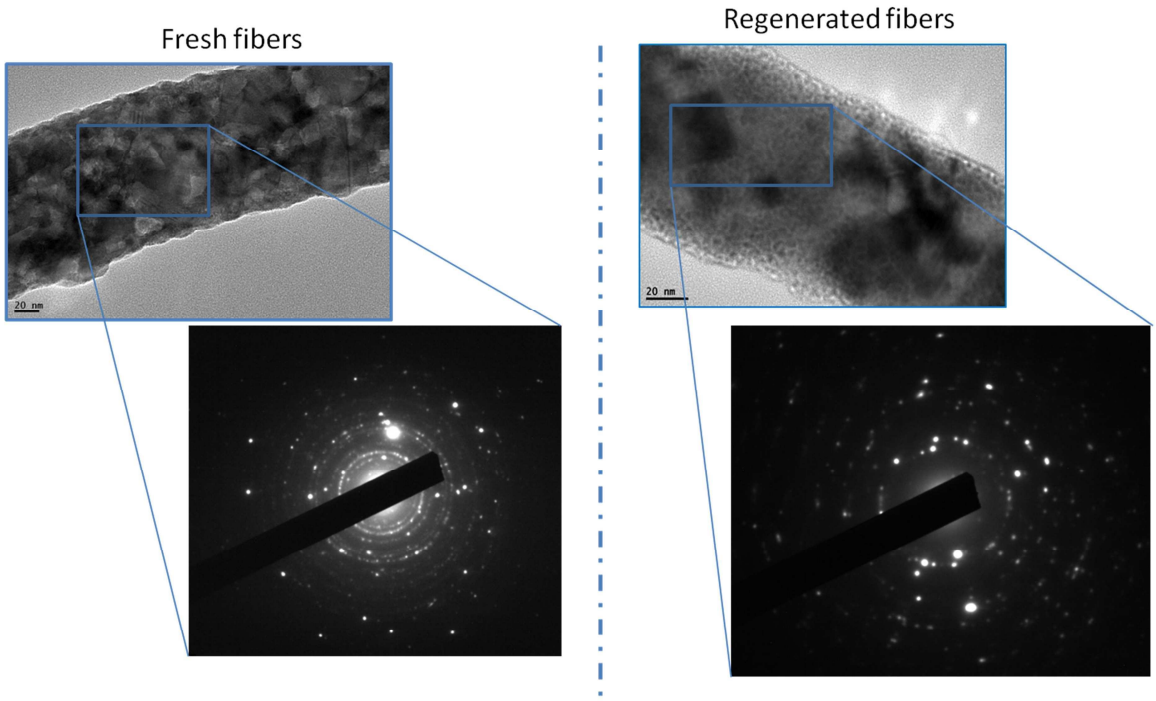

Figure-4.21: SAED analysis via TEM (Sample-1, regenerated at 600^{o}C)

4.6.4. EDX results for the regenerated samples

Fig-4.22 compares the EDX results for the fresh and the regenerated specimens from Sample-1 & Sample-2a (sulfidation and regeneration performed at 600^{o}C). As can be seen from the figure, the zinc-to-titanium ratio in the regenerated specimens from Sample-1 is lower than the fresh sample. This can be attributed to the fact that Sample-1 suffered a lot of zinc loss during the reduction step. EDX analysis of Sample-2, however, revealed that this ratio is well

preserved in the regenerated specimen, if the fresh sorbent is mainly composed of a mixed metal oxide which is sufficiently resistant to zinc loss by reduction ($ZnTiO_3$ in the present case).

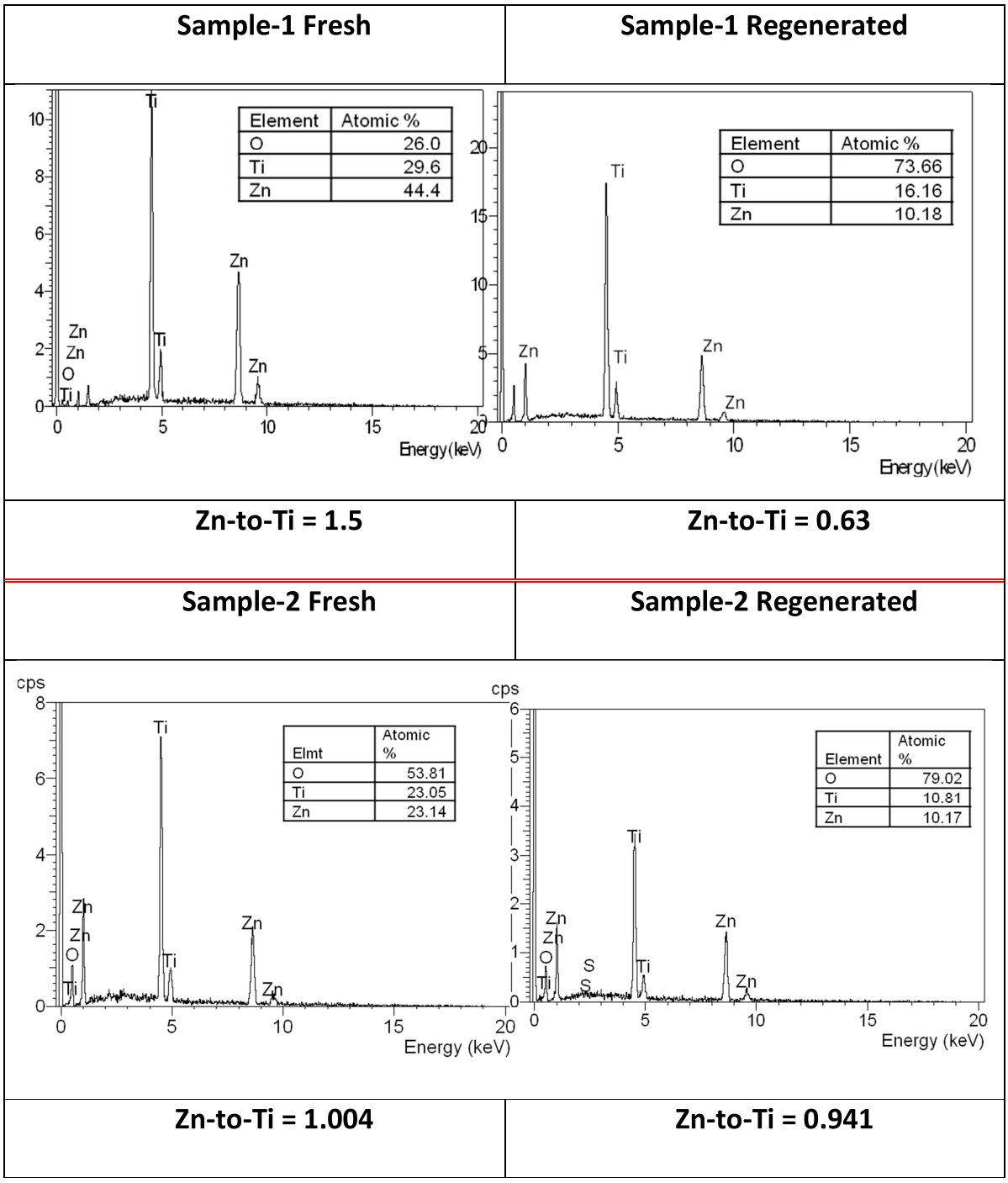

Figure-4.22: EDX analysis of Sample-1 & Sample-2a, regenerated at 600^{o}C

4.6.5. Post-regeneration XPS analysis

Fig-4.23 & 4.24 compares the resolved XPS peaks of a fresh specimen against a regenerated sample (for Sample-2a & Sample-1 respectively). Peaks were resolved for the Zn, Ti, O and S and were analyzed using suitable profile fitted curves (using 30% Gaussian / 70% Lorentzian peak shapes). As it can be seen, there is almost no noticeable shift in the peaks for Zn and Ti. For O, there is an addition peak at 533.3eV (Sample-2a). The two peaks, around 530.2 and 532.0 eV, were seen in both fresh & regenerated specimens. They were attributed to oxygen in TiO_2 (and possibly in some ZnO, which also shows up around 530.2eV) and in a zinc titanate phase (most likely zinc metatitanate, $ZnTiO_3$) respectively. The appearance of third peak in the regenerated specimen suggests presence of another zinc titanate phase (probably as zinc orthotitanate, Zn_2TiO_4). XRD analysis was done (Sec. 4.6.7) to further confirm the presence of multiple zinc titanate phases in the regenerated specimen, each being in a distinct crystalline phase. Sulfur, in any of its chemical state, was found to be absent.

Figure-4.23: Comparison of different elemental peaks in the XPS spectra of fresh and regenerated Sample-2a

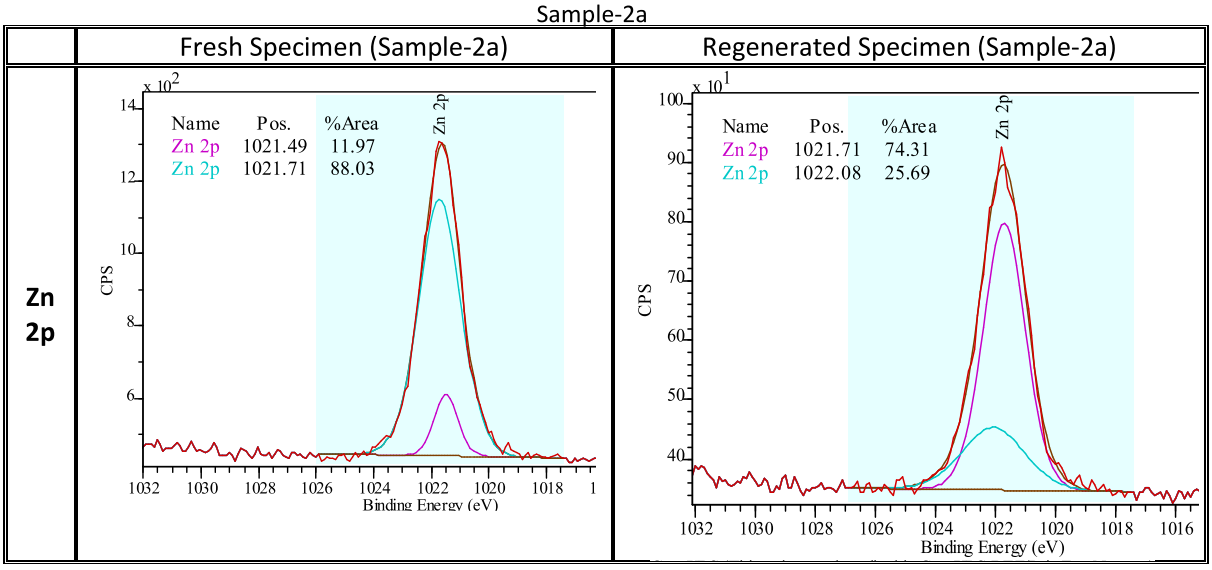

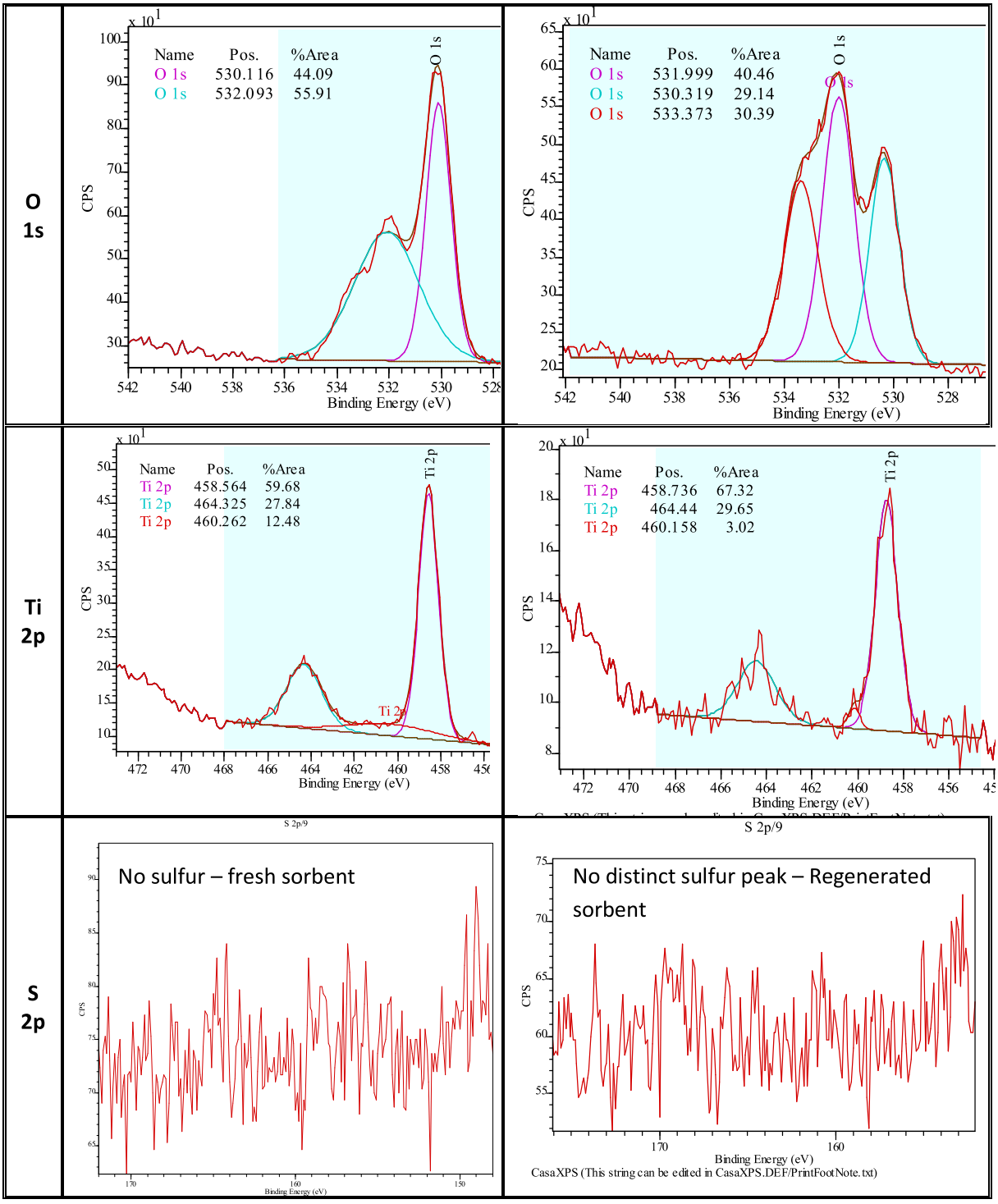

Figure-4.23 (Cont.): Comparison of different elemental peaks in the XPS spectra of fresh and regenerated Sample-2a

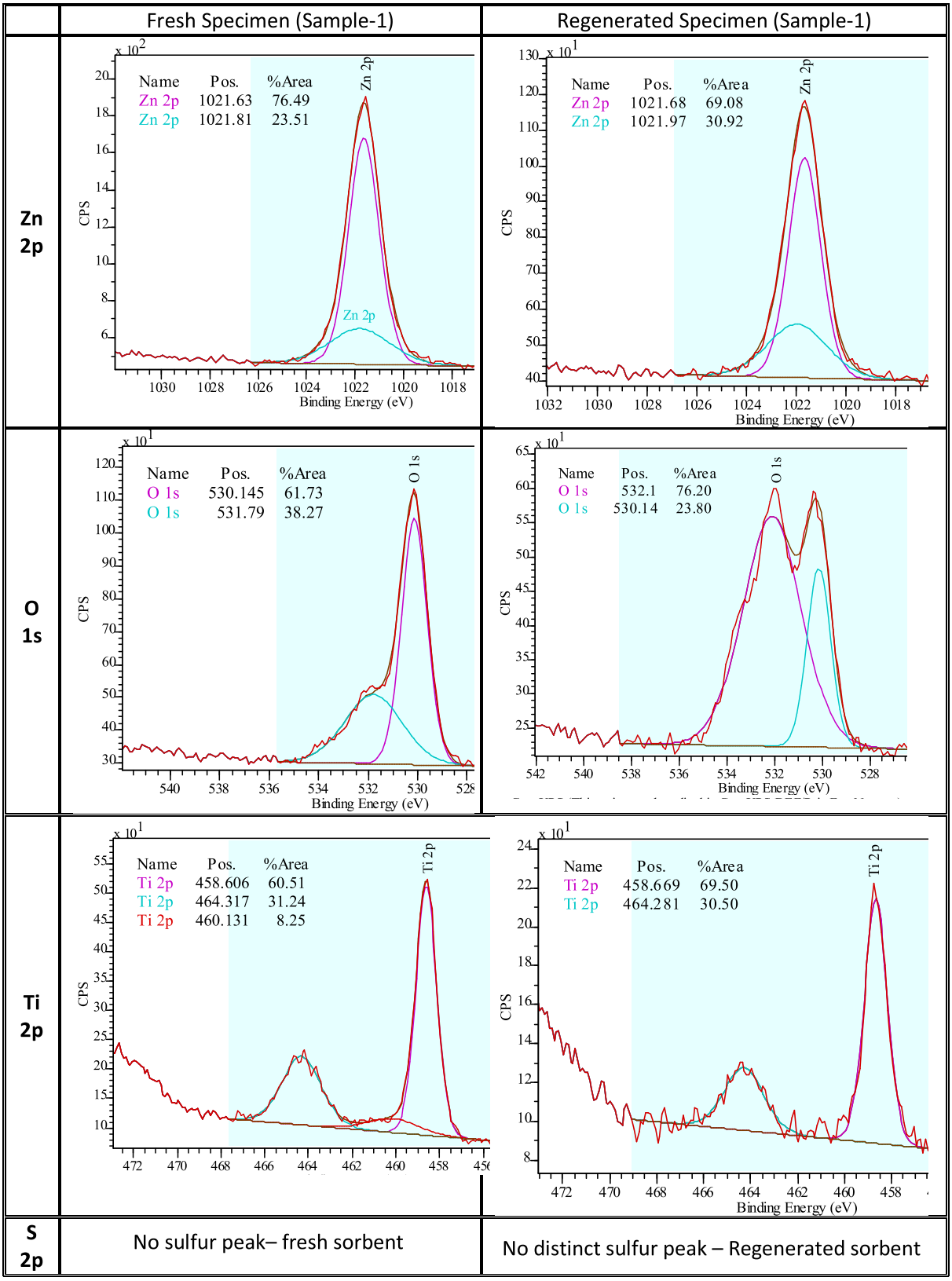

Figure-4.24: Comparison of different elemental peaks in the XPS spectra of fresh and regenerated Sample-1

4.6.6. Results from the XRD analysis

Fig-4.25 shows the XRD spectrum for the regenerated specimen (Sample-1). Note: The large hump seen at lower angles ($2\theta < 40^{o}$) was due to the glass substrate onto which the small amount of specimen was loaded. Profile-fitted peaks were used (generated using the help of a dedicated software (JADE®)) to quantitatively estimate the relative composition of the different phases present in the regenerated specimen (Fig-4.26). The major components identified were the two different phases of zinc titanate: $ZnTiO_3$ (Zinc metatitanate / Ecandrewsite) and Zn_2TiO_4 (Zinc orthotitanate). Rutile phase of Titania along with some zincite (ZnO) were also present.

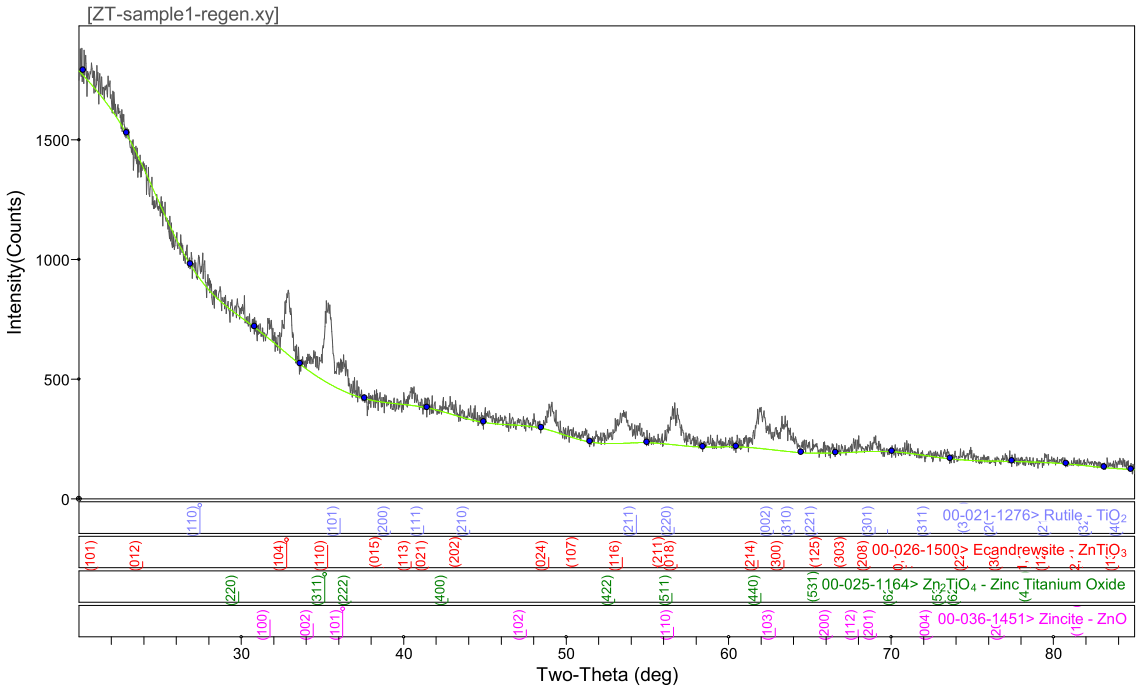

Figure-4.25: XRD spectrum of the regenerated Sample-1

Zn_2TiO_4 (a = 8.46Å) has a cubic inverse spinel structure (AB_2O_4-type), where Zn atoms occupy the A-site and the B-site is occupied by randomly arranged Zn and Ti ions. In the inverse spinel structure, the A-site generally is occupied by a larger cation and the B-site is occupied by a smaller cation. The Zn atom has a tendency to prefer the A-site; thus, surplus Ti^{4+} ions occupy octahedral sites and vacancies are created (most probably at tetrahedral sites) to compensate

the charge. $ZnTiO_3$ was found in a hexagonal ilmenite structure (a:c = 1:2.74, with the following lattice parameters values: a = 5.08 Å & c = 13.93 Å). Manik & Pradhan (2006) found the reflections from $ZnTiO_3$ overlapping with the spinel phases, with peaks being broad and overlapping. Thus, they proposed that the estimation of the quantity of individual phase, even with the help of Rietveld analysis, is difficult and should only be taken as an approximation

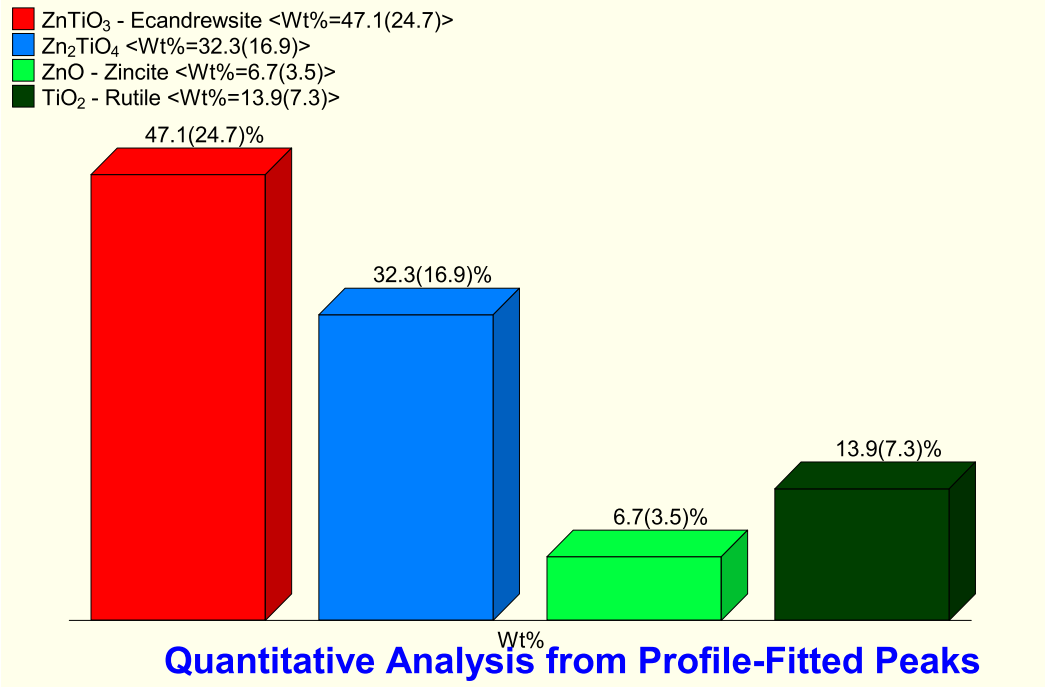

Figure-4.26: Quantitative compositional estimation of the different crystalline phases present in regenerated Sample-1

Clearly, the regenerated specimens have a chemical composition dominant in mixed metal oxides. No indication of zinc sulfide was present in the spectrum indicating that a complete regeneration was achieved, strengthening the proposition of the previously analyzed results obtained from the other characterization methods.

Table 4.5 compares the average grain sizes and the atomic plane spacings (d-spacings) of the regenerated and the fresh specimens. Grain size estimation was also done on the software (Jade) by first performing curve-fitting followed by application of the DeBye-Scherrer equation. As it can be seen, the average grain sizes are very much of the same

order and only a little grain growth appears to have occurred. Restoration of grain size post-regeneration is an important indication of sustainment of the structural properties of the fresh sorbent.

Table-4.5: Comparison of the grain sizes and the d-spacing for the fresh & regenerated specimen (Sample-1)

Regenerated specimen			Fresh specimen		
Phase	Grain size(nm)	Plane spacing d(Å)	Phase	Grain size(nm)	Plane spacing d(Å)
$ZnTiO_3$	16.47	2.09	$ZnTiO_3$	15.05	3.23
ZnO	13.13	2.23	ZnO	12.53	2.27
Zn_2TiO_4	16.60	1.50	Zn_2TiO_4	9.00	2.99

4.7. Multi-cycle sulfidation and regeneration experiments

As discussed earlier, commercial applicability of any sorbent is determined by examining the reusability and the performance of the sorbent during a repeated recycling operation. Thus, in order to examine whether the as-spun adsorbents from this work are reusable, another TGA experiment, incorporating a multi-cycle sulfidation-regeneration operation, was conducted. A consecutive sulfidation and oxidation step constitutes as one cycle. The sample was subjected to 6 such cycles. A sorbent specimen from sample-S2 was used for this purpose. The specimen was placed inside the sample holder of the instrument and the temperature was ramped to 650^oC at the rate of 15^oC/min. Once the set temperature was achieved, a gas stream containing 4% H_2 (in N_2) was introduced. This sorbent-pre-reduction continued for 15 minutes, after which H_2 stream was taken-off and a stream containing 1% H_2S in N_2 was introduced. This started the first cycle. After 60 minutes of sulfidation, H_2S stream was taken off and a stream containing 3% of O_2 (in N_2) was introduced. This regeneration step lasted for another 70 minutes. This step completed the first cycle. The specimen underwent six such cycles before it was allowed to cool for performing ex-situ material characterization. Figure-4.27 shows the corresponding changes in sample weight during the cyclic operation.

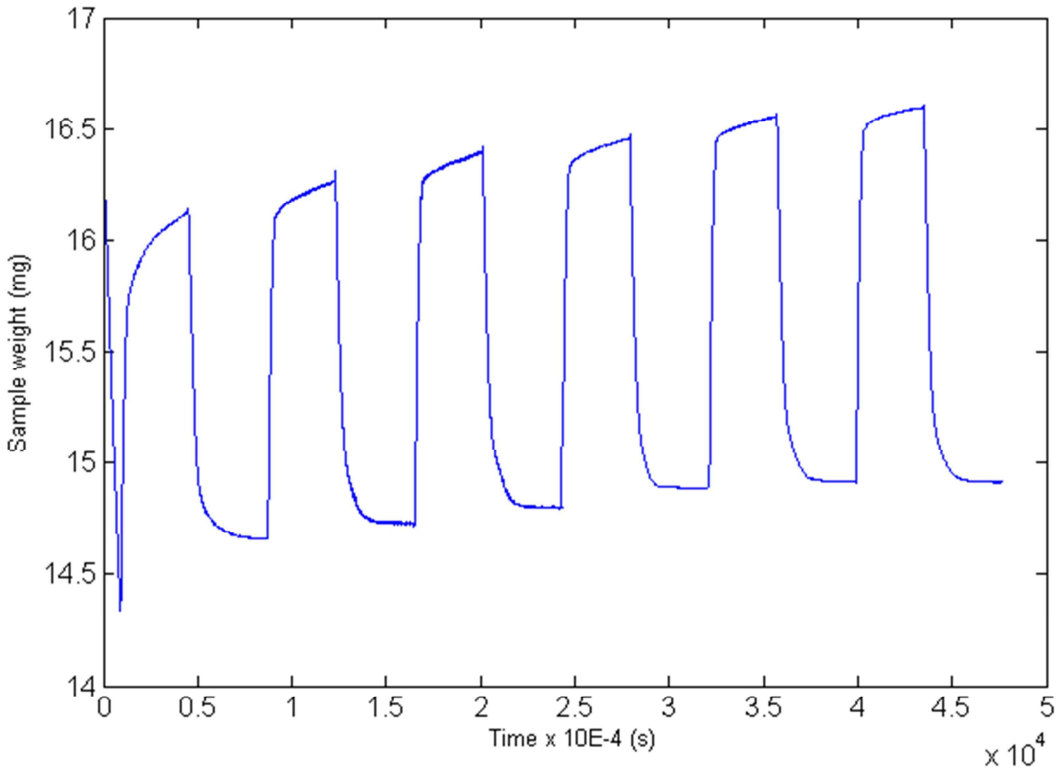

Figure-4.27: Weight change vs. Time for Sample-2a during the cyclic sulfidation-regeneration process

The initial drop in the sample weight was attributed to the volatilization of zinc metal that may have formed during the reduction of the sorbent first to zinc oxide and subsequently to zinc metal which tends to volatilize rapidly at temperatures above 550^{o}C. The first cycle starts with a gain in sorbent weight that is linked to the zinc sulfide formation; the successive drop in the weight is associated with the oxidation step. Similar alternating gain and loss in weight, corresponding to sulfidation and regeneration steps, can be observed for the other 5 cycles as well, indication of successful regeneration at the end of every cycle.

When presented in terms of fractional weight change (Fig.-4.28, a & b), the data can be used to interpret the extent of sulfidation i.e. the sulfur capacity of the sorbent specimen for each of the cycles (Fig.-4.29).

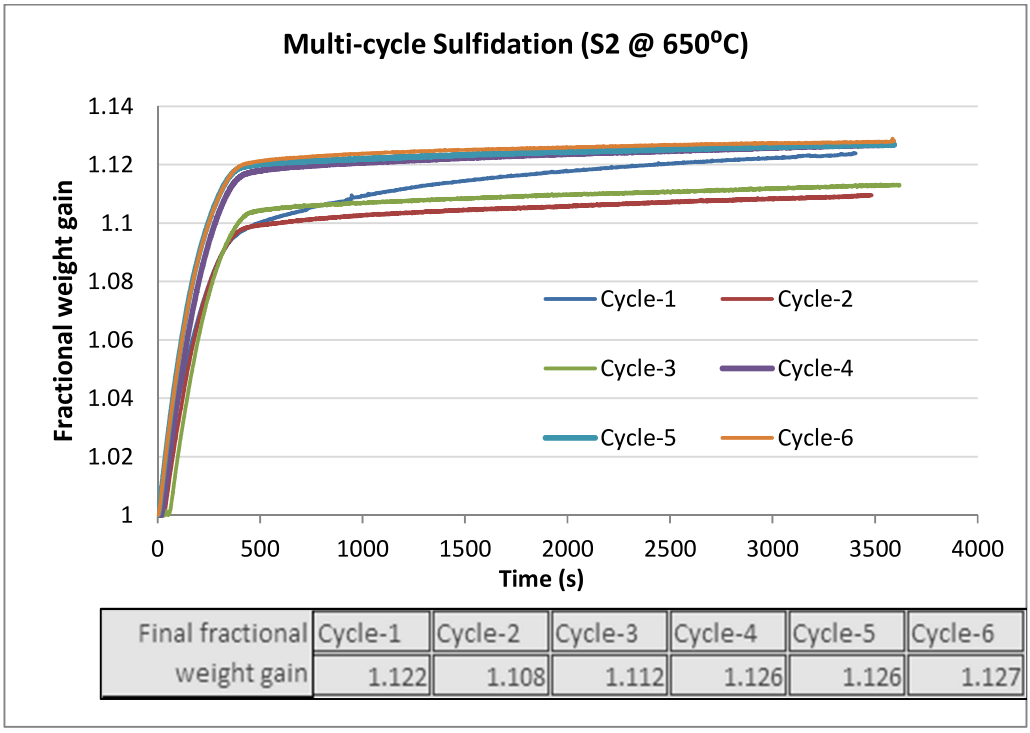

Final fractional weight gain	Cycle-1	Cycle-2	Cycle-3	Cycle-4	Cycle-5	Cycle-6
	1.122	1.108	1.112	1.126	1.126	1.127

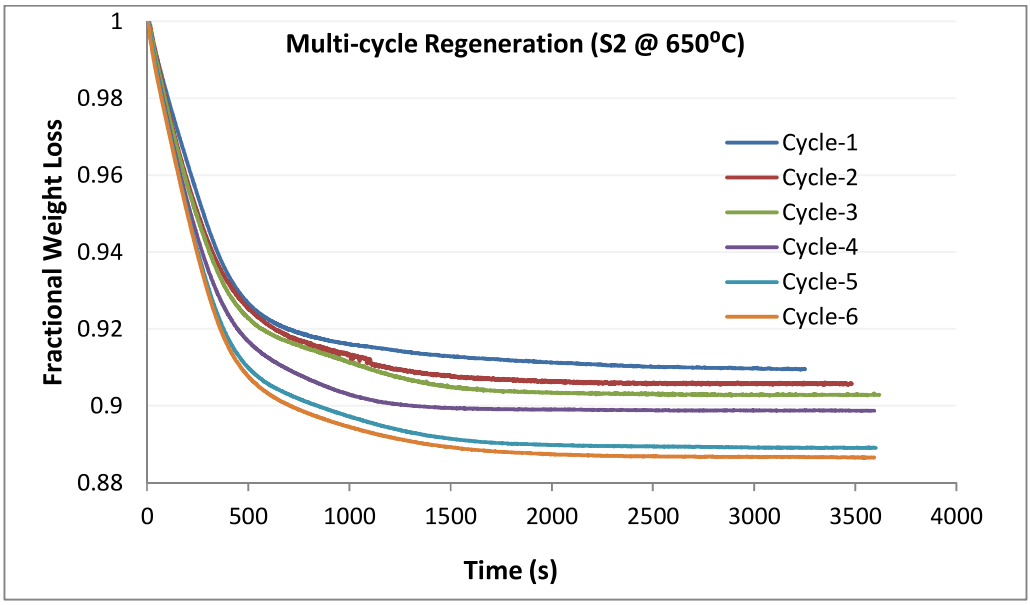

Figure-4.28: **a)** Fractional weight changes (top) during the sulfidation steps. **b)** Fractional weight changes during the oxidation steps (bottom) (all at 650°C)

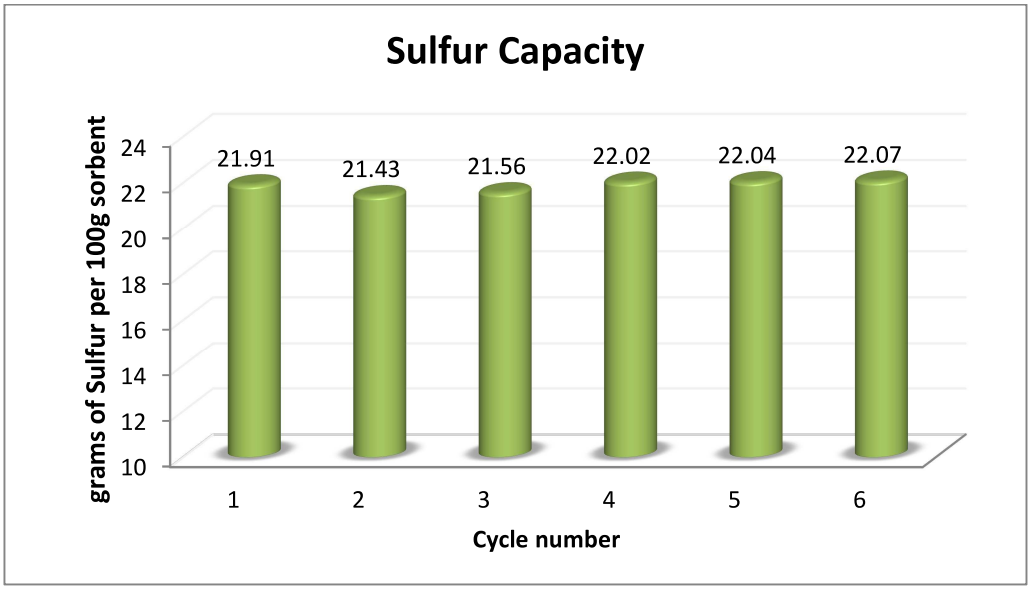

Figure-4.29: Sulfur capacity after first 50 mins of the sulfidation step for each of the cycles

Consistent gain in the fractional weight during each cycle (Figure 4.28a) reflects good regenerability of sorbent's sulfur capacity. The slight decrease at the beginning of the second cycle may be attributed to the small change in the crystal phase composition. These changes quickly even-out and from the fourth cycle onwards, the sulfidation capacity remains high consistently. The theoretical sulfur capacity based on the phase composition information obtained from the quantitative XRD analysis (Chapter-2, Section-2.4.1), performed during the material characterization of the fresh sorbent, gave a value of 21.41 grams of sulfur per 100 grams of sorbent specimen. All the experimentally obtained sulfur capacities (Fig-4.29) were found to be close to this value. Again, the observation that some of the experimental values were in fact higher can be understood by considering the fact that the theoretical value was calculated from the chemical stoichiometry of the component phases involved in the sulfidation reaction based on the *initial* sorbent composition. Sorbent composition may have changed as the sorbents were partially reduced at the beginning. Also, stoichiometric changes in the component phases, for instance, a portion of meta-zinc titanate ($ZnTiO_3$) going to its ortho phase (Zn_2TiO_4), could have occurred (XRD analysis after the 6^{th} cycle, Fig-4.30).

Fig-4.30 shows the XRD spectrum from the sample-S2 after it underwent a multi-cyclic operation. All the peaks were identified and assigned to the corresponding crystal phases. The major phases identified were: Titania (anatase & rutile), meta- and ortho-zinc titanate (ZnTiO3 & Zn2TiO4) and a small quantity of wurtzite (zinc sulfide). The phase compositions were calculated by carrying out the profile-fitting of the diffraction peaks in MDI-Jade®. Composition of the fresh sorbent has also been included for comparison. It can be seen that the concentration of titania has increased. This increase is partly attributed to the loss of volatile zinc during the initial reduction step; while titania being inert to hydrogen at 650°C, remains intact in the sample. Presence of small amount of ZnS can be attributed to the possibility that the regeneration was not complete for the duration of the oxidation step and the test should have run a little longer. However, XPS (Fig-4.32) and EDX analysis (Fig-4.31), performed on another portion of the same sample, show that there was no sulfur present. These results indicate that there is a possibility that a minute amount of sulfur may have been left unreacted. Also, as can be seen from Fig4.28b, increasing the number of cycles was aiding the regeneration by attaining a little higher conversion after every cycle. This seem to suggest that if the cyclic regeneration was to continue for few more cycles, as would happen in any commercial application, this would have led to a further improvement in sorbent utilization. This proposition is further supported by the SEM images (Fig-4.33) that the average fiber diameter in the multi-regenerated sample is smaller than the fiber diameter of the fresh sample (Fig-4.34). Furthermore, the mean grain sizes of the different phases remain statistically similar to those present in the fresh sample (Table-4.6). In addition, the specific surface area of the regenerated sample is expected to be greater than that of the fresh sample due to the growth of dendritic structures as can be seen in Fig-4.33(c). Also shown in the figure (inset in Fig-4.33c) is the high-magnification image of the fiber surface. It is to be noted that this dendrite-like growth in Sample-2 (multi-regenerated) is similar to the one seen in Sample-1 (Fig-4.5). Such growth during the sulfidation-regeneration reactions seems to be unique to the nanostructured adsorbents since the only product geometry reported in the literature is the core-shell (reactant-product) structures seen during the sulfidation-regeneration of pellet or extrudate shaped adsorbents.

All these observations indicate a sort of “textural-refining” that may be going on during the repeated regeneration, in effect leading to a progressively better utilization of the sorbent with each cycle.

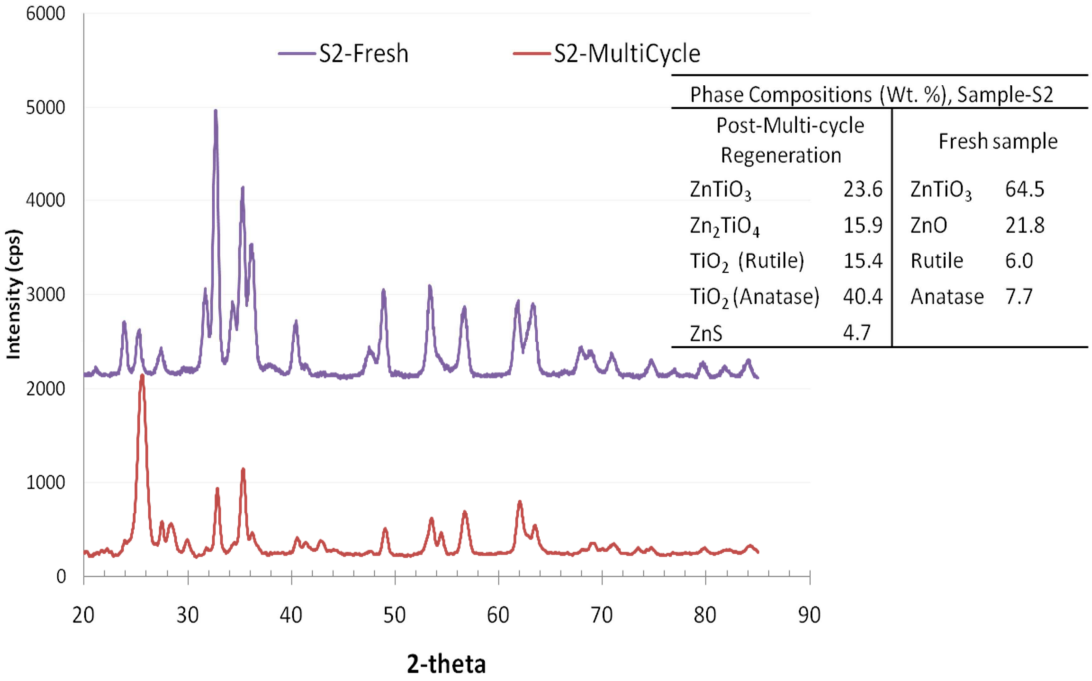

Figure-4.30: XRD spectra for fresh (top) and multi-regenerated (bottom) Sample-2a

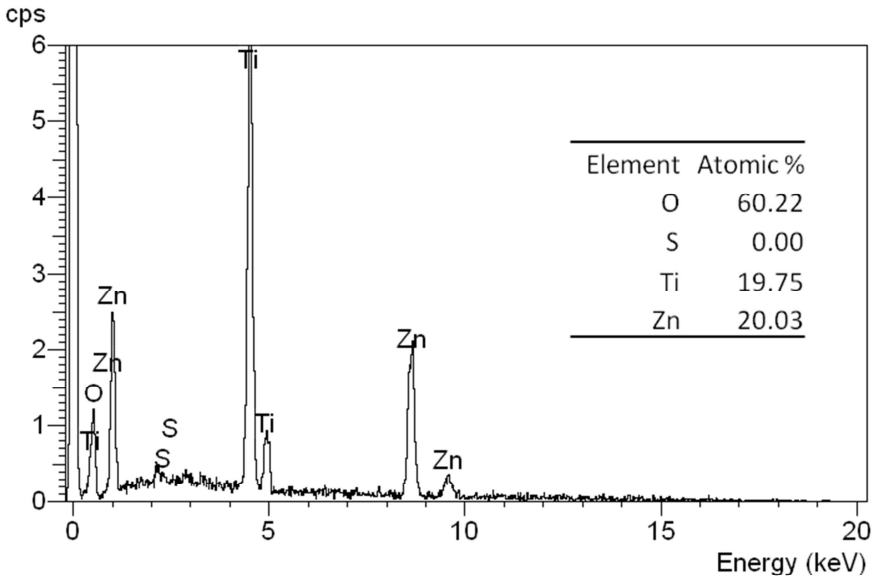

Figure-4.31: EDX spectrum with atomic concentration of the elements detected

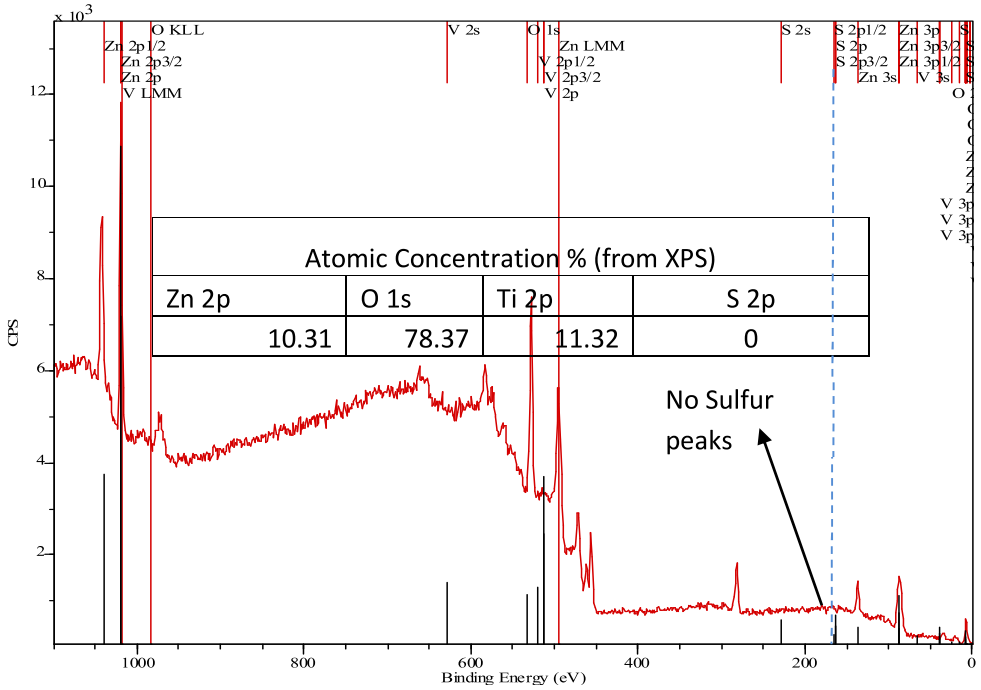

Figure-4.32: XPS spectrum with atomic concentration of the elements detected

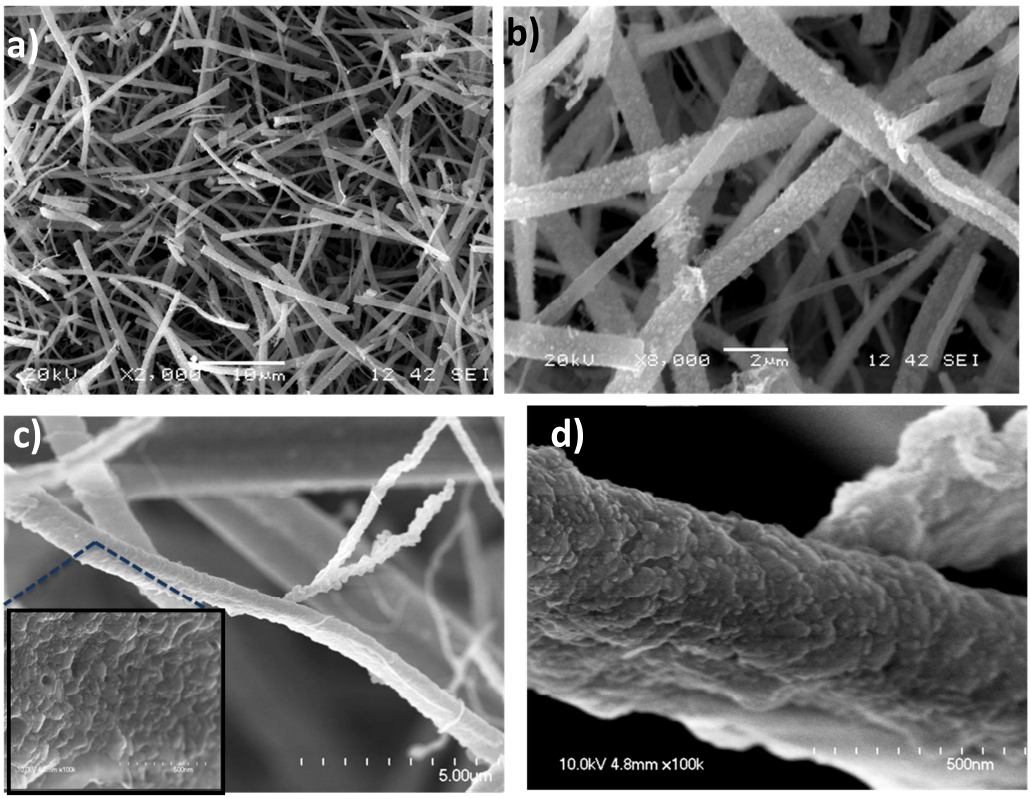

Figure-4.33: SEM images of Sample-2a after multi-cycle experiment at a magnification of **a)** 2000X, **b)** 8000X , **c)** 20000X with an inset showing the fiber surface at 100000X, **d)** another image of fiber surface at 100000X

Fiber diameter (µm)post-multi-regeneration	
Mean	0.577
SD	± 0.217
Min	0.26
Max	1.182

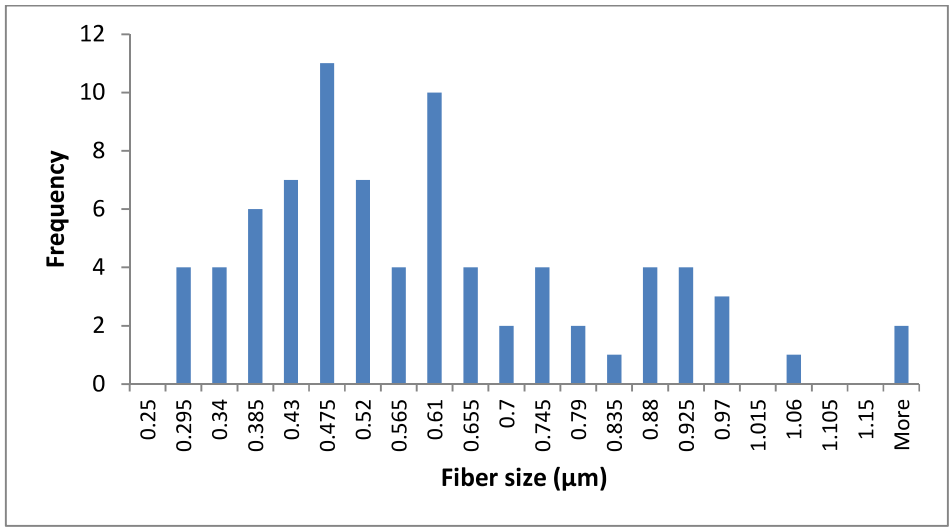

Figure-4.34: Fiber size distribution after multi-cycle regeneration

Table-4.6: Grain size estimation using XRD data

Grain Size (nm) Sample-2			
Post-Multi-cycle Regeneration		Fresh sample	
ZnTiO3	17.2	ZnTiO3	14.5
Zn2TiO4	18.0	ZnO	13.6
rutile	23.0	rutile	14.5
anatase	9.0	anatase	17.1

4.8. Effect of temperature – Calculation of activation energy

The purpose here was to determine the activation energy (E_a) associated with the sulfidation reaction. More specifically, impact of the nano-fibrous morphology of the as-synthesized sorbents on the energy barrier associated with the reaction between the H_2S and zinc titanate will be examined. To this end, sulfidation was carried out at four different temperatures: 500°C, 550°C, 600°C and 650°C, and the initial reaction rates (R_0) were calculated corresponding to each temperature while the flow rate and the H_2S concentration of the gas stream were kept constant (200 ml and 1% v/v). The experiments were done using the same TGA setup as described in the previous sections of this thesis. Initial reaction rates were calculated by monitoring the change in the sample weight with time, as described earlier by using this equation:

$$R_0 = \frac{(dW/dt)_0}{A_0 \cdot (M_{ZnS} - M_{ZnO})}$$

R_0 was calculated for different temperatures and an Arrhenius-plot was drawn (Fig-4.35) using this relation:

$$R_0 = kC_{H_2S}^n = k_0 \exp(-\frac{E_a}{\breve{R}T})C_{H_2S}^n = (k_0 C_{H_2S}^n).\exp(-\frac{E_a}{\breve{R}T}) = k^{'}.\exp(-\frac{E_a}{\breve{R}T})$$

$$\ell n(R_0) = \ell n(k^{'}) - \left(\frac{E_a}{\breve{R}}\right)\frac{1}{T}$$

Activation energy is obtained from the slope of the plot between $\ln$ (R_0) and 1/T. The reaction order, with respect to reactants, has been assumed to be not varying with temperature. The activation energy thus obtained is compared with the value of the activation energy as reported by Lew et al. (1992), who investigated the response of zinc titanates to sulfidation.

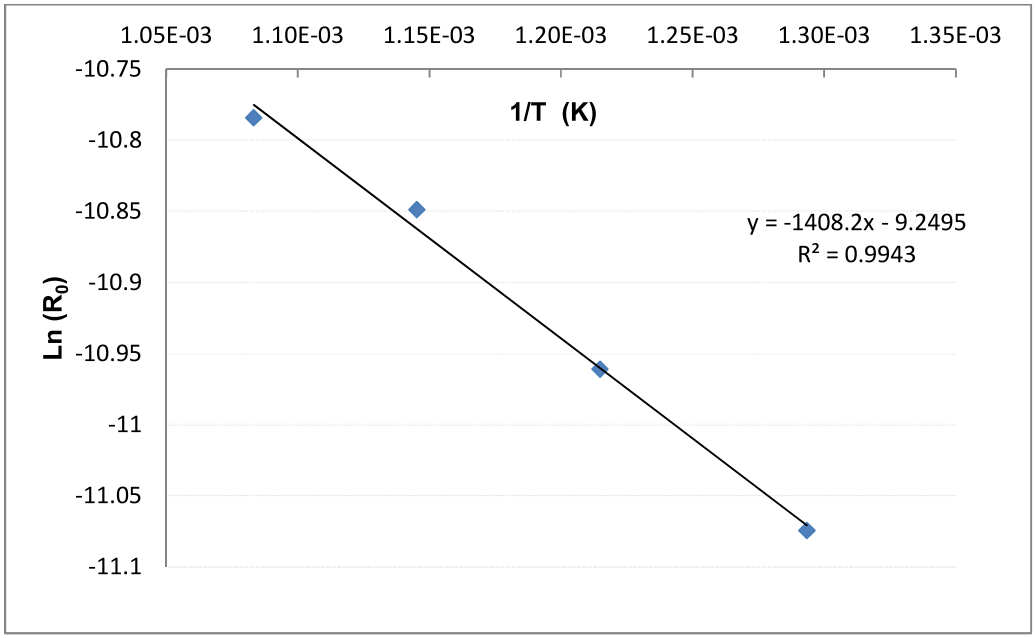

Figure-4.35: Arrhenius plot for the estimation of activation energy in the temperature range: 500^{o}C – 650^{o}C

Table-4.7: Comparison of activation energy with literature

Sorbent design	Material	Method of Synthesis	E_a Kcal/mol
Nano-fibrous mats	Zinc Titanates	Sol-gel based electrospinning	2.8
Extrudates, powder *	Zinc Titanates	Co-precipitation	9.0 – 10.5

***Lew et al. (1992)**

As can be seen in Table-4.7, the activation energy associated with nano-fibrous morphology is much smaller than the powder or pellet-based geometries. This difference suggests that the proposed sorbent design, i.e. the fiber-mat morphology, may have a lower energy barrier for the sulfidation reaction and may actually be more suitable for the applications requiring mid-high temperatures where the conventional high temperature, zinc titanate based sorbents tend to have lower reactivity. The difference in activation energy may also be an indication that a reaction mechanism that is different than the one reported for the bulk (Lew et al., 1992) may be going on during the sulfidation of nanostructured adsorbents. Further research in this area can help in confirming this hypothesis.

4.9. Summary of the results

Results from sulfidation experiments

1. Mixed metal oxide (Zn-Ti ratio ≈ 1.1) based nanofibrous sorbent specimens (Sample-2a) found to be equally or more reactive than the specimens rich in free zinc oxide (Zn-Ti ratio ≈ 3.7, both specimens being pre-reduced). This may suggest higher density of active sites and surface defects in polycrystalline complex oxides when compared to simple metal oxide surface. Conventional bulk-scale polycrystalline materials are composed of grains which are micrometers in size containing millions of atoms, a grain of a nanocrystalline material, on the other hand, typically contains only a few thousand atoms. A reduction in the grain size results in an increase in the density of grain boundaries and thus an increase in the fraction of atoms lying in interfaces compared to those at regular lattice positions, giving rise to larger density of active adsorption sites. This effect may be more pronounced for the case of mixed metal oxides than simple oxides.
2. Chemical reaction step found to be the rate-controlling step rather than the product layer diffusion step for the majority of the reaction duration – an indication of minimal mass transfer resistance offered by the nanofibrous sorbent specimens.
3. Growth of hierarchical / dendritic structures, emanating from the parent composite fiber, was observed during the sulfidation reaction. This was attributed to a specific simultaneous occurrence of the polar planes of ZnS/ZnO as fiber outer surface along with locally high gas (H_2S) / vapor (Zn) concentration. These structures may lead to increased specific area.
4. Post-sulfidation, no sulfate formation was detected. Absence of formation of any sulfate compounds during the sulfidation of nanofibrous zinc titanate adsorbent is expected to improve the chances of achieving complete regeneration.
5. Formation of wurtzite during sulfidation, a distinct crystal form of zinc sulfide, was seen as another potential advantage of using nanostructured sorbent morphology. Wurtzite

tend to oxidize directly to zinc oxide whereas oxidation of sphalerite (another ZnS crystal form) has been reportedly linked with the formation of $ZnSO_4$ and $Zn_3O(SO_4)_2$.

Results from regeneration experiments

1. Again, sorbent specimens rich in zinc titanate showed faster kinetics than the zinc oxide sorbents (both pre-reduced).
2. Complete regeneration was achieved at the same temperature at which the sulfidation was carried out (600C). Typically, the regeneration time needs to be raised by at least a couple of hundred degrees centigrade before the regeneration even begins.
3. No sulfate formation detected post-oxidation even when the regeneration temperature was kept same as the sulfidation temperature. This can be partly attributed to the formation of wurtzite form of ZnS.
4. Structural properties of the sorbent specimen like the fibrous morphology, grain size of the fresh sorbent remained intact in the regenerated specimens

Results from multi-cycle sulfidation and regeneration experiments showed the nanofibrous design of the as-synthesized adsorbents is highly effective in cyclic operations. It was found that nanofibrous mats of zinc titanate can successfully withstand repeated sulfidation-regeneration operations whithout suffering microstructure degradation while maintainng high sulfur capacities close to the theoretically predicted values. These results were inferred by the outputs from TGA, SEM-EDX, XRD and XPS. Progressive improvement in the textural properties of the fiber and growth of distinct structural features unique to nanometer-scale size of te grains (dendritic growth) were proposed to be the reason for this enhancement in the sorbent performance.

Furthermore, sulfidation experiments performed at different temperature suggested that the proposed sorbent morphology offered much lower energy barrier to the reaction, suggesting higher reactivity of the sorbent even at lower temperatures.

Chapter-5

Summary and Conclusions

Sol-gel based electrospinning was used to synthesize composite zinc and titanium oxide adsorbents in the form of non-woven fiber-mats. Two such samples, with different zinc-to-titanium atomic ratio were selected. The Zn-to-Ti ratio for the first sample (Sample-1) was 3.69 and for the second sample (Sample-2a) it was 1.17. Sol-gels, with a desired proportion of Zinc-to-titanium, were first prepared as a polymeric-metal salt precursor solution. Calcination of the as-spun fibers at 600^{o}C for 4hrs resulted in zinc-titanate fiber-mats free from polymer. These fiber mats were characterized by substantially high specific surface areas: 151.7 and 90.1 m^2/g respectively. The average fiber diameter for Sample-1 was found to be 435 nm and for the second sample it was 714 nm. Fibers were then characterized for their internal crystal structure and surface morphology using the techniques of XRD, SEM and TEM. The major findings from the characterization of the fresh specimens are as follows:

- XRD results and selected electron diffraction done using TEM confirmed that the electrospun fibers, obtained after the heat-treatment (post-sintering), are multi-phase and polycrystalline in nature. The crystallites formed within a fiber are within the range of 10 – 15 nm in size.
- Fiber diameters, ranging from 165 nm to 830 nm, were obtained. It was found that the use of inorganic binders, like lithium polysilicate, can help in reducing the spread in the fiber diameters.
- Sol-gel based electrospinning process, which uses zinc acetate and titanium isopropoxide as the ceramic precursors, can result in formation of at least two distinct

phases of Zinc titanate, namely hexagonal ilmenite zinc meta-titanate ($ZnTiO_3$) and cubic inverse spinel - zinc orthotitanate (Zn_2TiO_4) (post-calcination at 600°C).

- Any zinc or titanium, present in excess of stoichiometric quantity, ends up as zinc oxide or titanium oxide respectively. But if sintering is being carried out at higher temperatures (greater than 600 C), any free zinc tends to get lost rapidly (before solid-solid or gas-solid reaction can occur) due to its highly volatile nature and pure zinc oxide may not be present in the product mixture. As a result, mixed metal oxide phase ($ZnTiO_3$) may again become the major crystalline component (for starting Zn/Ti > 3).

These fresh specimens were subsequently tested for their high temperature reduction behavior. Investigation of the reduction behavior is important for any cyclic sulfidation-regeneration operation as it determines the durability and resistance of the sorbent specimens to the potential deactivation that may occur due to highly reducing gases present in the raw syngas. Temperature controlled reduction was carried out using a Thermo-gravimetric Analyzer (TGA). Fiber-based sorbents with Zn-to-Ti ratio closer to one were found to be more resistant to deactivation caused by reduction. The major findings from the reduction experiments are as follows:

- Nanocomposites (zinc + titanium oxides) were found to possess much higher resistance to the deactivation caused by the reduction. The effect was particularly strong if the zinc-to-titanium ratio was closer to one.
- During the reduction reaction, different compositions of the mixed oxide sorbent exhibited different regimes with different rate-controlling steps. More zinc content in the sorbent implied that the overall reaction rate was controlled by the gas-film diffusion step.
- Product layer diffusion step becomes rate controlling if there is comparable zinc-to-titanium content (as in Sample -2a). In such sample, shrinking-core mechanism can be seen in operation in which inert product layer grows as the active core shrinks. This is distinct from the shrinking – particle mechanism (as seen in sorbents with higher zinc

content), in which the main product is not solid (Zinc vapors) and the reaction proceeds as the entire sorbent unit starts shrinking in size.

- The weight loss was attributed to the free zinc oxide. The sorbent with higher mixed metal oxide content was found to be almost immune to reduction.
- No evidence of surface accumulation of elemental zinc was found.

Sulfidation experiments were carried out at isothermal conditions of 600°C in a TGA with 1% H_2S (rest N_2) gas stream. Following is the summary of the major results from the sulfidation experiments

- Mixed metal oxide (Zn-Ti ratio ≈ 1.1) based nanofibrous sorbent specimens (Sample-2a) found to be equally or more reactive than the specimens rich in free zinc oxide (Sample-1 with Zn-Ti ratio ≈ 3.7, both specimens being pre-reduced). This may suggest higher density of active sites and surface defects in polycrystalline complex oxides when compared to simple metal oxide surface.
- Equivalent grain model was used for identification of regime and the rate-controlling step. For majority of the reaction duration, chemical reaction step was found to be the rate-controlling step rather than the product layer diffusion – an indication of minimal mass transfer resistance offered by the nanofibrous sorbent specimens (Regime analysis performed on Sample-2a only).
- Growth of hierarchical / dendritic structures, emanating from the parent composite fiber, was observed during the sulfidation. This was attributed to specific simultaneous occurrences of the polar planes of ZnS/ZnO as fiber outer surface along with locally high gas (H2S) / vapor (Zn) concentration. These structures may lead to increased specific area.
- Post-sulfidation, no sulfate formation was detected. Absence of formation of any sulfate compounds during the sulfidation of nanofibrous zinc titanate adsorbent is expected to improve the chances of achieving complete regeneration.
- Formation of wurtzite phase during sulfidation, a distinct crystal form of zinc sulfide, was seen as another potential advantage of using nanostructured sorbent morphology.

Although bulk wurtzite is only metastable at temperatures less than 1020°C, wurtzite, in its nanocrystalline form, was found to be stable at lower temperatures as well (≈ 600°C). Wurtzite tend to oxidize directly to zinc oxide whereas oxidation of sphalerite (another ZnS crystal form) has been reportedly linked with the formation of $ZnSO_4$ and $Zn_3O(SO_4)_2$.

Regeneration experiments were carried out at the same temperature as the sulfidation (600^{o}C) with a gas stream containing 3% O_2 (rest nitrogen) flowing at 200 ml /min.

- Sorbent specimens rich in zinc titanate showed faster kinetics than the zinc oxide sorbents (both pre-reduced).
- Complete regeneration was achieved at the same temperature at which the sulfidation was carried out (600°C). Typically, the regeneration time needs to be raised by at least a couple of hundred degrees centigrade before the regeneration even begins.
- No sulfate formation detected post-oxidation even when the regeneration temperature was kept same as the sulfidation temperature. This can be partly attributed to the formation of wurtzite form of ZnS.
- Structural properties of the sorbent specimen like the fibrous morphology, grain size of the fresh sorbent remained intact in the regenerated specimens

Multi-cycle sulfidation and regeneration tests found that the nanofibrous design of zinc titanate sorbents can successfully withstand repeated sulfidation-regeneration operations whithout suffering microstructure degradation while maintainng high sulfur capacities close to the theoretically predicted values. Improvement in the textural properties of the fiber due to growth of dendrite-like structures and surface roughening were proposed as the reason for this enhancement in the sorbent performance.

Above-mentioned findings are promising and tend to confirm the main propositions of this work that the sorbent morphology and overall structure influence the sorbent performance as much as the compositional modifications. In fact, some of the troubling aspects about the compositionally-enhanced metal oxides like lower reactivity, requirement of high regeneration temperatures, mass transfer controlled overall rate and the resultant incomplete regeneration, were found to be absent in the above nanostructured sorbent specimens. These additional benefits of such structurally-enhanced sorbents when combined with the advantages mixed metal oxide compositions can help in the development of multi-cycle fully regenerable sorbents with longer lifetimes, as required by any economic process. These results may serve as a basis for further studies on regenerable nanostructured sorbents.

Recommendations for future research work

In future, one focus area for experiments investigating such nanostructured sorbents could be the identification and examination of the active sites on the surfaces of such specimens. The reported finding that when nanostructured, the pre-reduced zinc titanates become more reactive than the simple zinc oxide specimens could probably be explained more rigorously if the surface density and the nature of the active sites is well-understood.

Another interesting area for future studies will be a detailed study of the effect of temperature on the sulfidation and regeneration kinetics on such nanofibrous sorbents. A preliminary study was done during the course of this thesis which found that the activation energy associated with the reaction is smaller than those reported for bulk sorbent. A future study can help in estimating other kinetic parameters (like the pre-exponential factor) associated with these reactions. Finding the precise reason for the observed lower energy barrier can help in revealing the probable alternate reaction mechanism. Knowing all the details of the reaction mechanism can then help in the sorbent synthesis step i.e. tailored sol-gel preparation and electrospinning.

In the present study, only a simplified grain model was used to figure out the rate-controlling step. In future, more complex forms of kinetic modeling, like overlapping grain model, can also be used to predict the overall mechanism and associated evolution in the sorbent structure and reactivity.

Also, such nanostructured sorbents may also be considered for different applications like purification of the inlet gas to high temperature solid oxide fuel cells (SOFCs) which operate on fuels with some sulfur loading (like gasoline). Because of the fast overall reaction rates associated with such nanostructured sorbents, they can potentially be used as sulfur sorbents in applications where rapid cycling is equally important as the net capacity. Even applications requiring multi-component adsorption by a single sorbent can benefit from such structured sorbents. The results from such investigations may help in identifying the different ways in such nanostructured sorbents could prove to be useful.

Bibliography

1. Baird, T.; Denny, P.J.; Hoyle, R.; McMonagle, F.; Stirling, D.; Tweedy, J. J. (1992). Chem. Soc., Faraday Trans., 88 (22), 3375–3382
2. Cheah, S., Carpenter, D. L., & Magrini-Bair, K. (2009). Review of mid- to high-temperature sulfur sorbents for desulfurization of biomass- and coal-derived syngas. Energy & Fuels, 23(11), 5291-5307.
3. Chang, Y. S., Chang, Y. H., Chen, I. G., Chen, G. J., & Chai, Y. L. (2002). Synthesis and characterization of zinc titanate nano-crystal powders by sol-gel technique. *Journal of Crystal Growth, 243*(2), 319-326.
4. Dai, Y., Liu, W., Formo, E., Sun, Y., & Xia, Y. (2011). Ceramic nanofibers fabricated by electrospinning and their applications in catalysis, environmental science, and energy technology. *Polymers for Advanced Technologies*, 22 (3), 326-338.
5. Dooley, K. M., Kalakota, V., & Adusumilli, S. (2011). High-temperature desulfurization of gasifier effluents with rare earth and rare Earth/Transition metal oxides. *Energy & Fuels, 25*(3), 1213-1220.
6. Flytzani-Stephanopoulos, M. (1986). Detailed studies of novel regenerable sorbents for high temperature coal gas desulfurization. Proceedings of the sixth annual meeting on containment content in coal-derived gas streams, DOE/METC-86/6042, p.257.
7. Flytzani-Stephanopoulos, M.; Li, Z (1998). Kinetics of sulfidation reactions between H2S and bulk oxide sorbents. In Desulfurization of Hot Coal Gas, Atimtay, A. T.; Harrison, D. P., Springer: Berlin, Vol. 42, pp 179-211.
8. Focht, G.D., Sa, L.N., Ranade, P.V., Harrison, D.P. (1989). High-temperature desulfurization using zinc ferrite: Solid structural property changes. *Chemical Engineering Science, 44*(2), 215-224
9. Froessling, N. (1938). The evaporation of falling raindrops. *Beitr. Geophys.* 52, p. 170.
10. Gibson, J. B., & Harrison, D. P. (1980). The reaction between hydrogen sulfide and spherical pellets of zinc oxide. *Industrial & Engineering Chemistry Process Design and Development, 19*(2), 231-237.
11. Grunze, M. & Hirschwald. W. (1974). Vacuum microbalance investigations of heterogeneous surface reaction mechanisms. *J. Vac. Sci. Technol.,* 11, 424-428.

12. Harrison, D. P. (1998). Performance analysis of ZnO-based sorbents in removal of H2S from fuel gas. In Desulfurization of Hot Coal Gas, Atimtay, A. T.; Harrison, D. P., Springer: Berlin, Vol. 42, pp 213-242.
13. Huiling, F., Yanxu, L., Chunhu, L., Hanxian, G., & Kechang, X. (2002). The apparent kinetics of H2S removal by zinc oxide in the presence of hydrogen. *Fuel, 81*(1), 91-96.
14. Jothimurugesan, K., & Gangwal, S. K. (1998). Regeneration of zinc titanate H2S sorbents. *Industrial & Engineering Chemistry Research, 37*(5), 1929-1933.
15. Jun, H. K., Tae, J. L., Ryu, S. O., & Kim, J. C. (2001). A study of Zn−Ti-based H_2S removal sorbents promoted with cobalt oxides. *Industrial Engineering Chemistry Research, 40*(16), 3547.
16. Kobayashi, M., Shirai, H., & Nunokawa, M. (2002). Estimation of multiple-cycle desulfurization performance for extremely low-concentration sulfur removal with sorbent containing zinc ferrite-silicon dioxide composite powder. *Energy Fuels, 16*(6), 1378.
17. Kobayashi, M., Shirai, H., & Nunokawa, M. (1997). Investigation on desulfurization performance and pore structure of sorbents containing zinc ferrite. Energy & Fuels, 11(4), 887-896.
18. Levenspiel, Octave. (1999) *Chemical reaction engineerin,* 3rd Ed. New York: Wiley.
19. Lew, S., Jothimurugesan, K., & Flytzani-Stephanopoulos, M. (1989). High-temperature hydrogen sulfide removal from fuel gases by regenerable zinc oxide-titanium dioxide sorbents. *Industrial & Engineering Chemistry Research, 28*(5), 535-541.
20. Lew, S., Sarofim, A. F., & Flytzani-Stephanopoulos, M. (1992). The reduction of zinc titanate and zinc oxide solids. *Chemical Engineering Science, 47*(6), 1421-1431.
21. Lew, S. (1991). High temperature sulfidation and reduction of zinc titanate and zinc oxide sorbents. Ph. D. Dissertation, Dept. of Chemical Engineering, Massachusetts Institute of Technology, Cambridge, MA.
22. Li, D., & Xia, Y. (2003). Fabrication of titania nanofibers by electrospinning. *Nano Letters, 3*(4), 555-560.
23. Li, D., & Xia, Y. (2004). Electrospinning of nanofibers: Reinventing the wheel? Advanced Materials, 16(14), 1151-1170.
24. Li, D., McCann, J. T., Xia, Y., & Marquez, M. (2006). Electrospinning: A simple and versatile technique for producing ceramic nanofibers and nanotubes. Journal of the American Ceramic Society, 89(6), 1861-1869.

25. Liu, R., Ye, H., Xiong, X., & Liu, H. (2010). Fabrication of TiO2/ZnO composite nanofibers by electrospinning and their photocatalytic property. Materials Chemistry and Physics, 121(3), 432-439.
26. Manik, S. K., & Pradhan, S. K. (2006). Preparation of nanocrystalline microwave dielectric Zn2TiO4 and ZnTiO3 mixture and X-ray microstructure characterization by rietveld method. *Physica E: Low-Dimensional Systems and Nanostructures, 33*(1), 69-76.
27. Milbrandt, A. (2005). A Geographic Perspective on the Current Biomass Resource Availability in the United States. National Renewable Energy Laboratory (NREL) Publication.
28. Mojtahedi, W., & Abbasian, J. (1995). H2S removal from coal gas at elevated temperature and pressure in fluidized bed with zinc titanate sorbents. 2. sorbent durability. *Energy Fuels, 9*(5), 782-787.
29. Nagel, F. (2008). Electricity from wood through the combination of gasification and solid oxide fuel cells. Ph.D. Thesis, Swiss Federal Institute of Technology Zurich
30. Nolan, N. T., Seery, M. K., & Pillai, S. C. (2011). Crystallization and phase-transition characteristics of Sol−Gel-synthesized zinc titanates. *Chemistry of Materials, 23*(6), 1496-1504.
31. Pineda, M.; Fierro, J.L.G.; Palacios, J.M.; Cilleruelo, C.; Garcia, E.; Ibarra,J.V. (1997). Appl.Surf.Sci. 119 (1-2), 1–10.
32. Phillips, S.; Aden, A.; Jechura, J.; Dayton, D.; Eggeman, T. (2007). Thermochemical Ethanol via Indirect Gasification and Mixed Alcohol Synthesis of Lignocellulosic Biomass; NREL/TP-510-41168; National Renewable Energy Laboratory: Golden,CO.,.
33. Ramaseshan, R. and Ramakrishna, S. (2007). Zinc titanate nanofibers for the detoxification of chemical warfare simulants. J.Am.Ceram.Soc, 90(6), 1836-1842.
34. Ramaseshan, R., Sundarrajan, S., Jose, R., & Ramakrishna, S. (2007). Nanostructured ceramics by electrospinning.102(11), 17.
35. Ramakrishna, S. (2005). *An introduction to electrospinning and nanofibers.* World Scientific Pub Co Inc.
36. Ryu, S., Park, N. –K., Chang, C. H., Kim, J. C., & Lee, T. J. (2004). Multicyclic study on improved Zn/Ti-based desulfurization sorbents in mid-temperature conditions. *Industrial Engineering Chemistry Research, 43*(6), 1466-1471
37. Seitarides, T., Athanasiou, C., & Zabaniotou, A. (2008). Modular biomass gasification-based solid oxide fuel cells (SOFC) for sustainable development. Renewable and Sustainable Energy Reviews,12(5), 1251-1276.

38. Slimane, R. B. (2002). New ZnO-based regenerable sulfur sorbents for fluid-bed/transport reactor applications. *Industrial Engineering Chemistry Research, 41*(23), 5676.
39. Schultze, D. (1995). Thermal oxidation of ZnS modifications sphalerite and wurtzite. *Crystal Research and Technology, 30*(4), 553.
40. Shen, G., Chen, D., & Lee, C. J. (2006). Hierarchical saw-like ZnO Nanobelt/ZnS nanowire heterostructures induced by polar surfaces. *The Journal of Physical Chemistry B, 110*(32), 15689-15693.
41. Sasaoka et al. (1999). Modification of ZnO-TiO2 high-temperature desulfurization sorbent by ZrO2 addition. Industrial Engineering Chemistry Research, 38(3), 958.
42. Siriwardane, R. V., & Poston, J. A. (1990). Interaction of H2S with zinc titanate in the presence of H2 and CO. *Applied Surface Science, 45*(2), 131-139.
43. Siriwardane, R. V., Poston, J. A., & Evans, G. (1994). Spectroscopic characterization of molybdenum-containing zinc titanate desulfurization sorbents. Industrial Engineering Chemistry Research, 33(11), 2810.
44. Sohn, H. Y., & Szekely, J. (1972). A structural model for gas-solid reactions with a moving boundary—III : A general dimensionless representation of the irreversible reaction between a porous solid and a reactant gas. *Chemical Engineering Science, 27*(4), 763-778.
45. Steinfeld, A., Frei, A., Kuhn, P., & Wuillemin, D. (1995). Solar thermal production of zinc and syngas via combined ZnO-reduction and CH4-reforming processes. *International Journal of Hydrogen Energy, 20*(10), 793.
46. Sigmund, W., Yuh, J., Park, H., Maneeratana, V., Pyrgiotakis, G., Daga, A., (2006). Processing and structure relationships in electrospinning of ceramic fiber systems. Journal of the American Ceramic Society, 89(2), 395-407.
47. Siriwardane, R., Fisher, J. C., & Simonyi, T. (2010). Regenerable multifunctional sorbent development for sulfur and chloride removal from coal-derived synthesis gas. Energy & Fuels, 24(8), 4226-4230.
48. Ra, H-W., Khan, R., Kim, J.T., Kang, B.R. and Im, Y. H. (2010). The effect of grain boundaries inside the individual ZnO nanowires in gas sensing. Nanotechnology, 21 (8).
49. Torres, W., Pansare, S. S., & Goodwin, J. G. (2007). Hot gas removal of tars, ammonia, and hydrogen sulfide from biomass gasification gas. Catalysis Reviews: Science & Engineering, 49(4), 407-456.

50. Valsamakis, I., Si, R., & Flytzani-Stephanopoulos, M. (2010). Stability of lanthanum oxide-based H2S sorbents in realistic fuel processor/fuel cell operation. Journal of Power Sources, 195(9), 2815-2822.
51. Wang, Z., & Flytzani-Stephanopoulos, M. (2005). Cerium oxide-based sorbents for regenerative hot reformate gas desulfurization. Energy & Fuels, 19(5), 2089-2097.
52. Woods, M. C., Gangwal, S. K., Harrison, D. P., & Jothimurugesan, K. (1990). Reaction between hydrogen sulfide and zinc oxide-titanium oxide sorbents. 1. single-pellet kinetic studies. *Industrial Engineering Chemistry Research, 29*(7), 1160.
53. Westmoreland, P. R., & Harrison, D. P. (1976). Evaluation of candidate solids for high-temperature desulfurization of low-btu gases. *Environmental Science & Technology, 10*(7), 659-661.
54. Yuh, J., Perez, L., Sigmund, W., & Nino, J. (2007). Sol-gel based synthesis of complex oxide nanofibers. *Journal of Sol-Gel Science and Technology, 42*, 323-329.
55. Huang, J., & Wan, Q. (2009). Gas sensors based on semiconducting metal oxide one-dimensional nanostructures. *Sensors,9*(12), 9903-9924.
56. Du, G.H., F. Xu, Z.Y. Yuan and G. Van Tendeloo, Appl. Phys. Lett. **88** (2006), p. 243101
57. Li, G.R., X.H. Lu, D.L. Qu, C.Z. Yao, F.L. Zheng, Q. Bu, C.R. Dawa and Y.X. Tong, J. Phys. Chem. C 111 (2007), p. 6678.
58. Huang, M.H., S. Mao, H. Feick, H. Yan, Y. Wu, H. Kind, E. Weber, R. Russo and P. Yang, Science **292** (2001), p. 1897
59. Sun, Y., G.M. Fuge and M.N.R. Ashfold, Chem. Phys. Lett. 396 (2004), p. 21
60. Guo, C.F. , Y. Wang, P. Jiang, S. Cao, J. Miao, Z. Zhang and Q Liu, Nanotechnology 19 (2008), p. 445710.
61. Cheng, H., J. Cheng, Y. Zhang and Q.-M. Wang, J. Cryst. Growth 299 (2007), p. 34
62. Park, S. J., Chase, G. G., Jeong, K. U., & Kim, H. Y. (2010). Mechanical properties of titania nanofiber mats fabricated by electrospinning of sol–gel precursor. Journal of Sol-Gel Science and Technology, 54(2), 188-194.
63. Poston, J. A. (1996). A reduction in the spalling of zinc titanate desulfurization sorbents through the addition of lanthanum oxide. Ind.Eng.Chem.Res, 35(3), 875-882.
64. Ostermann et al. (2006). V_2O_5 nanorods on TiO_2 nanofibers: A new class of hierarchical nanostructures enabled by electrospinning and calcination. *Nano Letters, 6*(6), 1297.
65. Xu, L., Chen, Q., & Xu, D. (2007). Hierarchical ZnO nanostructures obtained by electrodeposition. *The Journal of Physical Chemistry C, 111*(31), 11560.

66. Wang, J. X., H. Zhang, X. T. Dong, G. X. Liu, Chin. 2010. ZnO-SiO2 coaxial nanocable: preparation via electrospinning and characterization. J. Inorg. Chem 26, 29.
67. Zhang, Z., Li, X., Wang, C., Wei, L., Liu, Y., & Shao, C. (2009). ZnO hollow nanofibers: Fabrication from facile single capillary electrospinning and applications in gas sensors. *The Journal of Physical Chemistry C, 113*(45), 19397-19403.
68. Zhang, H., Feng, J., Wang, J., & Zhang, M. (2007). Preparation of ZnO nanorods through wet chemical method. *Materials Letters, 61*(30), 5202-5205.
69. Zhao, J., Qin, L., & Zhang, L. (2009). Fabrication of ZnS/ZnO hierarchical nanostructures by two-step vapor phase method. *Materials Research Bulletin, 44*(5), 1003-1008.
70. Zhong, L. W. (2004). Zinc oxide nanostructures: Growth, properties and applications. *Journal of Physics: Condensed Matter, 16*(25) R829.
71. Park, N.-K., Lee, T. J., & Ryu, S. O. (2010). Study on deactivation of zinc-based sorbents for hot gas desulfurization. Industrial and Engineering Chemistry Research, 49(10), 4694-4699.
72. Siriwardane, R. V., & Poston, J. A. (1990). Interaction of H2S with zinc titanate in the presence of H2 and CO. Applied Surface Science, 45(2), 131-139.
73. Siriwardane, R. V., & Woodruff, S. (1995). FTIR characterization of the interaction of oxygen with zinc sulfide. Industrial & Engineering Chemistry Research, 34(2), 699-702.
74. Dulin, F. H., & Rase, D. E. (1960). Phase equilibria in the system ZnO-TiO2. *Journal of the American Ceramic Society, 43*(3), 125-131.
75. Yang, J., & Swisher, J. H. (1996). The phase stability of Zn2Ti3O8. *Materials Characterization, 37*(2-3), 153-159
76. Formo, E., Camargo, P.H.C., Lim, B., Jiang, M.J., Xia, Y.N. (2009). Chem.Phys.Lett. 476, 56.
77. Yin, L., & Bando, Y. (2005). Semiconductor morphology: Optimizing properties by tuning morphology. *Nat Mater, 4*(12), 883-884